

# A HEAT PIPE COOLED MICRO NUCLEAR REACTOR

MODELLING AND NEUTRONIC DESIGN OPTIMIZATION OF A HEAT PIPE  
COOLED MICRO NUCLEAR REACTOR

BY RAZIA NUSHRAT

A Thesis Submitted to the School of Graduate Studies in Partial Fulfilment of the Requirements  
for the Degree Master of Applied Science

McMaster University © Copyright by Razia Nushrat, April 2025

McMaster University Master of Applied Science (2025) Hamilton, Ontario (Engineering Physics)

TITLE: Modelling and Neutronic Design Optimization of a Heat Pipe Cooled Micro Nuclear Reactor

AUTHOR: Razia Nushrat, B.Sc. (Military Institute of Science and Technology, Dhaka, Bangladesh)

SUPERVISOR: Professor Dr. Adriaan Buijs

NUMBER OF PAGES: x; 74

## Abstract

This thesis presents the modelling and neutronic design optimization of a 5 MWt heat pipe-cooled Micro Nuclear Reactor (MNR) developed for deployment in remote and off-grid environments. Operating within a fast and intermediate neutron energy spectrum, the reactor is inspired by the Los Alamos National Laboratory's Design A concept but incorporates substantial enhancements to improve compactness, safety, and performance. Key innovations include the use of TRISO fuel embedded in a beryllium matrix, passive cooling through sodium heat pipes, and a hexagonal core layout designed for long-term, maintenance-free operation.

Extensive neutronic analyses were conducted using the OpenMC Monte Carlo code to evaluate neutron flux distributions, reactivity behaviour, fuel temperature coefficients, and depletion characteristics. Several design optimizations were implemented to achieve and sustain criticality despite the lower fissile content of TRISO fuel, such as pitch adjustment, cladding removal, and matrix material selection. The finalized core features 462 unit cells, surrounded by an alumina reflector and regulated by 12 hafnium hydride control drums and a central control rod to ensure precise reactivity control.

This study demonstrates the feasibility of a compact and inherently safe microreactor capable of 20 years of autonomous operation. Its robust, passively cooled design offers a promising solution for energy delivery in remote, austere, or emergency settings, supporting the broader goals of sustainable and decentralized nuclear power deployment.

## *Acknowledgements*

First and foremost, I would like to express my deepest gratitude to my supervisor, Dr. Adriaan Buijs, whose invaluable guidance, unwavering support, and inspiring mentorship have been instrumental throughout my thesis journey. Dr. Buijs's profound knowledge, constructive feedback, and continuous encouragement have greatly enriched my academic experience and motivated me to explore beyond my limits.

I sincerely thank my groupmates, Ariful Islam, Peter Kriemadis, and Cahit Alkan, for their continuous support, collaborative spirit, and willingness to assist me whenever needed. Their encouragement and shared insights significantly contributed to the successful completion of this work.

I also extend my heartfelt appreciation to my family for their unwavering support, patience, and encouragement throughout this journey. Their constant belief in my abilities provided me with the strength and motivation to persevere through all challenges.

Lastly, I would like to acknowledge the assistance provided by ChatGPT in refining the language and ensuring a professional presentation of this thesis.

Thank you all for being part of this important chapter of my academic career.

# Contents

1. Introduction.....	1
1.1 Special Purpose Reactor.....	2
1.2 Fast Reactor.....	4
1.3 Heat Pipe Cooled Reactor.....	7
1.4 TRISO Fuel.....	9
1.5 Reactor Physics.....	10
1.5.1 Neutron cycle:.....	10
1.5.2 Neutron Transport Equation.....	13
1.5.3 Monte Carlo Method.....	14
1.5.4 Multiplication Factor, Reactivity.....	16
2. Reactor Core Design Description.....	17
2.1 Benchmark Overview.....	17
2.2 Designed Micro Nuclear Reactor Overview.....	19
3. Simulation Methodology.....	24
3.1 OpenMC.....	24
3.2 Normalizing.....	25
3.3 Burnup Algorithms.....	26
3.3.1. Matrix Exponential Methods.....	27
3.4 Implementation in OpenMC.....	29

4. Result .....	30
4.1 Unit cell.....	30
4.1.1 Matrix Analysis.....	32
4.1.2 Optimization of Fuel Lattice Pitch .....	33
4.1.3 Flux Distribution Analysis.....	34
4.1.4. Fuel Temperature Coefficient .....	40
4.1.5. Burnup results.....	43
4.2 Full core.....	53
4.2.1 Core Layout: .....	53
4.2.2 Flux Distribution of the Central Core:.....	53
4.2.3 Optimization and Functionality of Absorbing Materials for Control Rods and Control Drums: .....	55
4.2.4 Impact of Control Rod and Control Drums on Reactor Flux Distribution:.....	59
5. Discussion of Results .....	68
5.1 Neutronic Optimization and Criticality Achievement.....	68
5.2 Fuel Burnup and Long-Term Reactor Viability .....	68
5.3 Neutron Flux Distribution and Core Performance .....	68
5.4 Reactor Control Mechanisms .....	69
5.5 Fuel Temperature Coefficient and Safety Implications.....	69
5.6 Comparison with Existing Micro Nuclear Reactor Designs .....	69

5.7 Challenges and Future Considerations .....	69
5.8 Conclusion.....	70

## List of Figures

Figure 1: Special Purpose Reactor concept schematic.[2].....	3
Figure 2: Neutron fission cross section for U-238 and Pu-239 [12].....	5
Figure 3: Working principle of high-temperature heat pipe [16].....	8
Figure 4: Micrograph of an actual TRISO fuel particle, as reproduced from Ref.[20] .....	9
Figure 5: Cross-sectional view of a single fuel element (pitch 2.79cm) [1].....	17
Figure 6: Cross-sectional view of the Design A core layout.[1].....	18
Figure 7: Cross-sectional view of a unit cell of hexagonal fuel matrix (pitch 5.2 cm). .....	20
Figure 8: Cross-sectional view of the full core layout with control devices. ....	21
Figure 9:Unit cell (edge length – 1.6086 cm, pitch- 2.7862cm).....	30
Figure 10: Unit cell of hexagonal fuel matrix with TRSIO particle (edge-1.6086 cm, pitch- 2.7862cm) without cladding material. ....	31
Figure 11: Final unit cell with beryllium matrix (pitch=5.17cm).....	34
Figure 12: Neutron spectra (lethargy flux) .....	35

Figure 13: Neutron spectra comparison for three different reactor designs (PWR, SFR and MNR)	36
.....	36
Figure 14: Flux energy distribution at BOL, MOL and EOL. ....	37
Figure 15: 2D flux distribution (fast and intermediate).....	38
Figure 16: 1D radial flux profile (fast and intermediate) for a unit cell. ....	38
Figure 17: 1D epithermal radial flux(left) and 1D thermal radial flux (right) profile for a unit cell.	39
.....	39
Figure 18: Capture cross section of sodium-23 from JENDL-5 data library.....	39
Figure 19: Reactivity variation with fuel temperature.....	41
Figure 20: Fuel Temperature Coefficient (FTC) with fuel temperature .....	42
Figure 21: Change of $k_{inf}$ with time for 20 years .....	43
Figure 22: Change of concentration of U-235 .....	44
Figure 23: Change of concentration of U-238 .....	45
Figure 24: Change of concentration of Pu-239.....	46
Figure 25: Change of concentration of Xe-135 .....	46
Figure 26: Change of concentration of I-135.....	47
Figure 27: Change of concentration of Pu-241 .....	48
Figure 28: Change of concentration of Pu-242.....	48
Figure 29: Change of concentration of Am-241 .....	49

Figure 30: Reaction rate of U-235 .....	50
Figure 31: Reaction rate of U-238 .....	50
Figure 32: Reaction rate of Pu-239 .....	51
Figure 33: Reaction rate of Xe-135 .....	52
Figure 34: Reaction rate of I-135 .....	52
Figure 35: Radial flux distribution of the core at the BOL .....	54
Figure 36: Absorption cross section of hafnium in HfH <sub>2</sub> [39] .....	58
Figure 37: 2D MNR core layout with control rod inserted and control drum facing inward .....	60
Figure 38: 2D plot of radial flux changes of the core inserting control rod in the middle of the core and rotating all the control drums facing inward the core. ....	61
Figure 39: 1D plot of radial flux changes of the core inserting the control rod in the middle of the core and rotating all the control drums facing inward the core. ....	61
Figure 40: 2D MNR core layout with control rod inserted and control drum facing outward. ...	62
Figure 41: 2D plot of radial flux changes of the core inserting a control rod in the middle of the core and rotating all the control drums facing outward the core. ....	63
Figure 42: 1D plot of radial flux changes of the core inserting the control rod in the middle of the core and rotating all the control drums facing outward the core. ....	63
Figure 43: 2D MNR core layout with control rod withdrawn and control drum facing outward.	64

Figure 44: 2D plot of radial flux changes of the core withdrawing control rod in the middle of the core and rotating all the control drums facing outward the core. .... 65

Figure 45: 1D plot of radial flux changes of the core withdrawing control rod in the middle of the core and rotating all the control drums facing outward the core. (250)..... 66

Figure 46: 1D plot of radial flux changes of the core withdrawing control rod in the middle of the core and rotating all the control drums facing outward the core. (220)..... 67

**List of Table**

Table 1: Nominal reactor design for 5MW Micro Nuclear Reactor(MNR) and LANL proposed 5MW SMR design concept..... 21

Table 2:  $k_{eff}$  values of the unit cell with a 2.8 cm pitch for the different matrix materials. .... 32

Table 3:  $k_{eff}$  values of the unit cell for various pitch sizes with 15% fuel enrichment. .... 33

Table 4:  $k_{eff}$  values of the unit cell for various pitch sizes with 20% fuel enrichment. .... 33

Table 5: Fuel Temperature Reactivity and FTC..... 40

Table 6:  $k_{eff}$  and reactivity variation calculation for different absorbing materials..... 56

# 1. Introduction

This thesis presents the neutronic design and optimization of a heat pipe-cooled Micro Nuclear Reactor (MNR) that works in a fast and epithermal energy region, specifically developed to serve remote and off-grid locations, thus directly benefiting humanity by providing reliable power where traditional energy infrastructure is absent or impractical. The proposed design is inspired by Los Alamos National Laboratory's (LANL) special-purpose reactor concept, known as Design A, a 5 MWt reactor. The original design comprises a hexagonal core structure, containing 1134 solid  $\text{UO}_2$  fuel elements with stainless steel cladding, potassium-cooled heat pipes, and helium-filled fuel gaps. However, substantial modifications have been introduced to enhance compactness, robustness, and operational flexibility for diverse remote applications.

As global demand for reliable, sustainable, and compact energy systems grows, nuclear innovations such as micro nuclear reactors have become increasingly important. This Micro Nuclear Reactor (MNR) has unique advantages, including high fuel efficiency, extended operational lifetimes, minimal maintenance requirements, and inherent safety, making it ideally suited for deployment in remote settlements, military installations, disaster-affected regions, and isolated communities. The reactor utilizes a hexagonal core structure with advanced TRISO (tristructural isotropic) fuel particles embedded within a beryllium matrix. TRISO fuel, notable for its exceptional safety attributes and resilience under high-temperature conditions, effectively confines fission products and maintains stable reactor performance under extreme scenarios.

A distinguishing feature of this reactor design is its operation in a fast and epithermal neutron energy spectrum, which eliminates the need for neutron moderators and significantly improves fuel efficiency. Incorporating advanced heat pipe technology, the reactor achieves fully passive cooling, greatly enhancing safety and reliability, particularly essential in isolated locations where maintenance capabilities are limited. The use of heat pipes eliminates the complexity of active cooling systems, thereby increasing the reactor's mechanical robustness and operational resilience.

This thesis undertakes detailed neutronic analyses and optimizations using iterative simulations performed with the OpenMC Monte Carlo code, enabling comprehensive modelling of neutron transport, flux distributions, and fuel burnup behaviours over a projected operational lifespan of 20 years. OpenMC is an open-source Monte Carlo particle transport code widely used in nuclear engineering for simulating neutron and photon transport. It allows detailed modelling of nuclear reactors, facilitating criticality analyses, neutron flux calculations, burnup studies, and reactor design optimizations. With its Python-based interface, OpenMC offers accessibility and flexibility, making it an excellent tool for students and researchers working on reactor physics and nuclear safety analyses [1]. Key innovations explored include leveraging a beryllium matrix for improved neutron economy and integrating advanced control mechanisms, such as hafnium hydride control drums and a centrally positioned control rod, to precisely manage core reactivity and enhance operational safety.

The primary objective of this research is to design and optimize a robust and efficient 5 MWt Micro Nuclear Reactor that works in fast and intermediate energy spectra, tailored for remote and humanitarian applications. Specifically, the thesis addresses the following goals:

1. **Neutronic Optimization:** Develop an optimized core layout to maintain criticality, enhance neutron economy, and ensure stable operation.

2. **Reactivity Control Analysis:** Evaluate the performance and effectiveness of innovative control systems, including control rods and control drums, in managing reactor reactivity under various operational conditions.
3. **Burnup and Fuel Cycle Analysis:** Examine the fuel depletion and accumulation of transuranic isotopes over the reactor’s 20-year operational lifespan to optimize fuel cycle performance.
4. **Flux Distribution Characterization:** Investigate neutron flux distribution radially and axially to ensure uniform power distribution and prevent thermal hotspots.
5. **Fuel Temperature Coefficient Analysis:** Analyze inherent safety features of the reactor through the study of temperature-reactivity feedback.
6. **Material Selection and Impact Analysis:** Assess the impact of different core materials on neutron absorption, leakage, and overall reactor performance to inform optimal material choices.

The subsequent chapters provide detailed discussions of the reactor design principles, simulation methodologies employed, and comprehensive results from neutronic and burnup analyses. Ultimately, this work demonstrates the feasibility and benefits of deploying a 5 MWt Micro Nuclear Reactor (MNR) in remote and off-grid environments, substantially contributing to the global pursuit of sustainable, advanced nuclear energy solutions accessible to underserved communities worldwide.

## 1.1 Special Purpose Reactor

This Micro Nuclear Reactor (MNR) is inspired by the first (Design A) of two LANL alternative core design concepts for the Special Purpose Reactor. The first LANL alternative core design concept, also known as Design A, is a 5MWt reactor. The active core of Design A retains the hexagonal shape of the LANL concept, with an inner central void for the emergency shutdown rods, and holds 1134 fuel elements surrounded by alumina filler elements on the periphery, which can add core reactivity if needed [2]. The unit cell of Design A is filled with solid  $\text{UO}_2$  fuel, and the heat pipe is cooled by potassium. The unit cell has stainless steel cladding with four different fuel gaps filled with pressurized helium gas.

Even though this reactor design is inspired by the mentioned reactor concept, we have made some changes to make it more compact, robust, and flexible. Our designed reactor core is a hexagonal fuel core with a unit cell filled with TRISO fuel particles surrounding the heat pipe in the middle. This unit cell is also hexagonal in shape but without any cladding material; instead, a beryllium matrix was used.

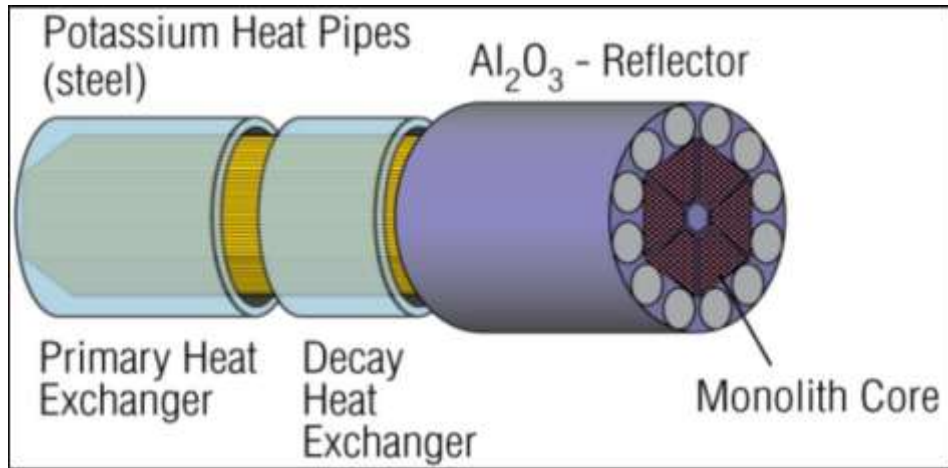


Figure 1: Special Purpose Reactor concept schematic.[2]

Special purpose reactors represent a category of nuclear reactors engineered for unique, often non-commercial applications, distinctly different from conventional reactors used for electricity generation. These reactors are designed to fulfill specialized missions such as scientific research, propulsion, medical isotope production, military operations, and industrial applications. Their tailored designs prioritize specific operational requirements, including compactness, adaptability to extreme environments, extended lifespans, and specialized fuel utilization. This versatility allows them to address challenges that conventional reactors cannot.

Research reactors are a quintessential example of special purpose reactors. Typically smaller and operating at lower power levels, they serve as invaluable tools for advancing scientific knowledge, testing materials, and producing isotopes essential for medicine, industry, and agriculture. For instance, materials testing reactors examine the behaviour of reactor components under radiation, while isotope production reactors focus on generating medical isotopes like technetium-99m, widely used for diagnostic imaging. Training reactors, commonly found in academic institutions, play a crucial role in educating the next generation of nuclear engineers and operators [3]. Facilities like the High Flux Isotope Reactor (HFIR) at the Department of Energy's Oak Ridge National Laboratory exemplify the importance of research reactors, producing medical isotopes and supporting cutting-edge experiments in neutron scattering [4].

Propulsion reactors, another significant type, are designed to power vessels and vehicles operating in environments where traditional energy sources are impractical. Naval propulsion reactors, for example, are vital for submarines and aircraft carriers, offering compact, robust designs capable of long-term operation without frequent refuelling. The S8G reactor, used in Ohio-class submarines from the US Navy, exemplifies this capability with its decades-long refuelling cycles [5]. Similarly, space propulsion reactors, like NASA's Kilopower Reactor, are engineered to provide reliable, long-term power for deep-space exploration, ensuring sustainability during missions to the Moon or Mars.

Medical isotope production reactors are indispensable in healthcare, producing radionuclides essential for diagnostics and treatments. Isotopes like technetium-99m and iodine-131 are crucial for medical imaging and cancer therapy, while cobalt-60 is widely employed in radiotherapy. These reactors, such as the OPAL reactor in Australia, ensure a steady supply of isotopes that support global healthcare systems[6].

Mobile and portable reactors, often referred to as microreactors or modular reactors, highlight the adaptability of nuclear technology. Designed for rapid deployment in remote or temporary locations, they provide electricity, heat, or process energy where conventional infrastructure is unavailable.

Test and prototype reactors play a pivotal role in the development and validation of new reactor designs, fuels, and safety systems. They provide platforms for assessing innovative technologies before their commercial deployment. For instance, the Experimental Breeder Reactor-II (EBR-II), a liquid-metal-cooled fast reactor (was located at the Argonne National Laboratory-West, which is now part of the Idaho National Laboratory (INL), near Idaho Falls, Idaho, USA), and was instrumental in testing advanced reactor concepts and nuclear fuel recycling technologies [7] [8].

Military reactors are highly specialized and often classified, serving defence-related roles such as powering naval vessels or contributing to nuclear weapons research. Compact reactors on submarines enable prolonged underwater operations, while reactors on aircraft carriers provide the immense energy required for propulsion and onboard systems. Examples like the S9G reactor illustrate the technological advancements enabling long-term operation without refuelling, essential for modern defence systems [9].

In summary, special purpose reactors demonstrate the adaptability of nuclear technology for non-commercial applications. Designed for specific missions, they enable operation in extreme environments, support defence, space exploration, scientific research, and medical isotope production. Their tailored features—such as compactness, extended operation without refuelling, and high thermal output—underscore their value in solving challenges conventional reactors cannot. Their adaptability allows them to meet complex operational demands, such as long-term deployment without refuelling, high-temperature thermal energy generation, and compact designs suitable for harsh or isolated environments. This makes them indispensable for applications like deep-space missions, military defence systems, and industrial processes, including hydrogen production and seawater desalination.

By pushing the boundaries of nuclear innovation, special purpose reactors contribute significantly to advancements in science, healthcare, defence, and sustainable energy. Their specialized functionalities demonstrate the potential of nuclear technology to solve some of the world’s most challenging problems while driving progress in diverse fields.

## 1.2 Fast Reactor

A fast reactor is a type of nuclear reactor designed to operate in a fast neutron spectrum, utilizing high-energy neutrons instead of the slow or thermal neutrons typical of conventional reactors. This distinction allows fast reactors to sustain fission chain reactions with neutrons that retain their kinetic energy, typically in the range of 1 MeV (Mega electron volts), compared to the thermal energy levels seen in thermal reactors. These unique operational characteristics make fast reactors instrumental to advancing nuclear energy technology, particularly in areas such as fuel efficiency, waste reduction, and sustainability. This design enables a more efficient use of fuel and the potential to reduce nuclear waste. According to the International Atomic Energy Agency (IAEA),

"The fast neutron spectrum allows fast reactors to largely increase the energy yield from natural uranium as compared to thermal reactors [10]."

Unlike thermal reactors, fast reactors do not use neutron moderators such as water or graphite to slow neutrons. This absence of moderation enables the fast neutron spectrum, which is essential for their operation. The chain reaction in these reactors relies on fissile materials such as uranium-235, plutonium-239, or uranium-233, which can sustain fission when struck by fast neutrons. Additionally, fertile materials like uranium-238 can be converted into fissile isotopes through breeding, though breeding is not a feature of all fast reactor designs. The compact core design of fast reactors ensures a high density of fuel, maximizing neutron interactions and maintaining criticality in a fast energy spectrum. The World Nuclear Association notes that "Fast neutron reactors (FNRs) are a technological step beyond conventional power reactors, but are poised to become mainstream" [11].

In this thesis, the reactor design primarily operates within the fast and epithermal neutron energy regions, as supported by the neutron cross-section graph shown in Figure 2.

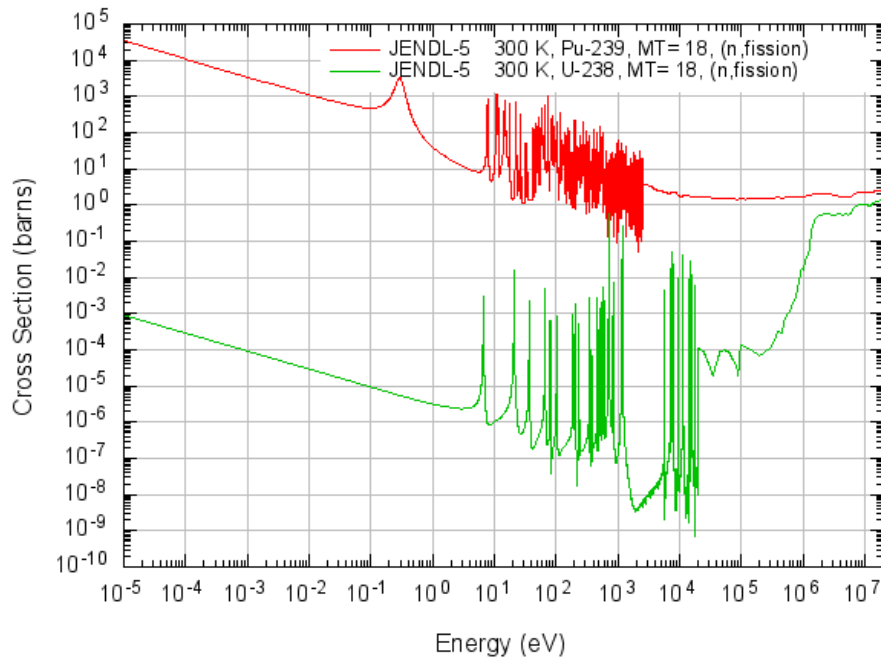


Figure 2: Neutron fission cross section for U-238 and Pu-239 [12].

From the cross-section curves, it is evident that uranium-238 exhibits pronounced resonance peaks at intermediate (epithermal) neutron energies. Due to these significant resonance peaks, U-238 absorbs neutrons effectively when neutrons are moderated towards intermediate energies. As the reactor temperature increases, Doppler broadening enhances these resonance peaks, increasing neutron capture probability further. Because the reactor operates at relatively high temperatures, neutrons are partially moderated to the epithermal range rather than fully thermalized. This moderation leads to increased resonance neutron absorption in U-238.

Moreover, in fast reactor conditions, Doppler broadening directly increases resonance neutron absorption by U-238 nuclei. This heightened neutron capture enhances the production rate of fissile plutonium-239 through neutron capture and subsequent decay processes. Thus, operating in the

fast-to-epithermal neutron spectrum, combined with the Doppler broadening effect at elevated temperatures, enhances the reactor's inherent safety through negative temperature feedback while also promoting efficient Pu-239 production.

Another significant reason for the reactor operating partially within the epithermal neutron energy region is the use of a beryllium matrix for embedding TRISO particles. Although primarily designed as a neutron multiplier due to its exceptional neutron multiplication characteristics, beryllium also acts as a moderate neutron moderator. This partial moderation shifts a fraction of the neutron spectrum towards intermediate energies, enhancing resonance interactions and further promoting both efficient neutron utilization and Pu-239 production. Thus, the inclusion of beryllium contributes directly to the reactor's neutronic performance in the fast-to-epithermal energy region.

The choice of coolant is crucial in fast reactors, as it must efficiently transfer heat while preserving the high energy of neutrons. The liquid sodium in sodium-cooled fast reactors (SFRs) offers excellent thermal conductivity and heat transfer capabilities. Other coolant options include lead or lead-bismuth eutectic, used in lead-cooled fast reactors (LFRs), and helium, used in gas-cooled fast reactors (GFRs). In this particular reactor design, sodium (liquid/vapour) is employed as the primary coolant due to its superior thermal properties, including high thermal conductivity, a high boiling point, and low neutron absorption. These characteristics enable efficient heat removal from the reactor core, maintain neutron energies within the desired fast and epithermal spectra.

Fast reactors offer significant advantages over traditional thermal reactors. By effectively utilizing depleted uranium and plutonium, fast reactors address the limitations of thermal reactors in managing these materials. Additionally, they have the capability to transmute long-lived radioactive isotopes, such as plutonium and americium, into shorter-lived or less radiotoxic forms. This capability not only reduces the volume and longevity of nuclear waste but also mitigates concerns surrounding the long-term storage of spent fuel.

Despite their advantages, fast reactors face notable challenges, and one of those is, fast reactor requires more fuel than thermal reactors because of their lower fission probability. In fast reactors, neutrons are not slowed (moderated) and remain at higher energies. At fast energies, the fission cross-sections (likelihood of a fission reaction) for fissile isotopes like U-235 and Pu-239 are much lower compared to thermal energies. To compensate for the reduced probability of fission, a higher density or quantity of fissile material is required to sustain the chain reaction.

Another important drawback of fast spectrum reactors is their lower delayed neutron fraction compared to thermal reactors. This happens for two main reasons:

1. Delayed neutrons are mostly emitted at lower energies, such as thermal and epithermal ranges, making them less effective in fast neutron environments.
2. Plutonium-239, which is commonly used or bred in fast reactors, emits fewer delayed neutrons relative to prompt neutrons compared to uranium-235. Although Pu-239 releases more neutrons overall, the smaller fraction of delayed neutrons makes reactor control more challenging.

Since delayed neutrons are essential for safely controlling reactor power, fast reactors require faster and more responsive control systems. Additionally, a notable drawback of fast reactors is the difficulty in reactivity control. Unlike thermal reactors, where large negative temperature

coefficients provide strong inherent safety feedback, fast reactors typically have weaker temperature feedback mechanisms. This means that even with rising temperatures, the decrease in reactivity is relatively small, making it harder to passively stabilize the reactor. The high-energy neutron environment accelerates irradiation damage to reactor materials, necessitating the development of advanced materials capable of withstanding such conditions. In some fast reactors (like sodium-cooled ones), losing coolant can increase reactivity. Furthermore, the complexity of fast reactor designs and their associated technologies contributes to higher initial costs and technical hurdles, underscoring the need for continued research and innovation.

Several operational and historical fast reactors have demonstrated the potential of this technology. Russia's BN-800, a sodium-cooled fast reactor, produces electricity while managing plutonium stocks [11]. The Experimental Breeder Reactor-II (EBR-II) in the United States showcased the feasibility of liquid-metal fast reactors and advanced fuel recycling technologies [8]. Other notable examples include France's Phénix and Superphénix reactors and Japan's Monju reactor, which contributed to the development of fast reactor systems despite operational challenges [13] [14].

In summary, fast reactors constitute a significant advancement in nuclear reactor technology. By operating in a fast neutron spectrum and utilizing innovative materials and designs, these reactors deliver improved fuel efficiency, waste management capabilities, and power density. Although challenges related to material durability, coolant management, and complexity persist, the ongoing development of fast reactors establishes them as a fundamental component of next-generation nuclear energy strategies. These strategies focus on achieving greater sustainability, safety, and efficiency to meet global energy demands.

### 1.3 Heat Pipe Cooled Reactor

A heat pipe-cooled reactor is a type of advanced nuclear reactor that uses heat pipes for passive heat removal, eliminating the need for traditional active cooling systems like pumps. A heat pipe is a fully sealed, passive two-phase heat transfer device that takes advantage of a fluid's high latent heat of vaporization to achieve extremely efficient heat transfer. A heat pipe-cooled nuclear reactor is a flexible and reliable power source for future Distributed Energy Resource Systems (DERS) that can provide a stable electricity supply to remote places. The structure of a megawatt heat pipe-cooled nuclear reactor, first proposed by Los Alamos National Laboratory, is shown in *Figure 1* [15]. Heat pipe technology offers a reliable and efficient method to transport heat from the reactor core to a heat exchanger or other cooling systems without the need for mechanical components. These reactors are typically small, modular designs aimed at providing power to remote areas, space missions, or other specialized applications where conventional cooling systems are impractical.

Here's a detailed explanation of the heat pipe-cooled reactor:

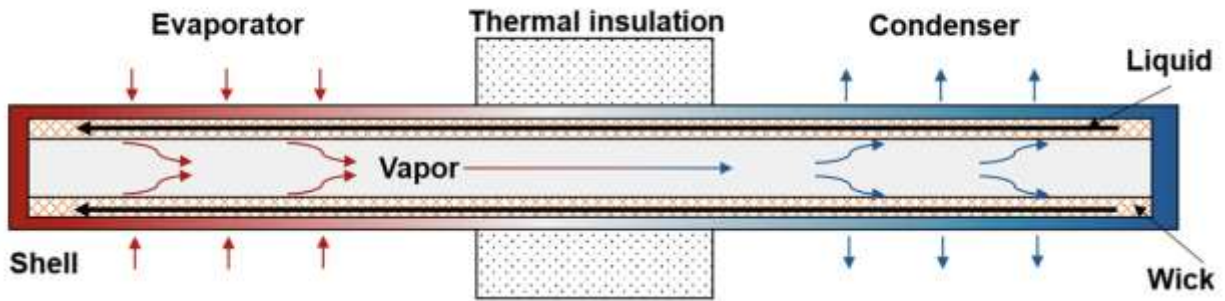


Figure 3: Working principle of high-temperature heat pipe [16]

A heat pipe is a passive heat transfer device that uses the phase transition of a working fluid to transport heat with minimal temperature difference. It consists of three main components:

1. **Evaporator section:** Located in the hot zone (e.g., reactor core), where the working fluid inside the pipe absorbs heat and evaporates.
2. **Adiabatic (Transport) Section:** In this section, the vapour travels from the evaporator to the condenser without any significant heat transfer to the surroundings. Its primary function is to transport the vapour to the cooler end of the heat pipe with minimal temperature change.
3. **Condenser section:** Located in the cooler region (e.g., heat exchanger), where the vaporized fluid releases heat and condenses.

In a nuclear reactor, heat pipes are embedded within the reactor core to remove heat generated by the nuclear fission process. Heat pipes move large amounts of thermal energy using evaporation and condensation. They use the latent heat of the coolant (e.g., sodium) to absorb heat at the core and release it at the heat exchanger without large temperature gradients. Heat pipes use phase change (latent heat) to move energy away from the core with minimal temperature drop. Heat pipes enhance safety by eliminating the need for active mechanical components like pumps. The U.S. Nuclear Regulatory Commission (NRC) highlights that "heat pipes are heat transfer devices that have been used for decades in other industries. They transfer heat via a working fluid that requires no pumps or forced circulation [17]."

Many heat pipe-cooled reactors operate in a fast neutron spectrum, employing advanced fuels like tristructural isotropic (TRISO) particles or metallic uranium [18] [19]. Fast spectrum operation allows for higher energy densities and improved fuel utilization. However, certain designs also use a thermal neutron spectrum, incorporating moderators like graphite to slow neutrons and enhance fission probabilities in specific fuel types. This flexibility enables heat pipe-cooled reactors to be tailored to diverse applications and performance requirements.

The versatility of heat pipe-cooled reactors extends to their applications. In space exploration, where reliability and compactness are paramount, they provide long-lasting power for missions to the Moon, Mars, and beyond. NASA's Kilopower reactor exemplifies this application, using sodium heat pipes to transfer heat from the reactor core to a Stirling engine for electricity generation. Similarly, the Los Alamos Megawatt Reactor demonstrates the scalability of this technology, with applications ranging from disaster response to military installations.

In conclusion, heat pipe-cooled reactors represent a paradigm shift in nuclear reactor design, offering unparalleled safety, reliability, and adaptability. Their unique combination of passive cooling, compactness, and long operational lifespans makes them a vital solution for environments where traditional reactors are unsuitable. As the demand for safe, efficient, and resilient power sources grows, heat pipe-cooled reactors stand out as a key technology for meeting the energy needs of the future.

## 1.4 TRISO Fuel

TRISO fuel (TRIstructural-ISotropic fuel) is a type of advanced nuclear fuel originally designed for high-temperature gas-cooled reactors (HTGRs) and small modular reactors (SMRs). It is known for its exceptional safety features, robustness, and ability to withstand extreme temperatures and radiation conditions. Here is an overview of its structure, characteristics, and applications:

TRISO fuel consists of small particles of nuclear fuel, typically uranium, which are coated with multiple layers of protective material. Each TRISO particle has a diameter of about 1 mm and is composed of the following layers:

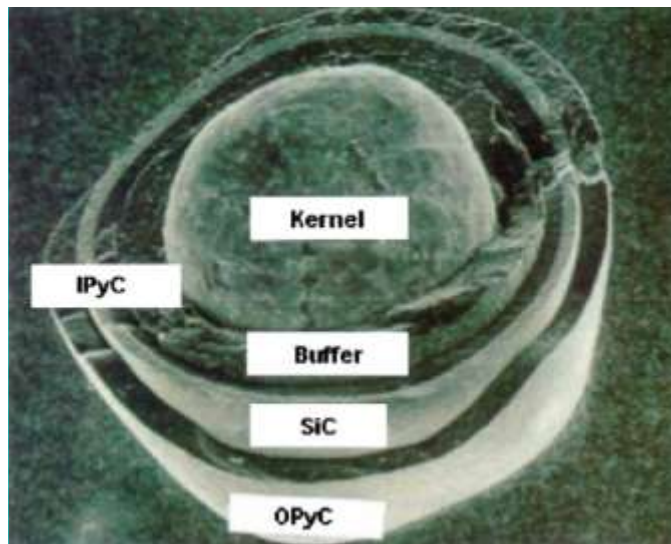


Figure 4: Micrograph of an actual TRISO fuel particle, as reproduced from Ref.[20]

1. Fuel Kernel: At the center is a tiny fuel kernel, typically made of uranium dioxide ( $\text{UO}_2$ ) or uranium oxycarbide (UCO). This is the actual nuclear fuel that undergoes fission.
2. Porous Carbon Buffer Layer: Surrounding the kernel is a carbon layer that absorbs fission gases generated during the nuclear reaction and provides space for the kernel to expand.
3. Inner Pyrolytic Carbon (PyC) Layer: This layer provides structural integrity and acts as a barrier to prevent the release of fission products.

4. Silicon Carbide (SiC) Layer: The SiC layer is a dense, strong ceramic material. The SiC layer acts as the main pressure vessel for the particle, withstanding the stresses from internal gas pressure buildup and other sources, and also provides a diffusion barrier to prevent the release of gaseous and metallic fission products (FPs). It also provides excellent resistance to high temperatures [21]
5. Outer PyC Layer: The final layer is an additional pyrolytic carbon layer, which further enhances the containment of fission products and adds mechanical strength.

TRISO fuel can operate at temperatures exceeding 1600°C (2900°F), which is much higher than conventional nuclear fuels, enhancing safety during accidents [22]. A significant benefit of TRISO particles are that the multi-layered structure ensures that **radioactive fission products remain contained within the particle, even under extreme conditions, reducing the risk of fission products leakage**, which is a very special purpose to use TRISO particles as fuel in this designed reactor. TRISO fuel is used in reactor designs where, even in the case of a coolant loss or other failure, the fuel can remain intact without releasing significant radioactivity. TRISO particles are designed to withstand the high radiation environment inside reactors, providing long-term stability.

TRISO fuel is primarily used in reactors, which are designed to operate at very high temperatures and do not melt at a very high temperature. TRISO is being considered for use in next-generation SMRs as well, such as Micro Nuclear Reactors (MNR), due to its high safety and performance. TRISO fuel has been researched for potential use in space and military applications, where safety and reliability are essential.

While TRISO fuel particles offer numerous advantages, such as superior fission product retention, high-temperature stability, and robust multi-layered containment, there are also some limitations to consider. One key drawback is the relatively low fissile material loading. Unlike conventional fuel pellets, where the entire volume contributes to fission, TRISO particles contain fuel only in the central ceramic fuel kernel, which occupies a small fraction of the total particle volume. The surrounding multiple coating layers (buffer, inner pyrolytic carbon, silicon carbide, and outer pyrolytic carbon) reduce the overall fuel density, thereby requiring larger core volumes or higher particle packing fractions to achieve comparable reactivity. The multi-layer structure of TRISO particles also demand precise fabrication techniques, increasing production cost and complexity.

## 1.5 Reactor Physics

### 1.5.1 Neutron cycle:

The fast neutron life cycle in a Micro Nuclear Reactor follows principles of neutron transport, fission chain reactions, and neutron economy specific to fast reactors. Fast and intermediate energy micro nuclear reactors are designed to operate with minimal neutron moderation, relying on fast neutrons to sustain fission. The neutron life cycle includes neutron production, interaction (fission or absorption), leakage, and reactivity control, all tailored to the compact, high-efficiency design of SMRs.

In fast SMRs, fast neutrons (with energies typically between 0.1 and 10 MeV) play a central role in the fission process. The following stages make up the fast neutron life cycle in a fast reactor:

### 1. Neutron Production (Fast Neutron Source)

- **Fission Reaction:** Fast neutrons are produced during the fission of fissile isotopes, such as U-235, Pu-239, or Pu-241. Each fission event releases about 2-3 fast neutrons.
- In MNRs, the fuel is often highly enriched uranium (HEU) or plutonium-based fuel like MOX (mixed oxide) to maximize neutron production.

### 2. Neutron Leakage

- Leakage refers to neutrons that escape from the reactor core without interacting with fuel or other materials. Leakage in fast reactors, especially in compact MMR cores, is a significant design concern, as neutron leakage can affect the reactor's efficiency and power output.
- In fast MNRs, advanced core designs, such as compact cores with reflector materials, are employed to reduce leakage and enhance neutron economy.

### 3. Neutron Absorption

- **Absorption by Fissile Material:** Fast neutrons are absorbed by fissile material (e.g Pu-239, U-235) and cause fission, releasing energy and more fast neutrons.
- **Non-Fissile Absorption:** Neutrons can also be absorbed by non-fissile materials (e.g., U-238, Th-232), leading to neutron capture and transmutation (e.g., breeding of Pu-239 from U-238).

### 4. Neutron Multiplication (Chain Reaction)

- The number of fast neutrons generated from fission events determines whether the chain reaction continues. A chain reaction occurs when the neutrons released during fission can cause other nuclei to fission, creating a self-sustaining process. The goal is to achieve a high **multiplication factor** ( $k_{\infty}$ ) in compact fast MNRs to ensure continuous fission and high power density.

- 1) The neutron life cycle can be described by a **neutron population balance equation**, which tracks changes in the neutron population due to production, absorption, and leakage. In steady-state conditions, the equation is:

$$\frac{dn}{dt} = \text{Neutron production} - \text{Neutron absorption} - \text{Neutron leakage} = 0$$

- 2) Fast Reactor Multiplication Factor ( $k$ ): The **multiplication factor** ( $k$ ) determines whether the chain reaction will sustain itself.

$$k = \frac{\text{Neutrons produced}}{\text{Neutrons lost (absorption + leakage)}} \quad (1)$$

$k = 1$  means the reactor is critical. The rate of production is equal to destruction.

$k > 1$  means the reactor is supercritical. The rate of production is larger than destruction.

$k < 1$  means the reactor is subcritical. The rate of production is less than destruction.

For a critical reactor,  $k = 1$ , indicating that neutron production balances absorption and leakage.

There are two types of multiplication factors:

1. Infinite Multiplication Factor ( $k_{\infty}$ ): The infinite multiplication factor ( $k_{\infty}$ ) is the ratio of neutrons produced in the next generation to those in the current generation in an infinite (unbounded) medium without leakage.
2. Effective Multiplication Factor ( $k_{\text{eff}}$ ): The effective multiplication factor ( $k_{\text{eff}}$ ) is similar to  $k_{\infty}$  but accounts for neutron leakage, making it more realistic for finite-sized reactors:

$$k_{\text{eff}} = k_{\infty} P_{\text{FNL}} P_{\text{TNL}} \quad (2)$$

Where,

$P_{\text{FNL}}$  = Fast neutron non-leakage probability (fraction of fast neutrons that remain in the core and do not escape)

$P_{\text{TNL}}$  = Thermal neutron non-leakage probability (fraction of thermal neutrons that remain in the core and do not escape)

Design Considerations for Fast SMRs:

**Core Design:** Fast SMRs have a high leakage probability. Materials with low neutron absorption cross-sections (like sodium or lead) are often used as coolants to avoid unnecessary neutron capture.

**Reflectors:** Neutron reflectors, typically materials with good scattering properties, are placed around the core to reflect escaping neutrons back into the core.

**Fuel:** The fuel is typically high in fissile material (HEU, plutonium, or MOX), and conversion is a common goal to extend fuel use.

### 1.5.2 Neutron Transport Equation

The neutron transport equation is the governing equation in nuclear reactor physics that describes the behaviour and movement of neutrons in a medium, being an exact deterministic equation for the continuity or conservation of neutrons. In short, the time-dependent neutron transport equation is an integro-differential form, describing the rate of change of neutron flux in terms of production and destruction in a differential volume at position  $\vec{r}$ , direction  $\vec{\Omega}$ , energy  $E$ , and time  $t$ . It considers the interactions of neutrons, such as scattering, absorption, and fission, as well as the spatial, energy, and angular distribution of neutrons. Mathematically, the neutron transport equation is given by -

$$\begin{aligned}
 & \underbrace{\frac{1}{v} \frac{\partial \phi(\vec{r}, E, \vec{\Omega}, t)}{\partial t}}_{1} = \underbrace{\frac{1}{4\pi} S(\vec{r}, E, t)}_{2} + \underbrace{\frac{\chi(E)}{4\pi} \int_{E'} v \Sigma f(\vec{r}, E', t) \phi(\vec{r}, E', \vec{\Omega}, t) dE'}_{3} \\
 & + \underbrace{\int_{\vec{\Omega}} \int_{E'} \Sigma s(\vec{r}, E' \rightarrow E, \vec{\Omega}' \rightarrow \vec{\Omega}) \phi(\vec{r}, E', \vec{\Omega}, t) dE' d\vec{\Omega}'}_{4} - \underbrace{\Sigma t(\vec{r}, E, t) \phi(\vec{r}, E, \vec{\Omega}, t)}_{5} \\
 & - \underbrace{\vec{\nabla} \cdot \vec{J}(\vec{r}, E, \vec{\Omega}, t)}_{6} \tag{3}
 \end{aligned}$$

$\Phi$  = neutron flux

$\vec{J}$  = neutron current

$S$  = external neutron source

$4\pi$  = solid angle integral over all 3D directions

$\chi$  = neutron energy spectrum

$v$  = fission neutron yield

$\Sigma f$  = fission cross section

$\Sigma s$  = neutron scattering cross section

$\Sigma_t$  = total cross section, defined as  $\Sigma_t = \Sigma_a + \Sigma_s$

$\Sigma_a$  = absorption cross section

- (1) rate of change in neutron density written in terms of  $\phi$
- (2) external neutron source
- (3) fission neutron production
- (4) neutron source scattered into  $\vec{r}, \vec{\Omega}, E$
- (5) neutron loss through absorption and scattering
- (6) neutron loss through leakage

The neutron transport equation is usually hard to solve because of its high dimensionality, complexity in interactions, and the nature of the underlying physics. The neutron transport equation is six-dimensional, with variables in both space (3D), angle (2D), and energy (1D). The equation couples spatial, angular, and energy variables through the scattering term, which involves an integral over all directions and energies. Apart from all these, it is also important to consider boundary conditions to solve the neutron transport equation, which can be even more complex depending on the geometry. The solution of the neutron transport equation is the main subject of most of the stochastic and deterministic nuclear computational solvers.

### 1.5.3 Monte Carlo Method

A Monte Carlo simulation is a model used to predict the probability of a variety of outcomes when the potential for random variables is present. The Monte Carlo method is a widely used computational technique for solving complex mathematical and physical problems using random sampling and statistical analysis. Monte Carlo simulations help to explain the impact of risk and uncertainty in prediction and forecasting models. A Monte Carlo simulation requires assigning multiple values to an uncertain variable to achieve multiple results and then averaging the results to obtain an estimate. A stochastic model is set up, and by sampling from the appropriate probability distribution functions, statistical methods are used to estimate a numerical answer [23]. The technique is particularly useful for systems that are too complex for deterministic models, involving numerous variables or random processes that influence the outcome. Sometimes the method generates random inputs or samples from a probability distribution to simulate the possible outcomes of a system or process. Again, sometimes it finds a solution by simulating many trials (often millions) using statistical properties like means, variances, etc., to estimate the result of a model. Monte Carlo simulations are the practical application of the Monte Carlo method, specifically involving running a large number of trials or simulations to analyze potential outcomes, and the process steps can be written as -

1. **Random Sampling:** The Monte Carlo method relies on generating random numbers to simulate the behaviour of a system.
2. **Simulation of Physical Processes:** It uses probabilistic distributions to represent physical phenomena (e.g., neutron interactions in reactors).
3. **Statistical Analysis:** By running thousands or millions of trials, statistical averages or distributions can be determined, leading to solutions that approximate real-world behaviour.
4. **Iterative Approach:** More simulations generally yield more accurate results, reducing statistical uncertainty.

For example, OpenMC, Serpent, and MCNP are some nuclear simulation tools that utilize the Monte Carlo method to model neutron transport in nuclear reactors.

In this thesis paper, OpenMC has been used to solve the neutron transport equation to calculate neutron flux, reactivity and burnup. It treats each neutron's journey, from its production in fission to its interaction with materials, as a probabilistic event. OpenMC is specifically designed for large-scale simulations of neutron behaviour in complex geometries.

Here's how OpenMC applies the Monte Carlo method:

1. **Neutron Transport:** The motion and interaction of neutrons with reactor materials are inherently random processes, governed by nuclear physics laws. OpenMC uses random sampling techniques to simulate neutron paths, scattering events, and absorption or fission reactions.
2. **Sampling and Randomness:** By using the Monte Carlo method, OpenMC randomly samples the distance a neutron will travel before interacting, the type of interaction it will undergo (e.g., scattering or absorption), and the outcome of these interactions based on known probability distributions from nuclear data libraries.
3. **Accuracy through Iteration:** OpenMC performs millions of simulations (neutron histories) to accurately estimate reactor properties such as power distribution, neutron flux, and criticality. By averaging the results of these simulations, OpenMC provides a statistical estimation of reactor behaviour.
4. **Parallel Computing:** OpenMC is optimized to run on large-scale parallel computing platforms, which allows it to simulate vast numbers of neutron histories in a reasonable time frame, significantly increasing the accuracy of its predictions.

In conclusion, OpenMC leverages the Monte Carlo method to simulate nuclear systems in a way that accounts for the inherent randomness of neutron interactions, offering a powerful tool for reactor design and safety analysis. The relationship between the Monte Carlo method and simulations is crucial in OpenMC's ability to handle highly complex nuclear physics problems.

### 1.5.4 Multiplication Factor, Reactivity

The multiplication factor ( $k$ ) measures how effectively a reactor sustains a fission chain reaction. Specifically, it indicates how the neutron population in a reactor changes from one generation to the next during fission processes. Two types of multiplication factors are generally used:  $k_{\infty}$ , which is valid only for infinite systems with no leakage, and  $k_{\text{eff}}$  for practical application that takes leakage of neutrons into account, which have been discussed before in section 1.5.1.

Reactivity ( $\rho$ ) is defined in terms of the multiplication factor  $k$  and describes deviations from the critical state [24]. Reactivity ( $\rho$ ) is a measure of how far a nuclear reactor is from criticality, which is the condition where the reactor is exactly sustaining a steady-state chain reaction ( $k_{\text{eff}}=1$ ).

Reactivity is given by the equation:

$$\rho = \frac{k_{\text{eff}} - 1}{k_{\text{eff}}} \quad (4)$$

Where:

$k_{\text{eff}}$  = the multiplication factor.

$\rho$  = reactivity, typically expressed in units like percent (%) or milli-k (mk).

Interpretation of reactivity ( $\rho$ ):

- $\rho=0$ : The reactor is critical ( $k_{\text{eff}}=1$ ), maintaining a constant power level.
- $\rho>0$ : The reactor is supercritical ( $k_{\text{eff}} > 1$ ), meaning the neutron population and reactor power are increasing.
- $\rho<0$ : The reactor is subcritical ( $k_{\text{eff}} < 1$ ), meaning the neutron population and reactor power are decreasing.

Reactivity is controlled in a reactor using devices such as control rods and moderators, allowing operators to adjust the chain reaction rate.

## 2. Reactor Core Design Description

### 2.1 Benchmark Overview

The Idaho National Laboratory (INL) proposed a special-purpose reactor concept developed by Los Alamos National Laboratory (LANL) in 2018. This design is called the "Special Purpose Reactor" (SPR). It aims to support various non-commercial missions, such as providing power in remote locations where conventional energy infrastructure is not feasible. It focuses on providing a reliable, compact, and transportable power source for off-grid locations, including military bases or space missions.

The LANL reactor design is a small, low-power, micro-reactor that can be easily transported and deployed. It's a compact nuclear reactor using advanced materials and fuels to ensure safety, reliability, and portability. It is modular in nature, meaning that it can be prefabricated and assembled on-site quickly, and it's mobile for transportability to remote locations, making it ideal for military or space missions. The reactor's power capacity is designed to be under 5 MW(e). The SPR uses High-Assay Low-Enriched Uranium (HALEU) as its fuel. HALEU contains a higher concentration of U-235 than traditional commercial reactors (20% U-235), offering greater efficiency and enabling more compact reactor designs. The design incorporates heat-pipe technology for passive heat removal, which enhances safety and reliability by minimizing the need for active cooling systems.

This SPR is designed to operate as a fast reactor, meaning it utilizes fast neutrons rather than thermalized (slower) neutrons. The design concept has a collection of individual fuel elements. It features a central heat pipe surrounded by a  $\text{UO}_2$  fuel pellet, with stainless steel cladding on both the inner and outer sides. The main purpose of the cladding is to contain the fuel and fission gases, not to act as a structural component.

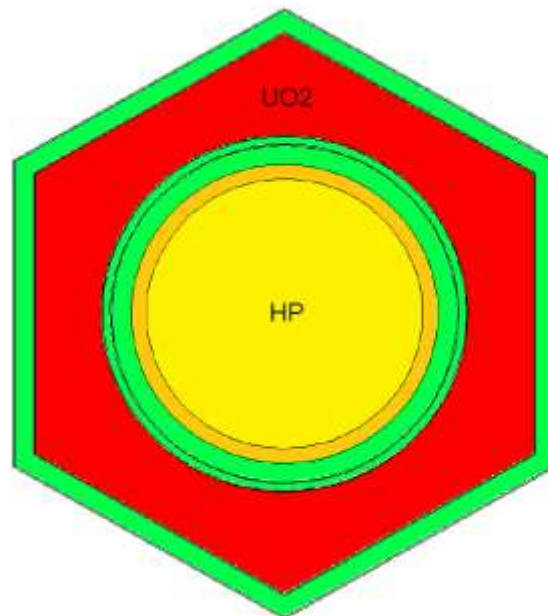


Figure 5: Cross-sectional view of a single fuel element (pitch 2.79cm) [1]

The fuel element's symmetrical design around the heat pipe simplifies stress distribution, leading to lower stress levels. The annular fuel pellet design allows for efficient use of  $\text{UO}_2$  fuel, optimizing the core space for both cladding layers. The outer surface of the fuel is hexagonal, allowing for tight packing of fuel elements in the core, while the low thermal gradients between them help minimize stress.

This design improves fuel loading efficiency and reduces mechanical stress, making it a viable solution for the reactor's operation in challenging environments.

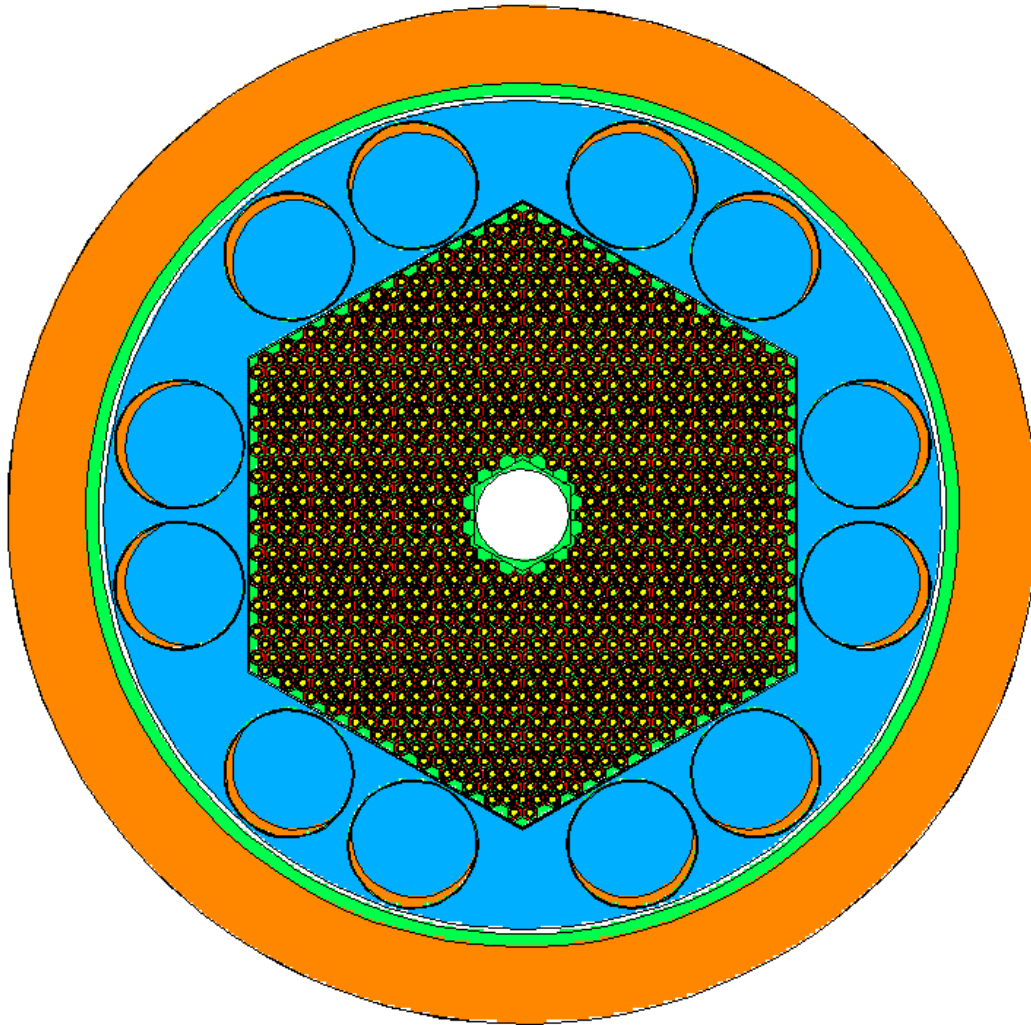


Figure 6: Cross-sectional view of the Design A core layout.[1]

This SPR design features a hexagonal core structure with an inner void for emergency shutdown rods. The core contains 1,134 fuel elements, with the option to add 72 additional fuel elements at the periphery to increase reactivity, if necessary, particularly during initial startup. This flexibility in fuel loading allows for easy adjustments to core reactivity.

Each fuel element consists of a central heat pipe surrounded by a hexagonal  $\text{UO}_2$  fuel pellet clad in stainless steel. The manufacturing process for these fuel elements is streamlined, allowing for individual fabrication and thorough testing of each component. This ensures reliability and quality

control. The ability to add more fuel elements also enhances the reactor's cooling capability, as each fuel element includes a heat pipe, improving the average thermal performance. The heat pipes are assembled and filled with liquid potassium in controlled environments, which increases their reliability and performance.

Overall, Design A emphasizes modularity, enabling efficient manufacturing and straightforward inspection and replacement of defective fuel elements, ultimately improving the reactor's operational reliability and flexibility.

## 2.2 Designed Micro Nuclear Reactor Overview

The core focus of this research is a 5 MWt Micro Nuclear Reactor (MNR), designed to operate for 20 years without refuelling. This reactor functions within the fast and epithermal neutron energy spectrum and utilizes TRISO fuel, known for its excellent resistance to neutron irradiation, corrosion, oxidation, and high temperatures [19].

However, compared to the benchmark unit cell design based on the LANL concept, which uses solid  $\text{UO}_2$  fuel pellets, it was more challenging to achieve criticality with TRISO particles. This difficulty arises from the lower fuel loading in TRISO particles, as only the central kernel contains fissile material, unlike the fully dense  $\text{UO}_2$  fuel pellets.

To overcome this and make the new reactor design critical, several modifications were necessary. These included:

- Increasing the pitch size to reduce neutron leakage,
- Removing the cladding material to increase fuel space, as TRISO particles have built-in containment layers that safely retain fission products, eliminating the need for traditional cladding.
- Changing the matrix material to one with better neutronic properties,
- Increasing the TRISO packing fraction to raise the overall fuel content.

These adjustments were essential to compensate for the lower fissile density in TRISO-based fuel and ensure the reactor achieved and sustained criticality under fast and intermediate-spectrum conditions.

Figure 6 presents the finalized unit cell design of the 5 MWt reactor, which operates in the fast and epithermal energy spectrum. This design reflects all the modifications discussed earlier.

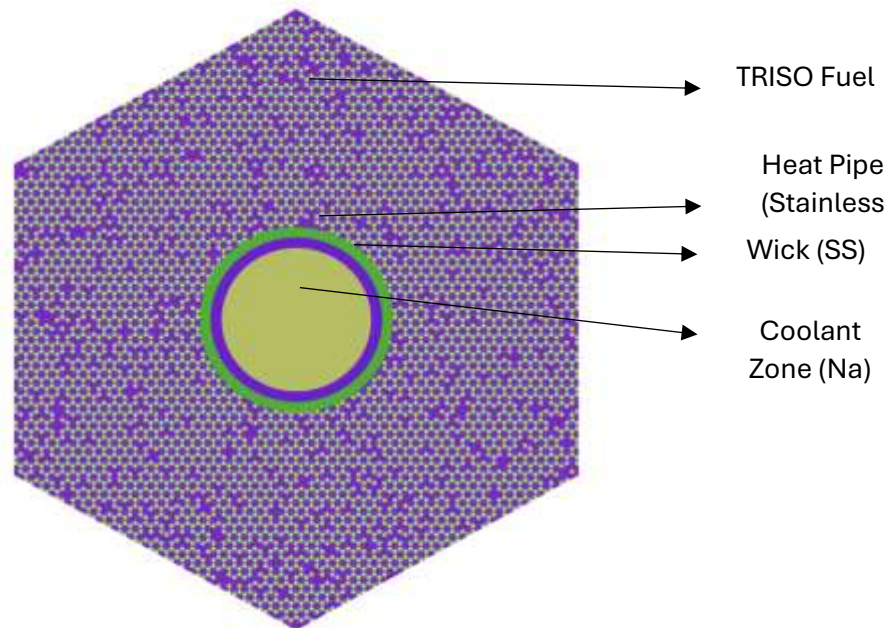


Figure 7: Cross-sectional view of a unit cell of hexagonal fuel matrix (pitch 5.2 cm).

Figure 7 shows materials associated with the fuel element of a unit cell. The heat pipe is characterized by an inner diameter of 1.575 cm and an outer diameter of 1.775 cm, with a wall thickness of 1.0 mm. All materials utilized in constructing this unit cell consist of high-temperature ceramic metals.

The core's defining feature is the heat pipe, with each heat pipe inserted into a hexagonal fuel element. As shown in Figure 7, each unit cell comprises a heat pipe working fluid surrounded by TRISO particles embedded in a beryllium matrix. The active core, illustrated in Figure 8, consists of 462 of these unit cells arranged in a hexagonal shape.

The core is encircled by an aluminum oxide ( $\text{Al}_2\text{O}_3$ ) reflector, which contains 12 rotatable control drums surrounding the core. The control drums can be rotated inward or outward to regulate the core's reactivity. When the control drums are positioned inward, the neutron-absorbing material faces the core, thereby increasing neutron absorption and reducing reactivity. Conversely, when the drums are rotated outward, the absorbing material is turned away from the core, and the reflector material faces the core, enhancing neutron reflection and increasing reactivity. Additionally, there is a control rod with a diameter of 19 cm at the center of the core, which can be inserted or withdrawn as needed to maintain criticality. Each control drum has a diameter of 24 cm and is placed within the reflector material that surrounds the core, with the reflector having a total diameter of 188 cm.

Furthermore, focusing on sustaining fast and intermediate energy nuclear reactions, the design of a complete core without control devices has been formulated and is presented below in Figure 8.

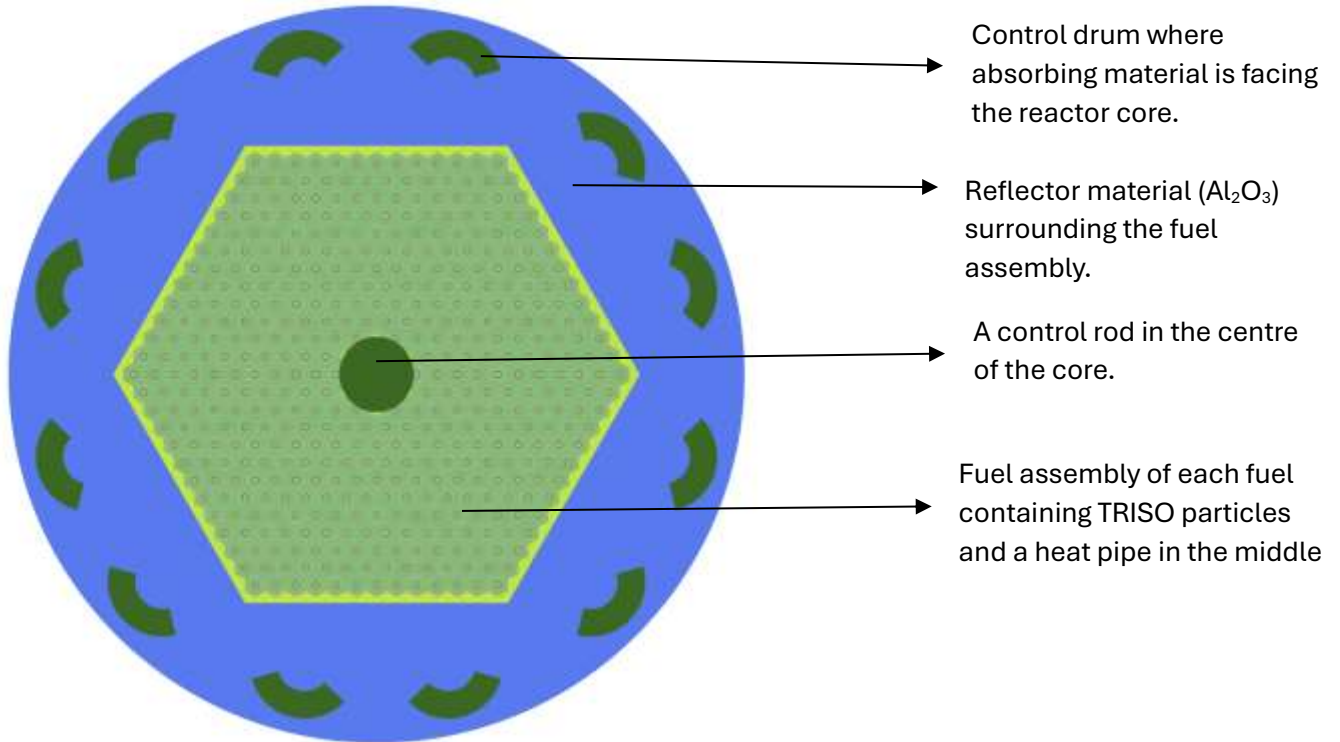


Figure 8: Cross-sectional view of the full core layout with control devices.

This reactor core is more compact in design compared to the INL proposed special purposed reactor because of the difference in their power. There are some similarities and differences between these two reactors. All these similarities and differences can be shown in Table 1-

Table 1: Nominal reactor design for 5MW Micro Nuclear Reactor(MNR) and LANL proposed 5MW SMR design concept

REACTOR	5MW MNR	LANL proposed 5MW SMR
Reactor thermal power	5MW	5MW
Reactor electric power	2MW	2MW
Reactor core orientation	Vertical	Vertical
Cycle Length	20 years	5 years
Coolant system	Heat pipes	Heat pipes
<b>POWER CONVERSION SYSTEM</b>		
Conversion cycle	Open-air Brayton	Open-air Brayton
Primary heat exchanger	Air convection over HPs	Air convection over HPs
Maximum air temperature	675°C	675°C
Cycle efficiency	40.3%	40.3%
<b>FUEL</b>		
Fuel form	UO <sub>2</sub> TRISO fuel	UO <sub>2</sub>
Theoretical density (TD)	10.96 g/cm <sup>3</sup>	10.96 g/cm <sup>3</sup>
Percent of TD	96.0%	96.0%
Density	11	10.52 g/cm <sup>3</sup>

U-235 enrichment	20 wt%	19.75 wt%
Fuel Pellet form	TRISO fuel embedded in beryllium matrix	Solid pellet
Fuel element geometry	Hexagonal fuel element with central heat pipe hole	Hexagonal with a central hole
<b>HEAT PIPES</b>		
Number of HPs in-core	462	1,134
Average HP power	10.822kW	4.41 kW
Pipe wall material	SS316	SS316
Pipe inner diameter	1.575 cm	1.575 cm
Pipe outer diameter	1.757 cm	1.757 cm
Pipe wall thickness	1.0 mm	1.0 mm
HP-to-HP pitch	5.17 cm	2.78 cm
Working fluid	Sodium (vapour/liquid)	Potassium (vapour/liquid)
HP length (evaporator)	1.5 m	1.5 m
HP length (adiabatic)	0.4 m	0.4 m
HP length (condenser)	2.1 m	2.1 m
HP total length	4 m	4 m
<b>FUEL ELEMENTS</b>		
No. of fuel elements in-core	462	1134
Element geometry	Hexagonal	Hexagonal
Geometry	Central heat pipe surrounded TRISO particle embedded in beryllium matrix	Central heat pipe surrounded by clad UO <sub>2</sub> fuel
Thermal bonding media	Helium/liquid metal	Helium/liquid metal
Helium gas pressure (fuel)	45 psi	45 psi
Fuel length	150.0 cm	150.0 cm
Clad inner diameter	No cladding	0.8939 cm (inner clad) 1.2867 cm (outer clad)
Clad outer diameter	No cladding	0.9339 cm (inner clad) 1.3867 cm (outer clad)
Clad thickness or minimum web thickness	No cladding	0.4 mm (inner) 1.0 mm (outer)
Cladding geometry	No cladding	Cylindrical tube (inner) Hexagonal tube (outer)
Fuel matrix material	Beryllium	No matrix
Matrix density	1.85 g/cm <sup>3</sup>	No matrix
Fuel pin or element pitch	5.17 cm	2.78 cm
<b>CORE</b>		
Type	Hexagonal fuel elements	Hexagonal fuel elements
Geometry	Hexagonal	Hexagonal
Core diameter	116.4 cm flat-to-flat	101.2 cm flat-to-flat
Active height	150.0 cm	150.0 cm
BOL core k-effective	1.063	1.028

<b>NEUTRON REFLECTORS</b>		
Reflector material	Alumina ( $\text{Al}_2\text{O}_3$ )	Alumina ( $\text{Al}_2\text{O}_3$ )
Side reflector thickness		19.4–27.3 cm
Reflector density	10 $\text{g}/\text{cm}^3$	3.9 $\text{g}/\text{cm}^3$
<b>CONTROL DRUMS</b>		
Control material	Hafnium hydride ( $\text{HfH}_2$ )	Boron carbide ( $\text{B}_4\text{C}$ )
Control material density	11.4 $\text{g}/\text{cm}^3$	2.51 $\text{g}/\text{cm}^3$
Number of control drums	12	12
Control drum outer diameter	28 cm (7 cm thickness)	25 cm
Single control drum worth	\$1.25	\$1.15
Total control drums worth	\$15	\$13.83
<b>EMERGENCY CONTROL RODS</b>		
Number of emergency control rods	1	2
Location in-core	Inside the core central hexagon volume	Inside the core central hexagon volume
Geometry	1 solid rod	1 solid rod 1 annular tube
Control material	Hafnium hydride ( $\text{HfH}_2$ )	Boron carbide ( $\text{B}_4\text{C}$ )
Control material density	11.4 $\text{g}/\text{cm}^3$	2.51 $\text{g}/\text{cm}^3$
Length	200 cm	200 cm

## 3. Simulation Methodology

This chapter presents the simulation methodologies employed in the design and analysis of the fast and intermediate energy spectra Micro Nuclear Reactor (MNR), focusing on the use of the OpenMC Monte Carlo code for neutron transport and depletion calculations. The primary areas of emphasis include neutron transport modelling, normalization techniques, burnup calculations, and advanced matrix exponential methods for depletion integration.

### 3.1 OpenMC

OpenMC is an open-source Monte Carlo code for neutron and photon transport simulations [1]. It is widely used for modelling nuclear reactor behaviour due to its high fidelity, support for complex geometries, and advanced features for depletion and burnup analysis. OpenMC employs stochastic methods to solve the neutron transport equation, making it suitable for complex nuclear systems.

OpenMC models the neutron transport process by tracking individual neutrons as they undergo interactions, including scattering, absorption, and fission, within the reactor core. These interactions are governed by probability distributions derived from nuclear data libraries, such as ENDF/B-VII.1 [26]. The neutron transport equation is the foundation of these simulations and OpenMC uses the neutron transport equation to calculate the neutron flux, which is essential for determining reaction rates, power distribution, and fuel depletion.

Key features of OpenMC include:

- **Flexibility in Geometry:** OpenMC supports various geometric configurations, allowing detailed modelling of reactor cores, including hexagonal and Cartesian lattices.
- **High-Accuracy Neutron Physics:** OpenMC uses continuous-energy cross-section data to model neutron interactions with high precision.
- **Depletion Analysis:** Through its `openmc.deplete` Python module, OpenMC enables time-dependent simulations of nuclide concentrations and burnup.

In this research, OpenMC is utilized for:

1. **Neutron Transport Simulations:** Modeling neutron flux, reaction rates, and power distribution within the reactor core.
2. **Depletion Calculations:** Estimating changes in fuel composition over time due to nuclear reactions and decay.

In this research, the OpenMC Python API was utilized to develop a 2D reactor model. The simulation was performed using 100 batches, with the first 20 batches discarded for convergence, and 100,000 particles per batch to ensure good statistical accuracy. Upon completion of the simulation, OpenMC generated a statepoint file in HDF5 data format containing all the simulation results. To efficiently extract and analyze these results, the built-in post-processing functions of the OpenMC Python API were employed.

## 3.2 Normalizing

Normalization in reactor physics ensures that the calculated neutron flux corresponds to the actual reactor power. This involves scaling the simulated reaction rates to match a specified thermal power level. The normalization process can be described mathematically as:

$$\text{Normalizing Factor} = \frac{P \times v}{E_f \times k_{\text{eff}} \times V} \quad (7)$$

Where,

P = Power in MW

v = Number of neutrons released per fission

$E_f$  = Energy released per fission in MeV (approximately 200 MeV)

$k_{\text{eff}}$  = Effective multiplication factor

V = Volume of the reactor

For the MNR design, normalization is performed to ensure the neutron flux corresponds to a thermal power output of 5 MW. This step is crucial for accurate predictions of burnup rates and material behaviour.

In OpenMC, normalization is achieved by scaling the reaction rates to match a specified reactor power level. The steps include:

1. **Calculation of Reaction Rates:** OpenMC computes reaction rates such as fission, absorption, and scattering based on neutron flux.
2. **Power Specification:** The user specifies the total reactor power or power density.
3. **Scaling Factor:** A scaling factor is derived to relate the simulated reaction rates to the actual reactor power, ensuring accurate representation of the physical system.

For the Micro Nuclear Reactor, normalization ensures that the calculated neutron flux and burnup rates correspond to a thermal power output of 5 MWt.

### 3.3 Burnup Algorithms

OpenMC uses advanced numerical methods to simulate fuel depletion, capturing the transmutation of nuclides and the generation of fission products. When materials are exposed to prolonged irradiation, their nuclides undergo transmutation due to nuclear reactions and radioactive decay. This time-dependent process, called depletion or burnup, alters the material composition, impacting transport equation solutions. Predicting these changes is crucial for accurate nuclear system analysis. The governing equation for nuclide transmutation and decay in an irradiated environment is given by:

$$\frac{dN_i(t)}{dt} = \underbrace{\sum_j [f_{j \rightarrow i} \int_0^\infty dE \sigma_j(E, t) \phi(E, t) + \lambda_{j \rightarrow i}] N_j(t)}_{\text{Production of nuclide i from nuclide j}} - \underbrace{\left[ \int_0^\infty dE \sigma_i(E, t) \phi(E, t) + \sum_j \lambda_{i \rightarrow j} \right] N_i(t)}_{\text{Loss of nuclide i}} \quad (5)$$

transmutation
decay
transmutation
decay

Where:

$N_i$  = Density of nuclide i at time t,

$\sigma_i$  = Transmutation cross section for nuclide i at energy E,

$f_{j \rightarrow i}$  = Fraction of transmutation reactions in nuclide j that produce nuclide i [26].

The equation essentially expresses that the rate of change of  $N_i$  is determined by the difference between its production and loss rates. Since the equation governing nuclide i is influenced by the densities of potentially numerous other nuclides, it forms a system of first-order differential equations.

OpenMC's depletion module calculates the evolution of nuclide concentrations in the reactor fuel over time using burnup algorithms [26].

The burnup calculation process includes:

1. **Input preparation:** Users define the reactor geometry, materials, neutron flux, and depletion chain file.
2. **Reaction rate calculation:** OpenMC computes reaction rates for all relevant nuclides in the depletion chain.
3. **Integration over time:** Numerical methods are applied to solve the Bateman equations and update nuclide concentrations for each time step.

### 3.3.1. Matrix Exponential Methods

Matrix exponential methods are advanced numerical techniques used to solve the Bateman equations efficiently and accurately. OpenMC supports several integration methods, including Predictor, CELT, CECM, and SCLI.

#### 1. Predictor

The predictor method uses reaction rates at the beginning of the time step to estimate nuclide concentrations at the end by assuming constant reaction rates and decay over the time step. It is expressed as:

$$n_{i+1} = \exp(hA(n_i))n_i \quad (6)$$

Where,

$n_i$  = Nuclide concentration vector at time step  $i$

$A(n_i)$  = Burnup matrix at  $n_{i-1}$ , containing decay constants and reaction rates

$h$  = Time step size

In this research, time steps were strategically selected to obtain burnup results at various stages of the reactor unit cell's operation. Initially, very small time steps were used to allow the buildup of xenon and ensure that an equilibrium xenon concentration was achieved. Subsequently, the time step size was gradually increased, starting from 0.25 days to 2 days, and then extended to 10, 25, 75, 170, 350, 700, 1200, 2000, 3200, 5200, and 7300 days to capture the burnup behaviour over a 20-year period. These values represent the time steps ( $h$ ) used to generate the burnup results throughout the reactor's lifetime.

#### 2. Constant Extrapolation and Linear Interpolation (CELI)

CELI improves on the predictor method by using constant extrapolation of reaction rates over the time step and applying a linear termination condition. This method, the Predictor method by blending reaction rates from the current and predicted time steps using linear interpolation. CELI stands for constant extrapolation on the predictor and linear interpolation on the corrector. The CELI method is for solving the burnup equations, which describe how nuclide concentrations change over time due to nuclear reactions and radioactive decay.

This algorithm is mathematically defined as:

1. Predictor step:

$$n_{i+1}^p = \exp(hA(n_i))n_i$$

- This step estimates the nuclide concentration  $n_{i+1}^p$  at the next time step using an exponential function of the burnup matrix  $A(n_i)$ . The matrix exponential  $\exp(hA)$  governs the evolution of nuclide densities over time.
- The burnup matrix  $A(n_i)$  contains reaction rates (such as fission, capture, transmutation) and decay constants.

- The time step size is represented by  $h$ . It determines how far forward in time the nuclide concentrations are projected in each step. Larger  $h$  values mean longer time steps, which improve computational efficiency but may reduce accuracy. Smaller  $h$  values lead to better accuracy but increase computational costs.

## 2. Corrector Step:

$$n_{i+1} = \exp\left(\frac{h}{12}A(n_i) + \frac{5h}{12}A(n_{i+1}^p)\right) \exp\left(\frac{5h}{12}A(n_i) + \frac{h}{12}A(n_{i+1}^p)\right) n_i \quad (7)$$

- The corrector step refines the nuclide concentration by using a combination of reaction rates from the previous  $A(n_i)$  and predicted  $A(n_{i+1}^p)$  time steps.
- Instead of assuming the reaction rates remain constant over the entire step (as in simpler methods like the predictor method), it uses a weighted combination of reaction rates:
  - $\frac{h}{12}A(n_i) + \frac{5h}{12}A(n_{i+1}^p)$  in the first exponential term.
  - $\frac{5h}{12}A(n_i) + \frac{h}{12}A(n_{i+1}^p)$  in the second exponential term.
- These terms represent a **linear interpolation** of the reaction rates between the previous and predicted values, which improves accuracy.

**Advantages:** Better accuracy than the predictor method for moderate time steps. Suitable for systems with moderate variations in reaction rates.

## 3. Constant Extrapolation and Constant Midpoint (CECM)

CECM evaluates reaction rates at the midpoint of the time step, providing a more accurate solution for systems with moderate changes in reaction rates. CECM employs constant extrapolation and evaluates reaction rates at the midpoint of the time step. This algorithm is mathematically defined as:

$$n_{i+1/2} = \exp\left(\frac{h}{2}A(n_i)\right) n_i \quad (8)$$

$$n_{i+1} = \exp(hA(n_{i+1/2}))n_i \quad (9)$$

**Advantages:** Provides a balance between computational efficiency and accuracy. Commonly used for steady-state and low-transient systems.

## 4. Stochastic Collocation Integration (SCLI)

SCLI incorporates stochastic sampling techniques to account for uncertainties in reaction rates [28]. It is particularly useful for systems with significant statistical variations or non-linear behaviour. SCLI uses stochastic techniques to handle uncertainties in reaction rates and flux distributions.

**Advantages:** High accuracy for systems with statistical variations or uncertain parameters. Ideal for advanced reactor systems with complex geometries or non-linear behaviours.

### 3.4 Implementation in OpenMC

The implementation of depletion calculations in OpenMC involves the following steps:

1. **Input Preparation:** Reactor geometry, materials, and initial nuclide concentrations are defined.
2. **Depletion Chain File:** A depletion chain file specifies transmutation pathways and decay constants. OpenMC uses chain files based on ENDF/B-VII.1 data [29].
3. **Neutron Transport:** OpenMC calculates reaction rates for all nuclides in the depletion chain.
4. **Matrix Solver:** The selected integration method (e.g., Predictor, CELT, CECM, SCLI) is applied to solve the Bateman equations [30].
5. **Post-Processing:** Results, including neutron flux, power distribution, and nuclide concentrations, are analyzed to assess reactor performance [27].

## 4. Result

### 4.1 Unit cell

The initial design of the Micro Nuclear Reactor (MNR) unit cell drew significant inspiration from the Los Alamos National Laboratory's (LANL) concept, characterized by a hexagonal geometry with a centrally positioned heat pipe and a uranium dioxide ( $\text{UO}_2$ ) fuel section. This design provided a baseline for developing a novel configuration tailored to the unique operational requirements of the MMR.

To align with the objectives of this study, the MMR unit cell maintained the hexagonal geometry of the LANL concept but incorporated advanced tristructural isotropic (TRISO) fuel instead of traditional  $\text{UO}_2$  pellets. TRISO fuel, known for its superior safety characteristics and high-temperature resilience, was initially packed with a 60% packing fraction within the fuel element. Despite this high packing density, the effective fuel mass within the unit cell was notably lower than that of the original  $\text{UO}_2$  design due to the inherently lower density of TRISO fuel particles. This presented a challenge in achieving the desired neutron economy and reactivity levels.

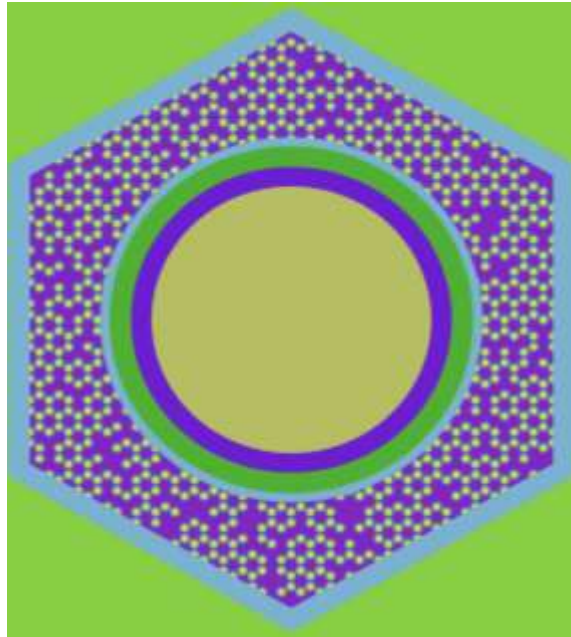


Figure 9: Unit cell (edge length – 1.6086 cm, pitch- 2.7862cm)

The pipe structure consisted of a stainless steel wick encased within a stainless steel cladding, ensuring durability and compatibility with the high-temperature environment of the reactor core. However, initial neutronic simulations revealed a significant limitation in this design. The calculated  $k_{\text{eff}}$ , or the effective neutron multiplication factor, was only 0.65. This value indicated that the reactor could not achieve criticality, rendering the design impractical for sustained nuclear fission. The presence of the stainless steel cladding around the TRISO fuel contributed to substantial neutron absorption, effectively reducing the availability of neutrons for sustaining the fission chain reaction. The results presented in the following sections detail the iterative

modifications and analyses undertaken to address this challenge, ultimately leading to a design capable of achieving criticality and fulfilling the intended operational objectives of the MMR.

Stainless steel, while durable, has a high neutron absorption cross-section, reducing the number of neutrons available for sustaining the fission chain reaction. This contributed to the initially low  $k_{\text{eff}}$  value of 0.65. Further investigation revealed that the cladding was unnecessary in this design. TRISO fuel is inherently capable of containing fission gases and solid fission products due to its multi-layered structure, including silicon carbide (SiC) and pyrolytic carbon (PyC) coatings. These layers provide sufficient containment without the need for additional cladding.

To address the issue, the stainless steel cladding was removed from the design to achieve a higher  $k$  eigen value, and Figure 10 shows the unit cell as a result without a cladding of stainless steel material. This design change resulted in a significant improvement in the reactor's neutron economy, as fewer neutrons were absorbed by the cladding in Figure 9. Consequently, the  $k_{\text{eff}}$  increased substantially, enabling the reactor to approach criticality.

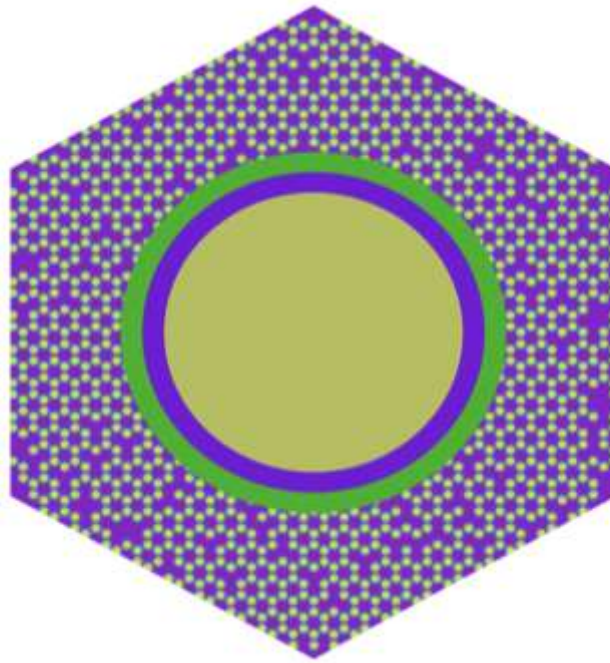


Figure 10: Unit cell of hexagonal fuel matrix with TRISO particle (edge-1.6086 cm, pitch-2.7862cm) without cladding material.

The enhanced design not only achieves criticality but also maintains the safety and robustness associated with TRISO fuel. The following sections detail the performance improvements resulting from this key modification. Following the removal of the stainless steel cladding from the TRISO fuel element, the  $k_{\text{eff}}$  value increased from 0.65 to 0.85. Substituting the values, the reactivity for  $k_{\text{eff}}=0.85$  is determined to be:

$$\rho = \frac{0.85 - 1}{0.85} \approx -0.176 \text{ or } -176 \text{mk}$$

The reactor remains subcritical. Additional modifications are therefore required to achieve a critical state ( $k_{\text{eff}}=1.0$ ).

The next step was to increase the unit cell size or pitch, allowing for a greater number of TRISO fuel particles to be incorporated into the fuel element. This adjustment is expected to enhance the neutron flux within the core and bring the reactor closer to achieving criticality.

#### 4.1.1 Matrix Analysis

The study so far has utilized stainless steel as the matrix material for TRISO particles, but due to the high neutron absorption cross-section of stainless steel in the fast and intermediate energy spectrum, alternative matrix materials were explored. The objective was to identify a material that minimizes neutron interaction, thereby enhancing the reactor's performance and facilitating criticality. For this purpose, several candidate materials, including helium, graphite, lead, and beryllium, were analyzed using the same unit cell pitch of 2.8 cm. The results are summarized in Table 2.

Table 2:  $k_{\text{eff}}$  values of the unit cell with a 2.8 cm pitch for the different matrix materials.

Matrix	$k_{\text{eff}}$
Ag-In-Cd	0.194
Stainless Steel	0.858
Zircaloy	0.902
HT9 alloy	0.908
He	1.039
Graphite	1.001
Lead	1.014
Beryllium (Be)	1.032

From the analysis of Table 2 results, helium, graphite, lead, and beryllium emerge as potential candidates for the matrix material. Helium, despite its favourable neutronic properties, is a gas and therefore unsuitable for physically containing TRISO particles in a matrix. Graphite, a widely used matrix material, demonstrates promising neutronic performance. However, Fast reactors need materials with low neutron absorption and low moderation. Graphite doesn't absorb many neutrons (which is good), but its moderation effect is the issue in this case. Even small amounts of graphite significantly alter the neutron energy spectrum, reducing fission probabilities of fast-spectrum-favouring isotopes

Lead, as a solid material, demonstrates promising potential but poses practical challenges in reliably containing TRISO particles due to its physical properties, like low melting point ( $\sim 327^\circ\text{C}$ ). A fast reactor typically operates at a higher temperature (more than  $500^\circ\text{C}$ ). So solid lead wouldn't remain solid, and liquid lead can't structurally contain TRISO particles in a matrix and manufacturing constraints. In contrast, beryllium stands out as a superior matrix material due to its low neutron absorption and minimal moderating effects, making it well-suited for maintaining a fast and intermediate neutron spectrum while effectively supporting the TRISO fuel structure.

The key advantage of beryllium lies in its neutron multiplication capability rather than neutron absorption. Beryllium has a high probability of undergoing the (n,2n) reaction, where an incoming neutron interacts with a beryllium nucleus, resulting in the emission of two neutrons instead of a single absorption event. This property is particularly beneficial in fast reactors, where maintaining a high neutron flux is crucial for sustaining fast and intermediate-spectrum fission reactions.

Based on this analysis, beryllium is identified as the most viable matrix material for the reactor design, given its compatibility with fast and intermediate spectrum operation and its ability to enhance neutron economy without significant interaction with neutrons. Further design and simulation studies using beryllium are expected to improve the reactor’s performance and facilitate its progression toward criticality.

#### 4.1.2 Optimization of Fuel Lattice Pitch

Beryllium has emerged as the optimal matrix material for this reactor design due to its excellent neutron multiplication properties. To ensure the criticality of the reactor, the unit cell must attain supercriticality. And to ensure the unit cell achieves excess reactivity, various pitch sizes were analyzed to evaluate their impact on the effective neutron multiplication factor ( $k_{\text{eff}}$ ). A series of simulations were conducted for pitch sizes ranging from smaller, more compact configurations to larger, less dense arrangements. The analyses were performed for two levels of fuel enrichment—15% and 20%—to assess the influence of enrichment on reactor performance.

The results of these studies are presented in the tables below, showing the  $k_{\text{eff}}$  values for each combination of pitch size and fuel enrichment. These results provide valuable insights into the relationship between pitch size, enrichment, and reactivity, guiding the selection of the optimal configuration for the reactor core.

Table 3:  $k_{\text{eff}}$  values of the unit cell for various pitch sizes with 15% fuel enrichment.

Edge length (cm)	Pitch (cm)	$k_{\text{eff}}$
1.61	2.79	1.032
1.66	2.88	1.042
1.76	3.05	1.069
1.86	3.20	1.083
1.96	3.39	1.101
2.19	3.79	1.119
2.97	5.17	1.165

Table 4:  $k_{\text{eff}}$  values of the unit cell for various pitch sizes with 20% fuel enrichment.

Edge length (cm)	Pitch (cm)	$k_{\text{eff}}$
1.61	2.79	1.032
2.19	3.79	1.106
2.986	5.17	1.154

The results indicate that increasing the pitch size allows for a higher number of TRISO particles to be accommodated within the unit cell, thereby improving the neutron economy and  $k_{\text{eff}}$ . The reactor demonstrates a more pronounced increase in reactivity at higher enrichments, highlighting the combined effect of fuel density and enrichment level on achieving criticality.

#### 4.1.3 Flux Distribution Analysis

Based on the outcomes of the simulation studies, the pitch size for the unit cell has been designated as 5.2 cm. This pitch size represents an optimal balance between maximizing the packing fraction of TRISO particles and maintaining adequate space for efficient neutron flux distribution within the reactor core. The increased pitch allows for improved reactivity while ensuring structural and thermal considerations are met.

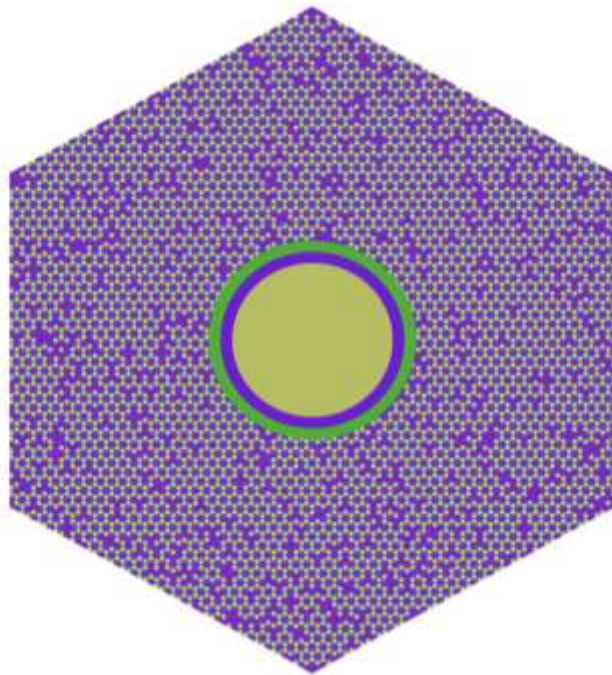


Figure 11: Final unit cell with beryllium matrix (pitch=5.17cm)

To further evaluate the performance of the selected configuration, an analysis of the neutron flux distribution and normalized flux distribution within the unit cell was conducted. Neutron flux distribution provides insights into the spatial variation of neutron intensity within the core, directly influencing fission rates, power generation, and fuel burnup. The normalized flux distribution is particularly significant as it allows for a relative comparison of flux values across different regions of the core, ensuring uniformity in power output and minimizing localized hot spots that could affect reactor safety and efficiency.

The simulation study focused on capturing the behaviour of neutrons within the selected unit cell geometry under steady-state conditions. The results of the flux distribution analysis serve as a validation tool to confirm that the reactor design facilitates uniform neutron flux, effectively utilizes the fuel, and minimizes areas of neutron leakage or underutilization. By combining the

insights from the  $k_{\text{eff}}$  evaluation and the flux distribution analysis, the chosen pitch size of 5.2 cm has been demonstrated to meet the design objectives. To verify that the designed unit cell predominantly operates within the fast and epithermal energy region, the in-core neutron spectra have been plotted in terms of lethargy flux, as illustrated in Figure 12. This representation provides a comprehensive depiction of neutron energy-dependent behaviour within the reactor core [22]. Figure 12, the lethargy flux spectra, which offer a relative indication of neutron intensity across various energy ranges, independent of absolute flux magnitudes [27].

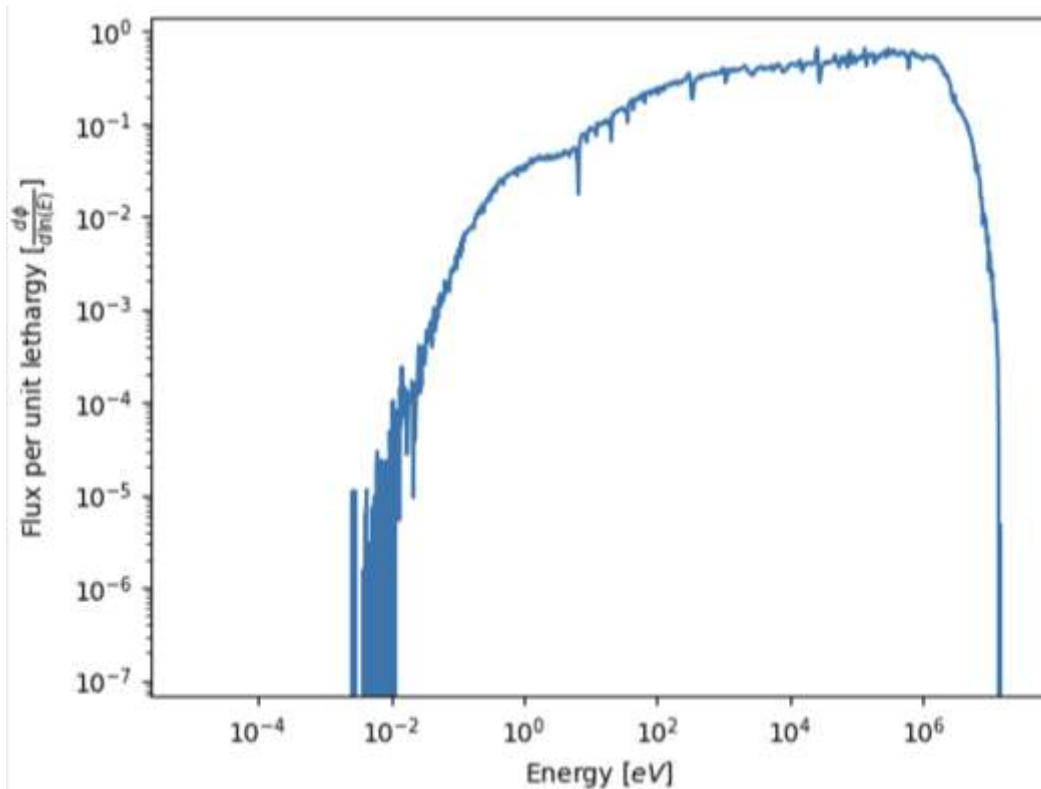


Figure 12: Neutron spectra (lethargy flux)

The lethargy flux spectra indicate a concentration of neutron interactions at higher energy levels and the normalized distribution also confirms the dominance of fast neutrons throughout the reactor core [31] [32]. This behaviour underscores that the reactor operates effectively within a fast and epithermal energy spectrum, aligning with the design objectives for fast and epithermal micro nuclear reactors, ensuring efficient fuel utilization [33].

A comparative neutron flux spectrum as a function of neutron energy (eV) can be studied and for that, in core neutron spectra of three distinct reactor types: Pressurized Water Reactor (PWR), Sodium-cooled Fast Reactor (SFR), and Micro Nuclear Reactor (MNR) are shown in Figure 13. Here, the PWR pin cell problem is based on Beaver's benchmark, representing a 4-loop light water-cooled PWR reactor [34]. The SFR case corresponds to the OECD/NEA benchmark for a sodium-cooled fast reactor (SFR) with a 3600 MWt oxide-fueled core [35].

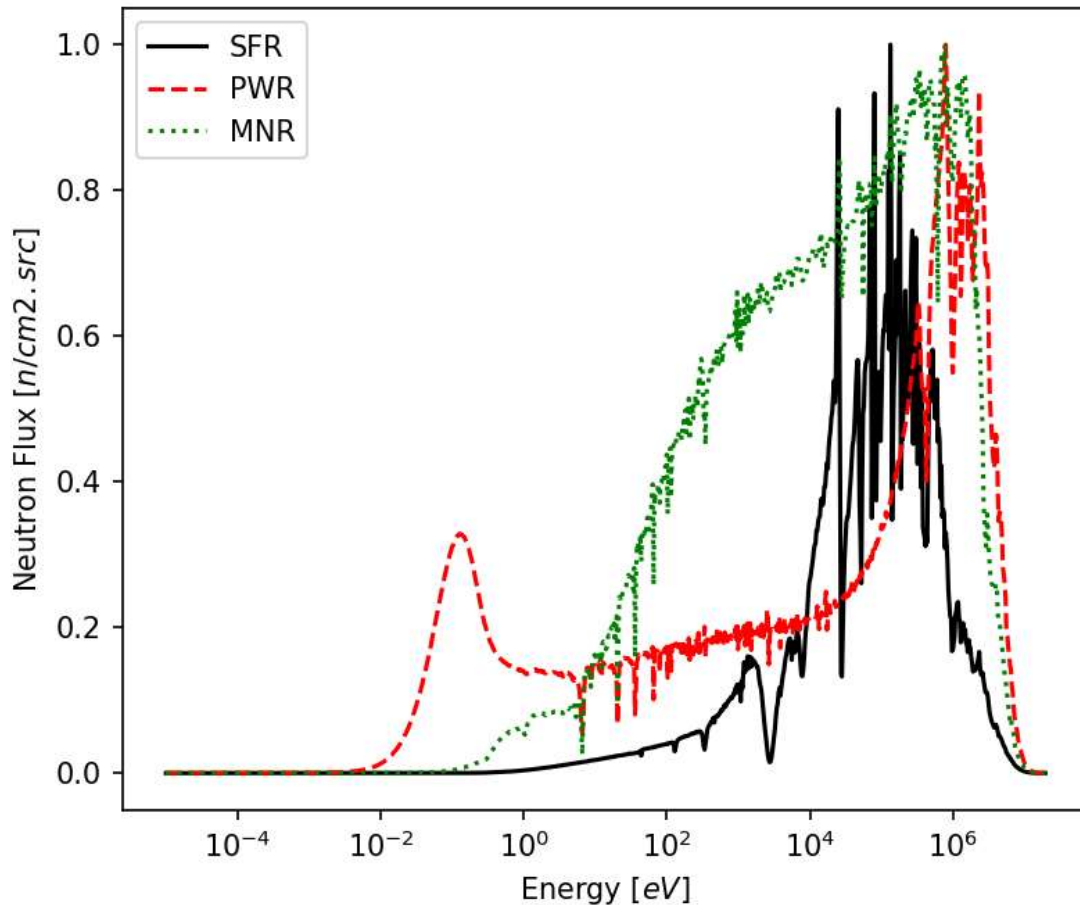


Figure 13: Neutron spectra comparison for three different reactor designs (PWR, SFR and MNR)

In Figure 13, The PWR spectrum (red dashed line) is distinctly thermal, exhibiting a prominent peak in the thermal neutron energy region ( $\sim 0.025$  eV), followed by a significant moderation tail extending into the epithermal region (up to  $\sim 1$  eV). This reflects the high neutron moderation characteristic of water-moderated reactors. The SFR spectrum (solid black line) is predominantly fast, showing negligible neutron flux in the thermal region, a sharply rising flux from approximately  $10^3$  eV (1 keV), and peaking significantly in the fast neutron energy region (from  $\sim 10^4$  to  $10^6$  eV). This distribution aligns with the minimal moderation provided by sodium coolant, supporting fast neutron interactions crucial for breeding and high neutron economy.

The MNR spectrum (green dotted line) demonstrates clear fast and intermediate reactor behavior, closely resembling the SFR spectrum but with broader neutron distribution extending slightly into lower (epithermal) energies (down to  $\sim 1$  eV). However, the primary neutron flux occurs in the fast and intermediate energy region, peaking around  $10^5$  to  $10^6$  eV. The presence of this extended spectrum toward epithermal regions suggests the moderation effects associated with structural materials, specially the carbon layer (buffer, silicon carbide layers) in the TRISO fuel.

To further illustrate this, the neutron spectrum from the unit cell has been plotted, where the flux energy distribution has been calculated at three key reactor stages: Beginning of Life (BOL), Middle of Life (MOL), and End of Life (EOL). The resulting plot is presented in Figure 14.

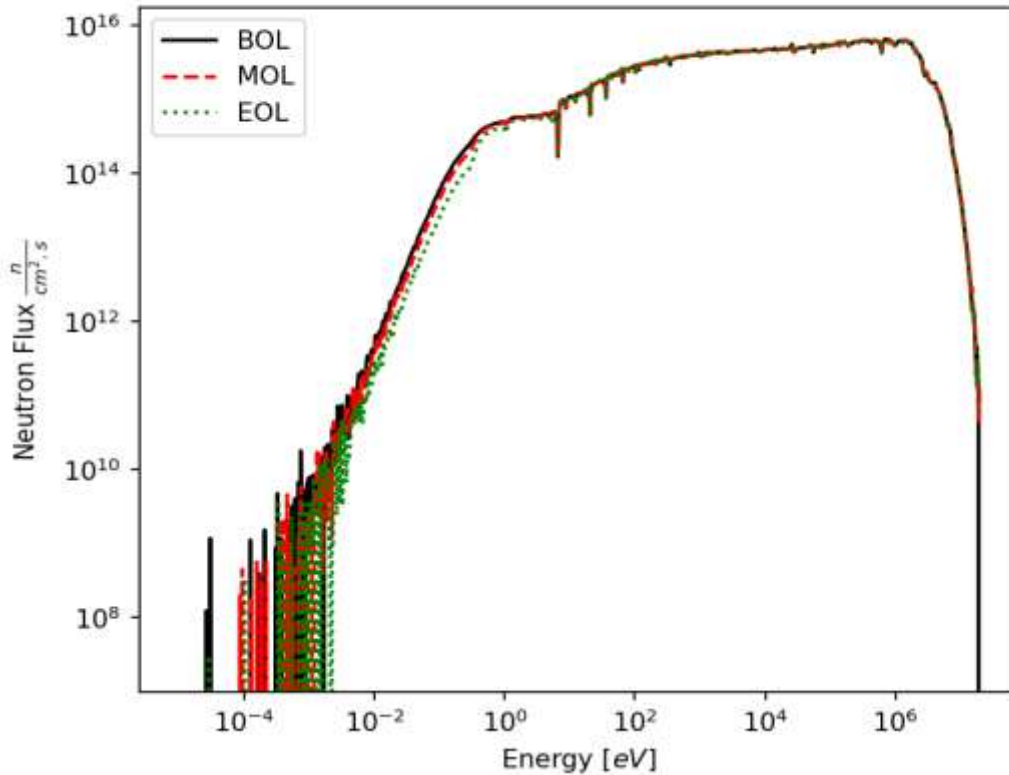


Figure 14: Flux energy distribution at BOL, MOL and EOL.

These findings provide evidence that the reactor's design supports the intended fast and epithermal spectrum operation throughout the lifespan of the reactor, a crucial aspect for achieving the desired performance and efficiency goals [31]. The data also validate the neutronic properties of the chosen materials and geometry, reinforcing the feasibility of the proposed reactor configuration [30].

After confirming that the reactor operates within a fast and intermediate energy spectrum, a 1D radial flux plot has been generated to visualize the radial flux distribution within the unit cell. Figure 16 presents the radial neutron flux distribution as a function of length (cm), with flux values expressed in  $n/cm^2 \cdot s$ . The central region exhibits a relatively uniform flux profile, indicating efficient neutron utilization for sustaining fission reactions. The flux values were initially obtained in  $n/cm^2 \cdot src$  and later converted to  $n/cm^2 \cdot s$  by multiplying by the total neutron source strength factor (S). This representation allows for direct comparison with experimental and theoretical reactor models. The equation for the multiplication factor S is given below-

$$S = \frac{P \times v}{E_f \times k_{eff} \times v}$$

Where, P = Power of the reactor = 5 MW

$v$  = Average number of neutrons released per fission = 2.43

$E_f$  = Energy released per fission = 200 MeV =  $200 \times 1.6 \times 10^{-13}$  J

$k_{\text{eff}}$  = Eigenvalue of unit cell

$v$  = Volume of mesh cell where flux is calculated in  $\text{cm}^3$

For the visualization of this 1D radial flux distribution, a  $50 \times 50$  mesh was constructed along both the x and y axes within a unit cell. The 1D flux profile was extracted along the x-axis at  $y=25$  to examine the radial flux behaviour within the unit cell. Additionally, to convert the flux unit from  $\text{n}/\text{cm} \cdot \text{src}$  to  $\text{n}/\text{cm}^2 \cdot \text{s}$ , a scaling factor of  $8.487 \times 10^{18}$  was applied to the flux values. This conversion ensures that the results are expressed in absolute physical units, allowing for direct comparison with experimental and theoretical reactor models. Both the 2D flux distribution and the 1D radial flux profile in the fast and intermediate energy spectra are illustrated in Figure 15 and Figure 16, respectively.

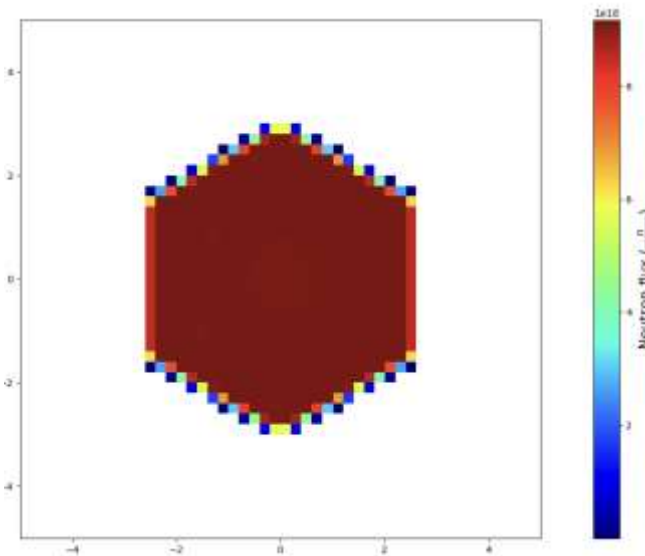


Figure 15: 2D flux distribution (fast and intermediate)

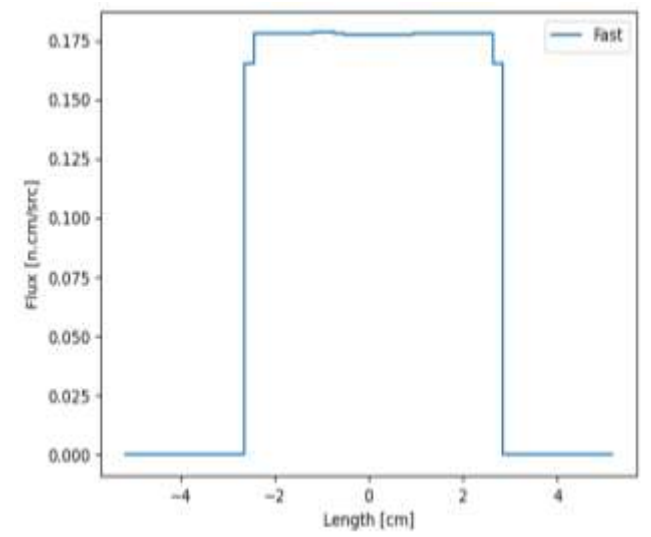


Figure 16: 1D radial flux profile (fast and intermediate) for a unit cell.

The 2D neutron flux distribution analysis shows uniform fast flux behaviour across the unit cell. The one-dimensional radial neutron flux distribution, plotted along the centerline of the unit cell and shown in Figure 16, exhibits a consistent fast flux profile, with peak values reaching approximately  $1.4 \times 10^{18} \text{ n}/\text{cm}^2 \cdot \text{src}$ . A noticeable corner dip is observed in the figure, which results from the use of a regular mesh in a hexagonal unit cell. In the hexagonal geometry, the corner mesh elements often do not intersect with any material due to the edge shape, leaving many corner meshes effectively empty. As a result, these regions lack neutron-producing material, leading to an absence of neutron flux and creating the observed corner dip in the flux distribution.

Although a sodium-cooled heat pipe is located at the center of the hexagonal unit cell, a study was conducted to determine whether any neutron capture effects are observable in the neutron flux distribution. As shown in Figure 16, there is no noticeable decrease in neutron flux at the center of the fast flux profile, indicating minimal neutron absorption by the heat pipe. To further investigate the neutron flux behaviour in the epithermal and thermal energy regions, Figure 17 has been plotted, where the epithermal flux distribution is presented on the left side and the thermal flux distribution is shown on the right side.

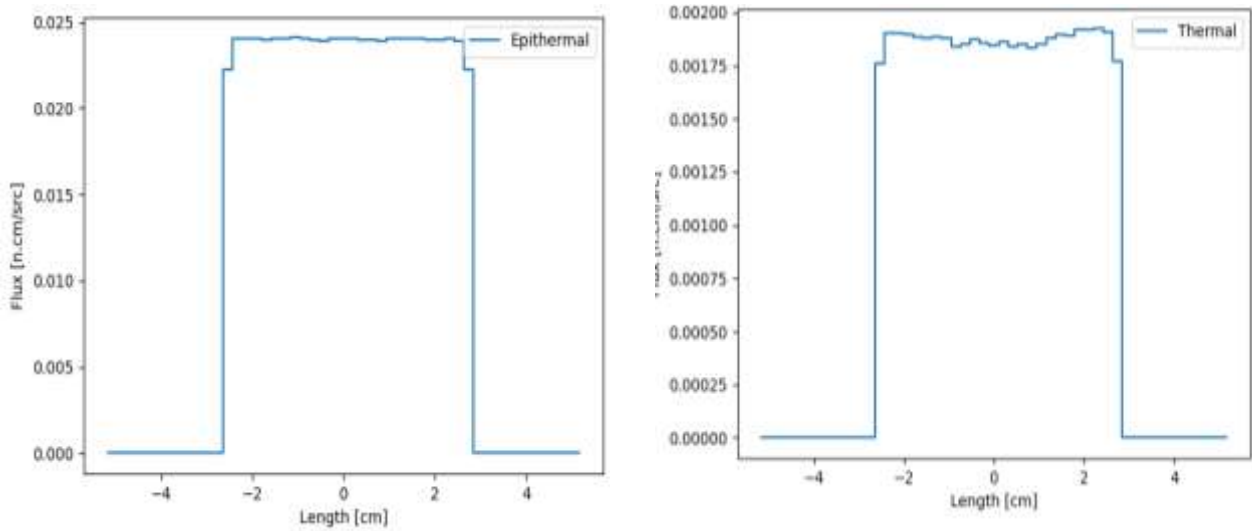


Figure 17: 1D epithermal radial flux(left) and 1D thermal radial flux (right) profile for a unit cell.

In Figure 17, the radial flux distribution in the epithermal energy region appears almost as uniform as that observed in the fast neutron region. However, a slight decrease in neutron flux is noticeable in the thermal energy region. This behavior can be attributed to the neutron absorption characteristics of sodium-23. Sodium-23 exhibits a tendency to capture neutrons predominantly at thermal energies, whereas its neutron capture probability is significantly lower in the fast and epithermal energy ranges. To further investigate this phenomenon, a neutron capture cross-section plot for sodium-23 was generated using data from the JENDL nuclear data library, as shown in Figure 18. The plot clearly illustrates that the  $(n,\gamma)$  reaction cross-section of sodium-23 is considerably higher in the thermal energy region compared to the fast and epithermal regions, thereby explaining the observed flux behavior in the thermal flux distribution.

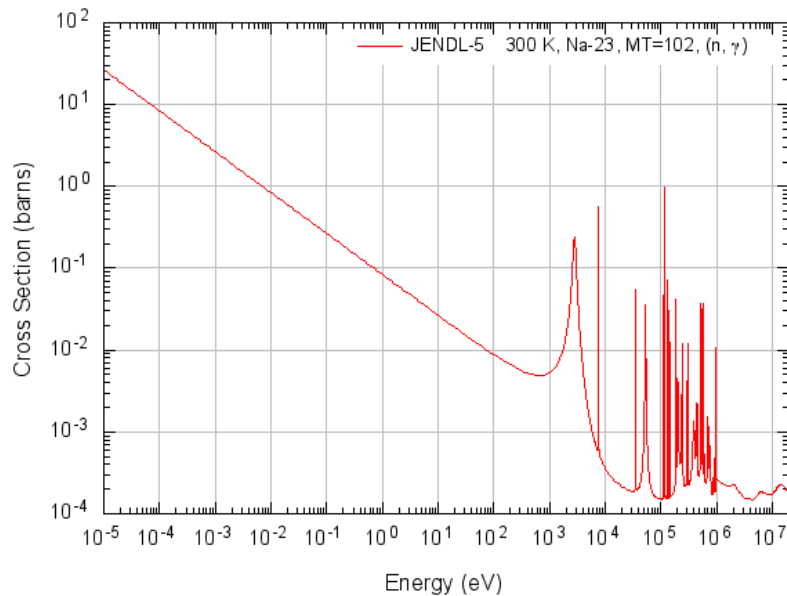


Figure 18: Capture cross section of sodium-23 from JENDL-5 data library.

#### 4.1.4. Fuel Temperature Coefficient

The fuel temperature coefficient of reactivity (FTC) plays a crucial role in governing the reactor's neutronic behaviour, especially in response to reactivity excursions. This parameter represents the change in reactivity due to variations in fuel temperature, and this sensitivity is quantified by the temperature coefficient of reactivity  $\alpha_T$  [36]. FTC or  $\alpha_T$  is mathematically defined as the rate of change of reactivity with respect to temperature:

$$\alpha_T = \frac{d\rho}{dT}$$

The sign of  $\alpha_T$  critically affects reactor behaviour. A positive  $\alpha_T$  means that as temperature increases, reactivity increases, which further raises reactor power and temperature, potentially causing unsafe conditions. Conversely, a negative  $\alpha_T$  means that increased temperature reduces reactor power. A negative FTC enhances the inherent safety of a nuclear reactor by introducing immediate negative feedback during a reactivity excursion, thereby stabilizing the reactor and preventing runaway conditions. Furthermore, the absolute magnitude of the fuel temperature coefficient determines the rate at which the reactivity transient progresses. A stronger negative FTC results in a faster stabilization of the reactor, whereas a weaker negative FTC may allow reactivity fluctuations to persist for a longer duration.

To determine the Fuel Temperature Coefficient of Reactivity (FTC), the following equation has been utilized:

$$\alpha_T = \frac{k_2 - k_1}{k_2 \times k_1 \times (T_2 - T_1)} \quad (10)$$

Where,

$\alpha_T$  = Fuel Temperature Coefficient of Reactivity

$k_1$  = Effective Multiplication Factors (k-effective) at temperature  $T_1$

$k_2$  = Effective Multiplication Factors (k-effective) at different fuel temperatures

$T_1$  = 773 K

$T_2$  = Different fuel temperatures

Using this formula, the calculated values of  $k_{eff}$  and FTC are presented in Table 5. The values of the FTC and reactivity changes, and how the temperature feedback effect evolves with temperature.

Table 5: Fuel Temperature Reactivity and FTC

Temperature	$k_{eff}$	Reactivity $\pm \sigma$ (mk)	FTC $\pm \sigma$ (pcm/K)
773	$1.1191 \pm 0.0005$		
900	$1.1083 \pm 0.0005$	$-10.9 \pm 0.5$	$-6.8 \pm 0.52$
1000	$1.1028 \pm 0.0004$	$-16.0 \pm 0.5$	$-5.8 \pm 0.28$
1100	$1.0957 \pm 0.0004$	$-23.0 \pm 0.5$	$-5.8 \pm 0.19$
1200	$1.0902 \pm 0.0004$	$-28.1 \pm 0.5$	$-5.5 \pm 0.14$
1500	$1.0771 \pm 0.0003$	$-40.5 \pm 0.5$	$-4.8 \pm 0.08$

1800	$1.0640 \pm 0.0004$	$-52.4 \pm 0.5$	$-4.5 \pm 0.06$
2100	$1.0512 \pm 0.0004$	$-63.8 \pm 0.5$	$-4.3 \pm 0.04$
2400	$1.0391 \pm 0.0004$	$-74.2 \pm 0.5$	$-4.2 \pm 0.03$

The results from Table 5 are shown in Figure 19. The graph shows the magnitude of reactivity variations, highlighting the reactor's increasing negative temperature feedback.

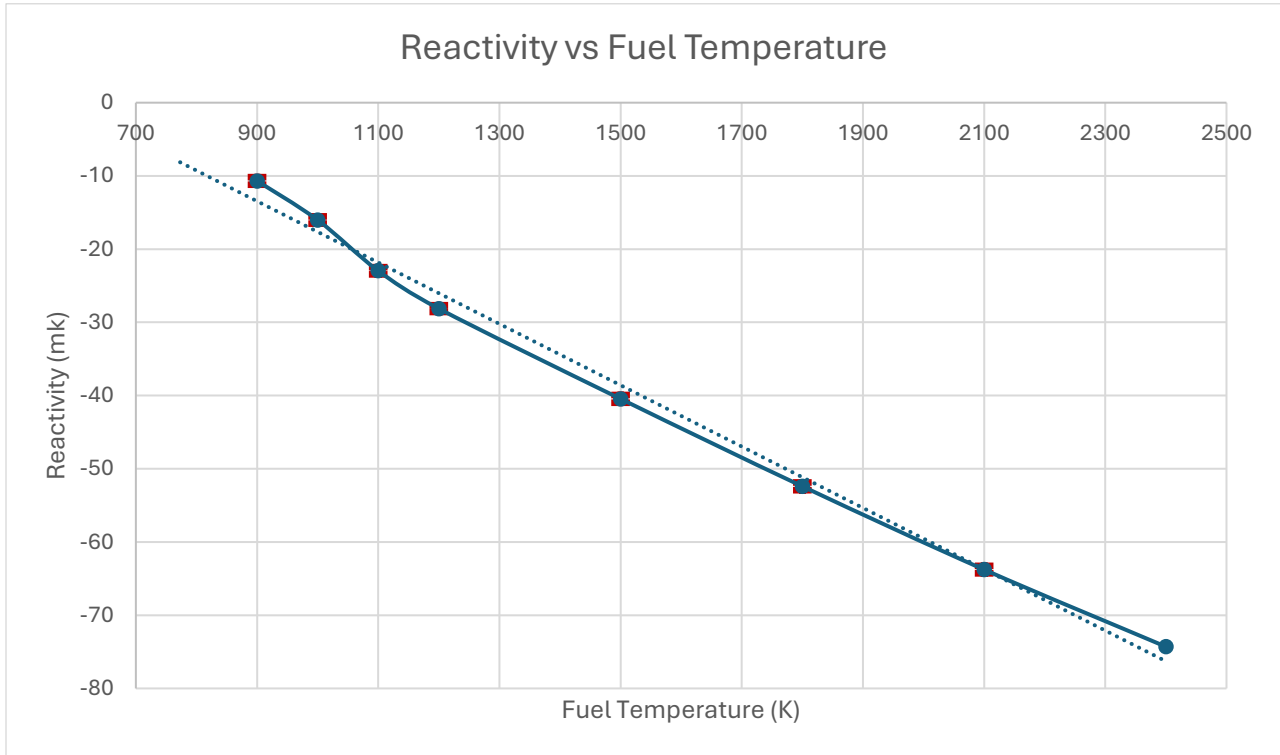


Figure 19: Reactivity variation with fuel temperature

Using the statistical error of the effective multiplication factor, the uncertainty for both reactivity and the Fuel Temperature Coefficient (FTC) has been calculated and represented with error bars in Figure 19 and Figure 20.

To calculate the uncertainty of reactivity, the following formula has been used-

$$\sigma_{\Delta\rho} = \sqrt{\left(\frac{\sigma_{k_1}}{k_1^2}\right)^2 + \left(\frac{\sigma_{k_2}}{k_2^2}\right)^2} \quad (11)$$

Where,

$k_1 = 1.1191$  (fixed at 773 K)

$k_2 = k$  effective that changes with temperature

$\sigma_{k_1}$  = Standard deviation (uncertainty) of  $k_1$

$\sigma_{k_2}$  = Standard deviation (uncertainty) of  $k_2$

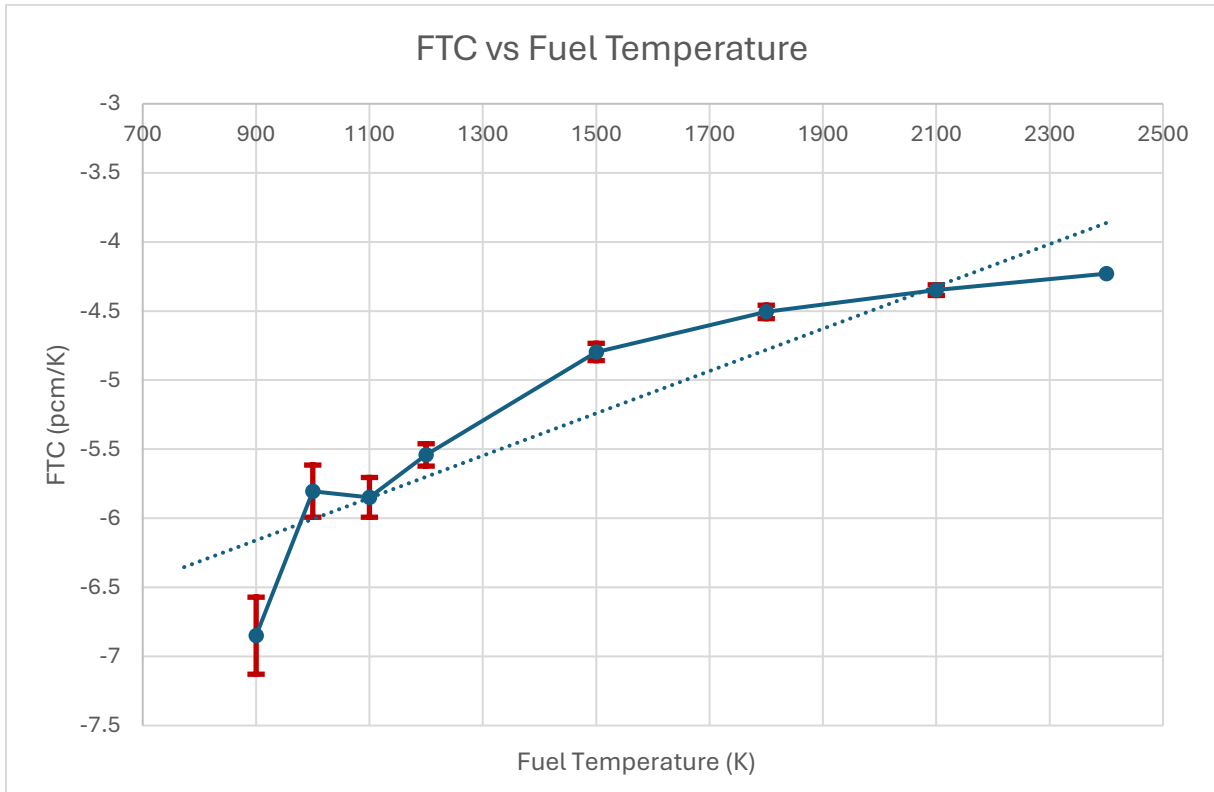


Figure 20: Fuel Temperature Coefficient (FTC) with fuel temperature

The uncertainty of FTC has been calculated using the following formula:

$$\sigma_{\text{FTC}} = \frac{1}{T_2 - T_1} \times \sqrt{\sigma_{\rho_1}^2 + \sigma_{\rho_2}^2} \quad (12)$$

Where,

$T_1 = 773 \text{ K}$

$T_2 = \text{Temperature}$

$\sigma_{\rho_1} = \text{Uncertainty of reactivity at } 773 \text{ K}$

$\sigma_{\rho_2} = \text{Uncertainty of reactivity at different temperatures}$

Only for uncertainty of reactivity at 773k =  $\frac{\sigma_{k_1}}{k_1^2} = \frac{0.00046}{1.1191^2} = 0.0003672 = 0.3672\text{mk}$

At 773 K,  $k_{\text{eff}}$  was 1.1191, decreasing to 1.0771 at 1500 K. The FTC was calculated as -4.8 to -6.8 pcm/K, indicating strong negative reactivity feedback, essential for passive stability during temperature excursions.

#### 4.1.5. Burnup results

The reactor unit cell was simulated for 20 years of continuous operation at 5MWt power, tracking fuel depletion and fission product accumulation. The simulation was conducted with a reduced number of particles to provide an initial understanding of the system's capability to sustain a controlled chain reaction over this period. The unit cell  $k$ -eigenvalue was simulated using boundary conditions around the hexagonal unit cell with 1 cm in height.

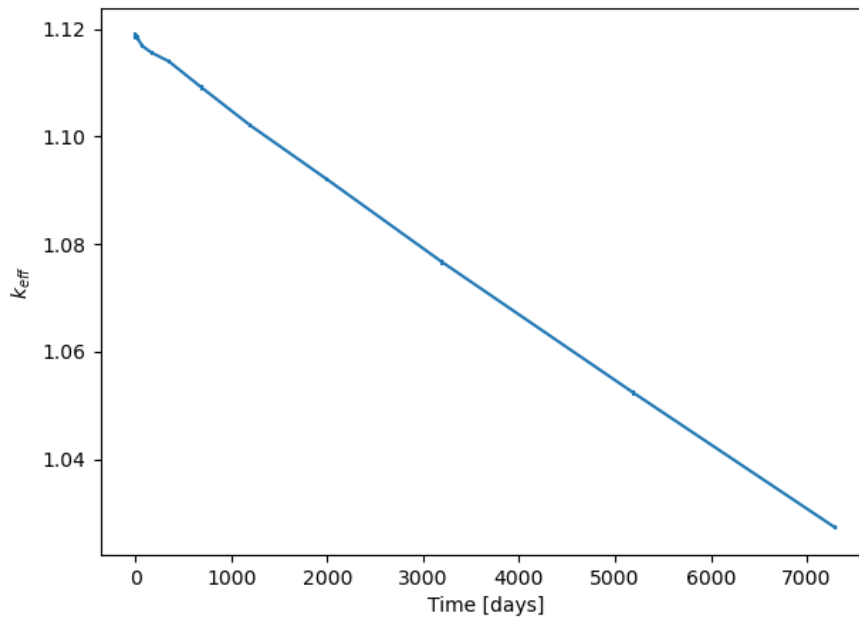


Figure 21: Change of  $k_{inf}$  with time for 20 years

The  $k_{inf}$  curve begins above 1.12, reflecting an initial excess reactivity required to offset neutron-absorbing fission products and fuel depletion. The visible oscillations, particularly at early time steps, are attributed to the use of fewer particles in the simulation, causing statistical noise. Despite this, the general trend is clearly observable. Throughout the 20-year period, the reactor remains critical. The curve demonstrates a gradual decline, consistent with the expected behaviour due to fuel burnup and the buildup of fission products.

The decline in  $k_{inf}$  appears linear with minor variations, suggesting that the design effectively compensates for reactivity losses over the simulated duration. Even with the reduced number of particles in the simulation, the results confirm the feasibility of operating the reactor unit cell for 20 years.

The following burnup and reaction rate results present the concentration profiles and temporal evolution of key isotopes, including essential fissile materials, high actinides, and their associated reaction rates, over the reactor's operational lifespan. The burnup curves illustrate the depletion of fuel, generation of transuranic elements, and accumulation of fission products, while the reaction rate curves provide insights into the neutron-induced reactions, such as fission and capture, that

drive these changes. Together, these results offer a comprehensive understanding of reactor behaviour, fuel utilization dynamics, and the underlying nuclear processes shaping the reactor's performance over time. The reactor exhibited a reactivity swing of  $-0.08 \Delta k/k$ , demonstrating a controlled depletion profile with sufficient reactivity margin.

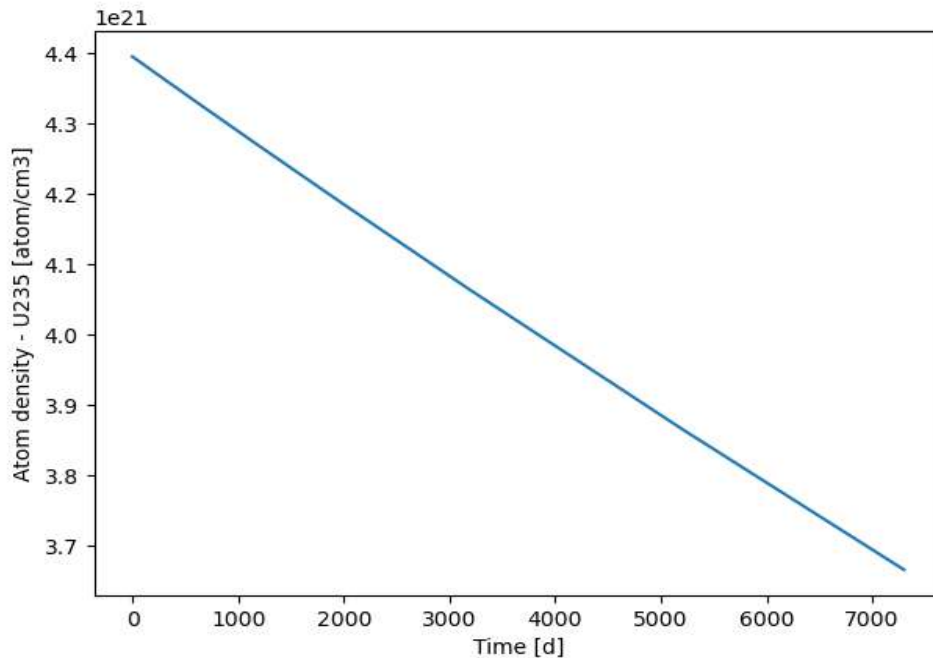


Figure 22: Change of concentration of U-235

The graph depicts the depletion of U-235 concentration over time, represented as a linear decline in the number of U-235 atoms/cm<sup>3</sup>. This trend indicates steady burnup behaviour in the reactor core, with U-235 atoms undergoing fission or decay processes. U-235 atom density decreased from 4.4e21 to around 3.7e21 over 20 years of time. This indicates that U-235 is being consumed through fission and capture reactions as expected in a functioning reactor core. The consistent slope suggests a uniform rate of fuel consumption, which is an important parameter in evaluating the efficiency and longevity of the reactor's operational cycle.

Figure 23 illustrates the linear decrease in the concentration of U-238 over the reactor's lifespan from around 1.76e22 atom/cm<sup>3</sup> to around 1.71 atom/cm<sup>3</sup>. This trend reflects the consumption of U-238 through neutron capture reactions, leading to the production of fissile isotopes such as Pu-239.

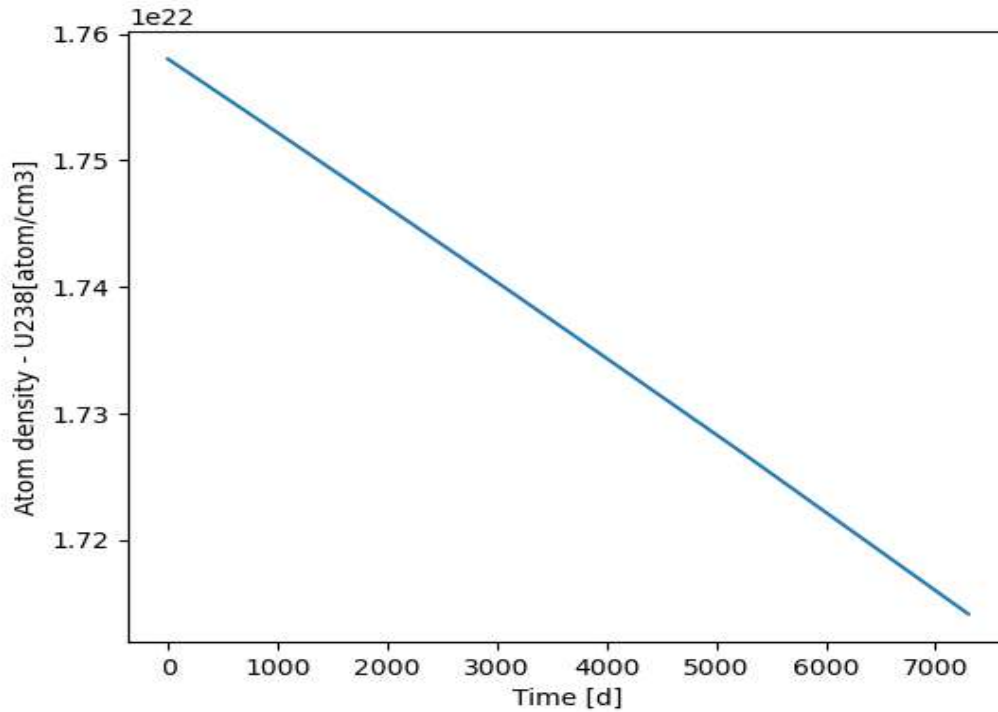
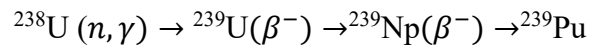


Figure 23: Change of concentration of U-238

The steady decline highlights the role of U-238 as a fertile material in sustaining reactor operations by contributing to the breeding of transuranic isotopes, which are crucial for maintaining reactivity in the later stages of the fuel cycle.

Breeding occurs when a fertile material like U-238 converts into a fissile material like Pu-239 through a neutron capture and subsequent decay :



To assess the production of Pu-239 from U-238 and evaluate the potential for breeding, Figure 24 has been plotted. This figure demonstrates a continuous increase in Pu-239 atom density, from 0 to approximately  $3.6 \times 10^{20}$  atoms/cm<sup>3</sup> over the reactor's operational lifetime, confirming that new fissile material is being generated from the fertile isotope U-238. Simultaneously, Figure 22 shows the depletion of U-235, allowing estimation of the total fissile material consumed during operation.

To quantitatively determine whether the reactor functions as a breeder, the breeding ratio (BR) can be calculated using the following relation:

$$\begin{aligned} \text{BR} &= \frac{\text{Fissile atoms produced (Pu - 239)}}{\text{Fissile atoms consumed (U - 235)}} \\ &= \frac{3.6 \times 10^{20} - 0}{4.4 \times 10^{21} - 3.7 \times 10^{21}} = \frac{3.6 \times 10^{20}}{7 \times 10^{20}} = 0.514 \text{ which is } < 1. \end{aligned}$$

Since  $BR < 1$ , the reactor is not classified as a breeder reactor.

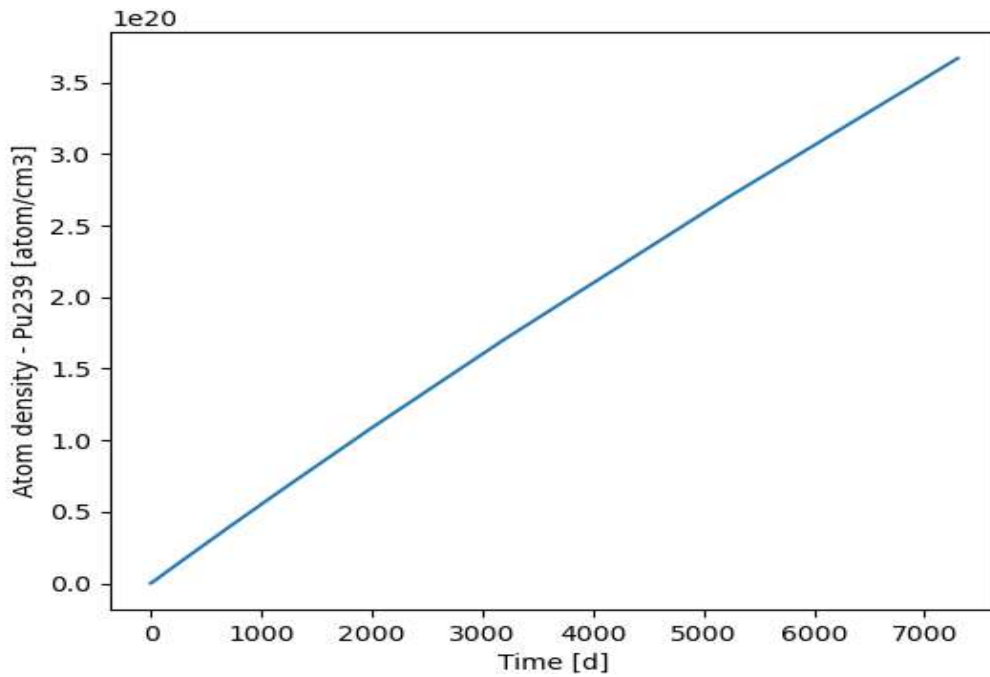


Figure 24: Change of concentration of Pu-239

However, the increasing concentration of Pu-239 in Figure 24 indicates that breeding is actively occurring, even though the amount of fissile material produced does not surpass that which is consumed.

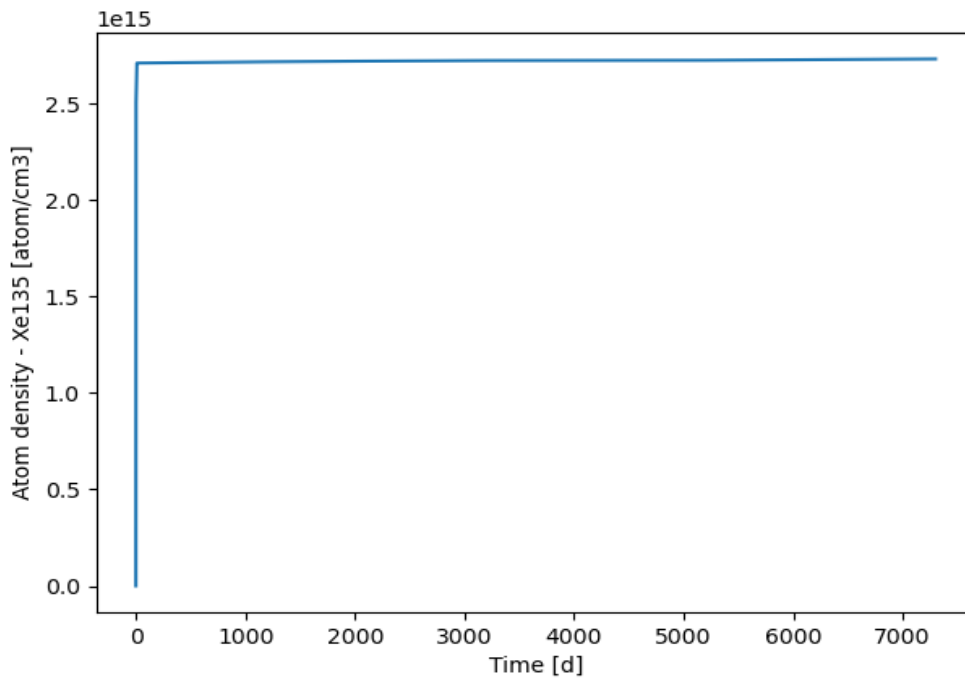


Figure 25: Change of concentration of Xe-135

In Figure 25, the graph represents the concentration of Xe-135 over time during the reactor's operational period. The sharp initial rise to a steady state concentration reflects the rapid production of Xe-135 to around  $2.6 \times 10^{15}$  atom/cm<sup>3</sup> as a fission product and reaching equilibrium quickly due to its high neutron capture cross-section and short half-life. Following this rapid buildup, the concentration stabilizes and remains almost constant throughout the reactor lifetime, indicating equilibrium between its production (from fission product decay), its burnout due to neutron absorption and decay into Cs-135, a stable isotope as Xe-135 has a half-life of approximately 9.1 hours. Xe-135, a strong neutron absorber, plays a significant role as a poison in the reactor.

In Figure 26, the iodine-135 (I-135) curve shows a rapid rise to a high concentration, reaching around  $1.8 \times 10^{15}$  atom/cm<sup>3</sup> due to the decay of its precursor, Xe-135.

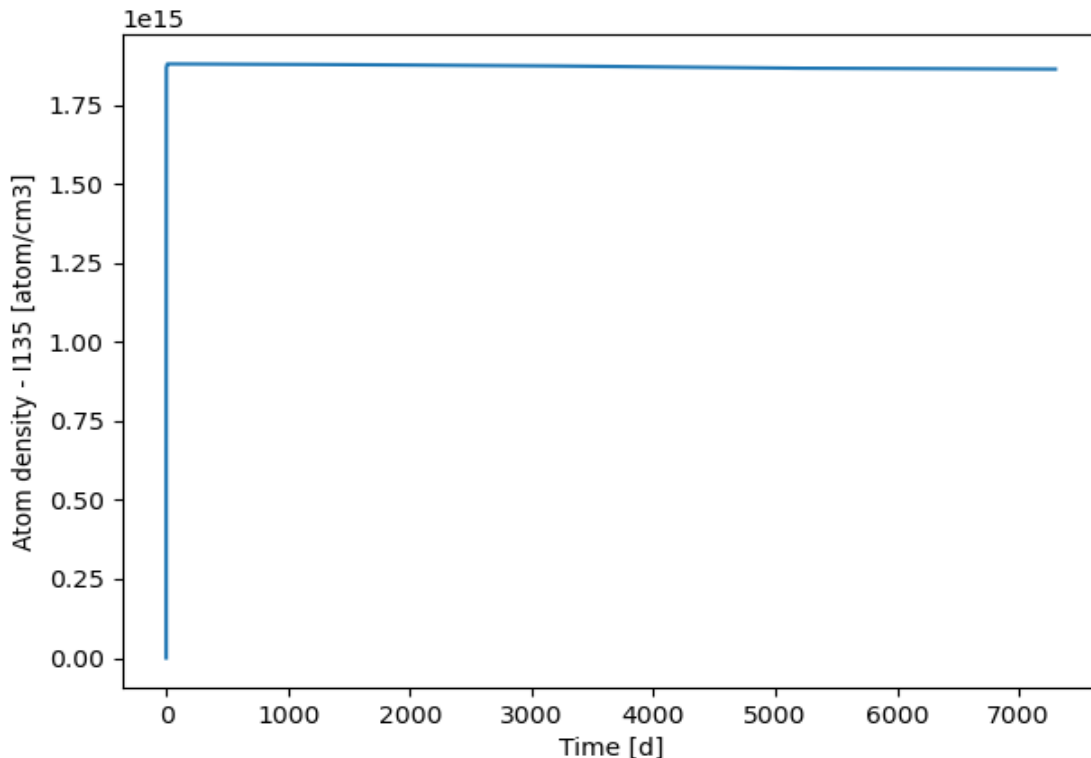


Figure 26: Change of concentration of I-135

This behaviour suggests that I-135 reaches a near-steady-state concentration quickly and remains relatively stable over the long term, indicating continuous production and decay equilibrium in the reactor environment. This steady-state reflects the balance between I-135 production from Xe-135 decay and its subsequent transmutation.

Figure 27 shows the buildup of Pu-241 concentration over the reactor's operational lifespan. Initially, Pu-241 concentration is minimal due to its absence in the fresh fuel but progressively accumulates as a direct result of neutron capture and transmutation reactions involving uranium isotopes, particularly uranium-238.

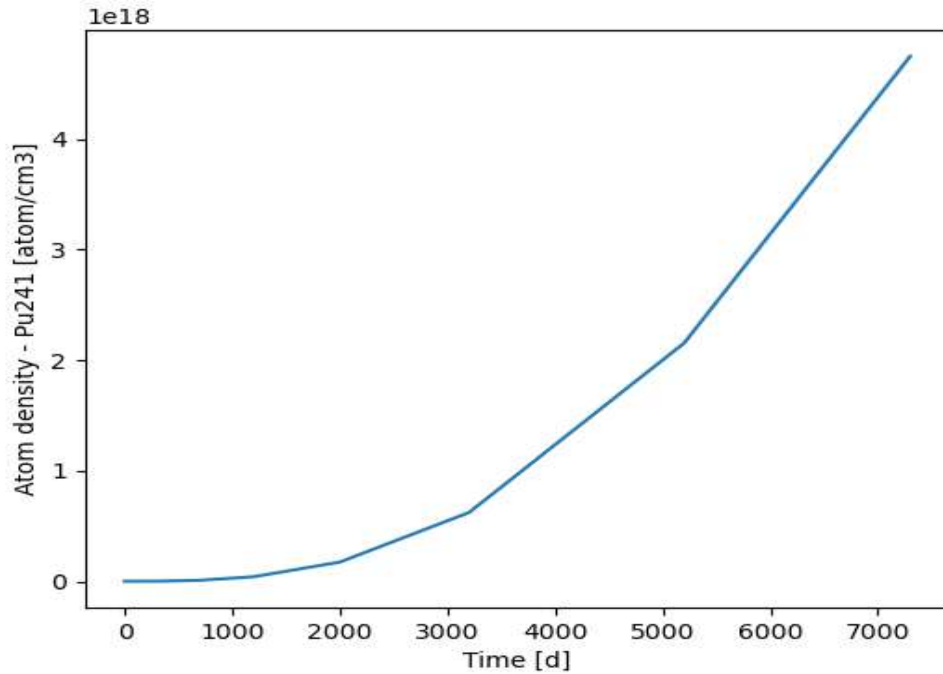


Figure 27: Change of concentration of Pu-241

The graph shows a slow initial increase, followed by an accelerated rise at later stages of reactor operation, reaching approximately  $2 \times 10^{18}$  atoms/cm<sup>3</sup> near the midpoint and approximately  $4.7 \times 10^{18}$  atoms/cm<sup>3</sup> at the end of the operational period. This trend indicates significant plutonium breeding over time, impacting the reactor's reactivity characteristics. However, as the reactor progresses, the rate of Pu-241 generation accelerates, reflected in the increasing slope of the curve.

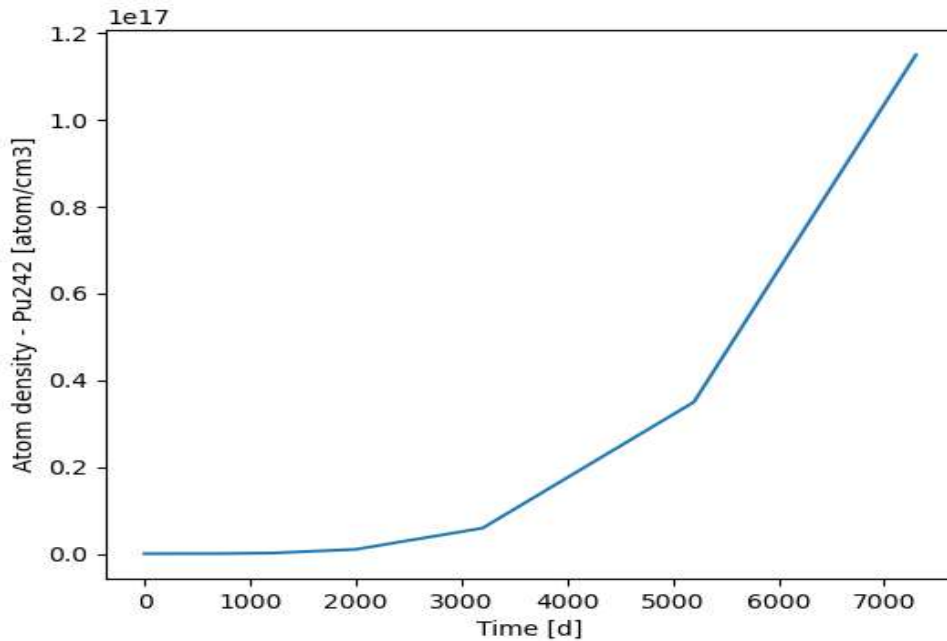


Figure 28: Change of concentration of Pu-242.

In Figure 28, the graph shows the ideal buildup of Pu-242 over the reactor's lifespan where initially, the Pu-242 concentration remains negligible but progressively accumulates due to successive neutron capture reactions occurring primarily in Pu-241. At around the midpoint (~3500 days), the concentration noticeably rises, reaching about  $2.0 \times 10^{16}$  atoms/cm<sup>3</sup>. By the reactor's end-of-life (~7000 days), the concentration significantly increases further, attaining approximately  $1.15 \times 10^{17}$  atoms/cm<sup>3</sup>.

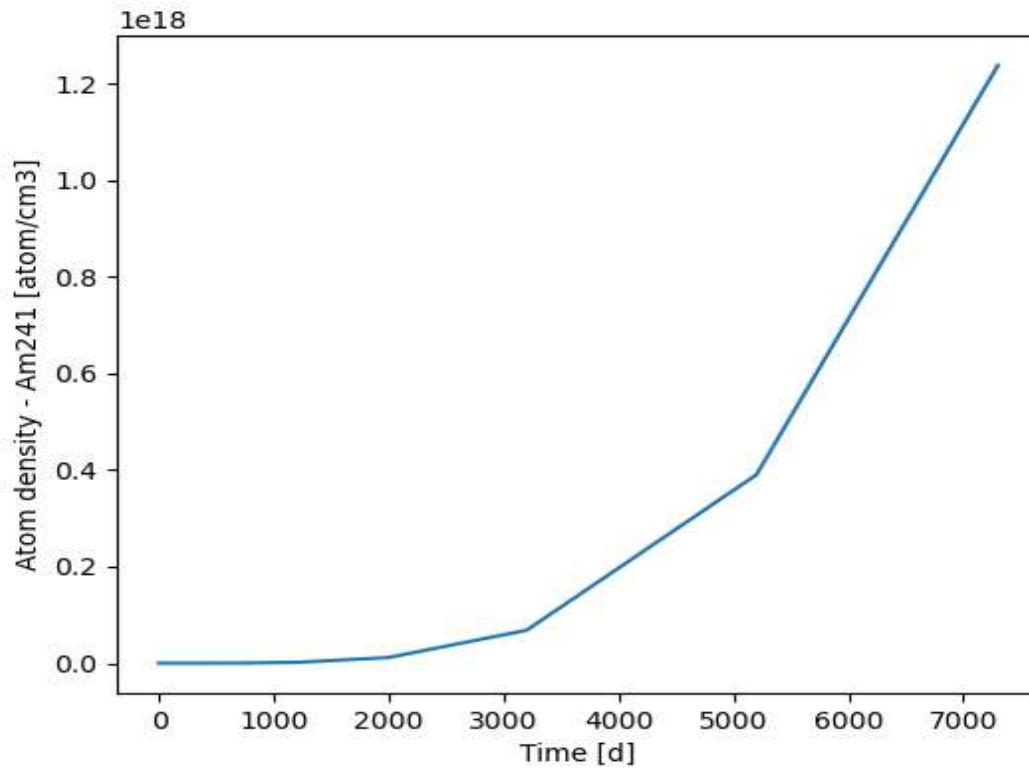


Figure 29: Change of concentration of Am-241

The graph shows the accumulation of Am-241 over time, with a slow initial increase followed by accelerated growth as the reactor operates. This behaviour aligns with the ideal shape, reflecting the gradual production of Am-241 from the decay of Pu-241 and subsequent neutron capture processes.

In Figure 30, the graph shows a gradual decline in the fission reaction rate over time, reflecting the expected depletion of fissile material and the steady burnup of fuel. The curve illustrates the reaction rate of uranium-235 (U-235) over approximately 7000 operational days.

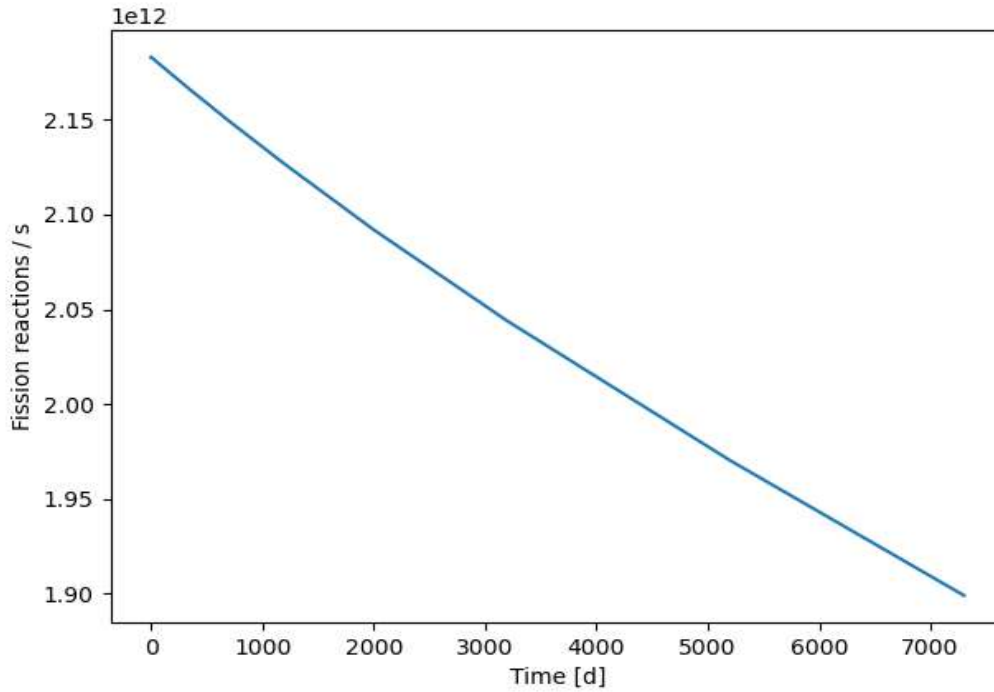


Figure 30: Reaction rate of U-235

It exhibits a steady and linear decrease, starting from approximately  $2.17 \times 10^{12}$  reactions/s at the beginning of life (BOL) and gradually declining to around  $1.9 \times 10^{12}$  reactions per second at the end of life (EOL).

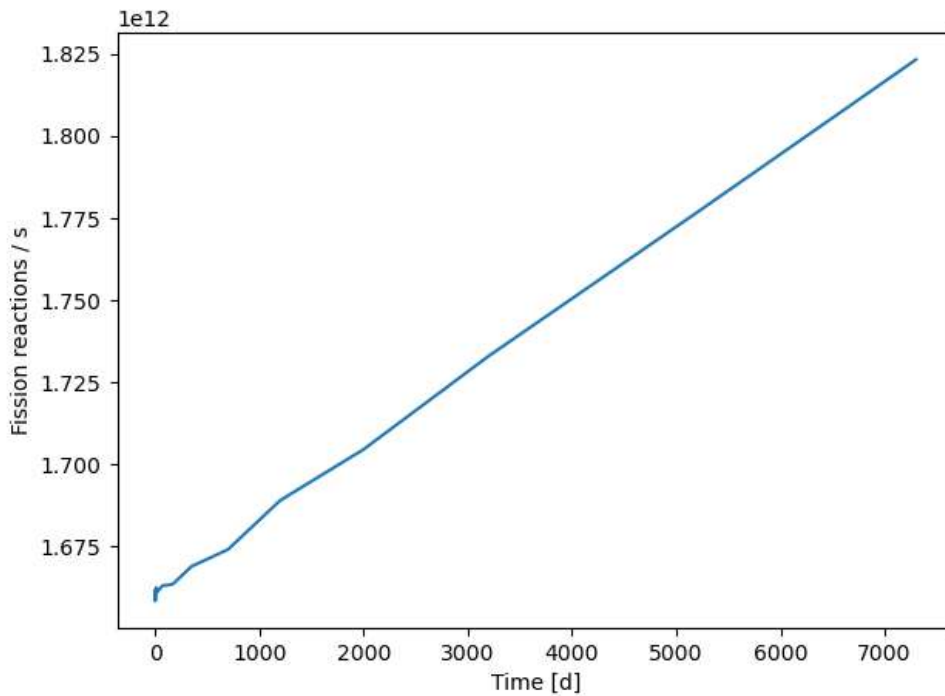


Figure 31: Reaction rate of U-238

The graph illustrates the fission reaction rate of plutonium-239 (Pu-239) over the reactor's operation period of approximately 7000 days. The reaction rate begins at about  $1.67 \times 10^{12}$  reactions/s, followed by a steady and gradual increase throughout reactor operation, reaching approximately  $1.83 \times 10^{12}$  reactions/s by the end-of-life. This increase indicates that Pu-239 progressively contributes more significantly to the total fission reactions within the reactor, compensating for the decrease in fission reactions from initial fissile isotopes such as uranium-235 (U-235). This behaviour is typical in reactors operating in a fast and intermediate neutron spectrum.

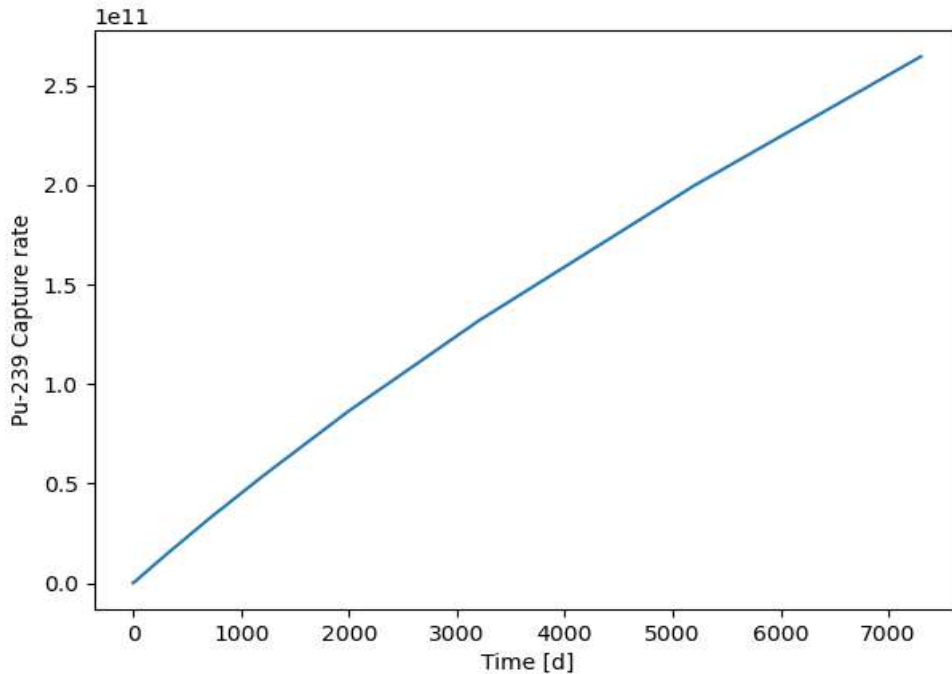


Figure 32: Reaction rate of Pu-239

The graph illustrates the Pu-239 capture rate increasing linearly over time, indicating a consistent accumulation of neutron captures in Pu-239. This behaviour aligns with the ideal shape for such a curve, reflecting the expected production of higher actinides due to continuous neutron flux exposure. The linearity demonstrates stable reactor conditions and efficient utilization of Pu-239 in the transmutation process.

Figure 33 precisely illustrates the neutron capture rate of Xenon-135 (Xe-135) over approximately 7000 days of reactor operation. The capture rate sharply peaks at about  $4.5 \times 10^8$  captures/s during the initial operation, then steadily declines over time to approximately  $2.8 \times 10^8$  captures/s by the end of the operation.

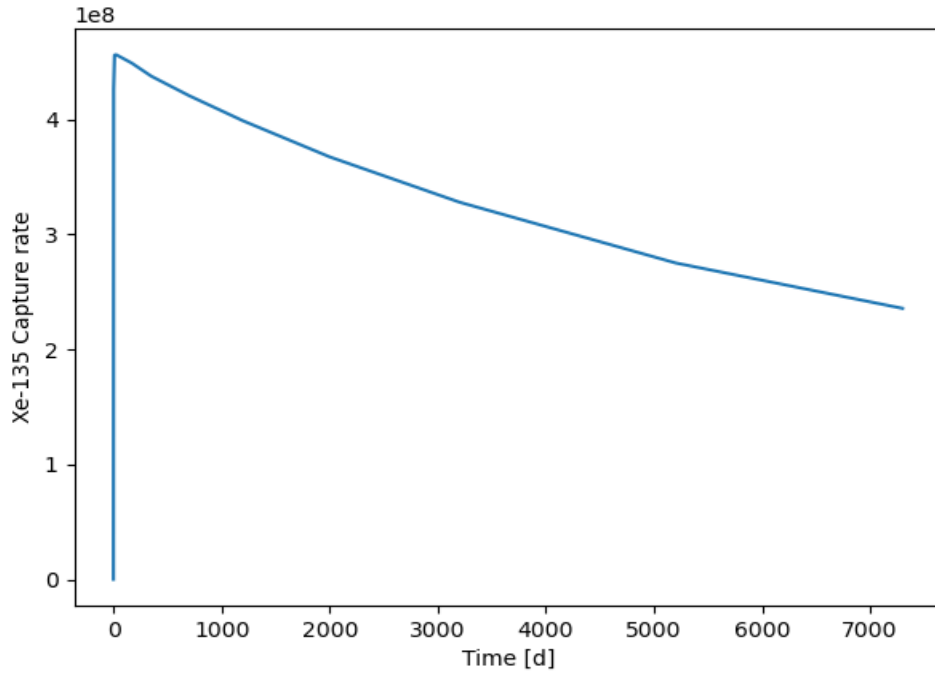


Figure 33: Reaction rate of Xe-135

This trend reflects Xe-135's rapid initial buildup from fission product decay, followed by a gradual reduction due to equilibrium conditions between production, absorption, and decay processes within the reactor core.

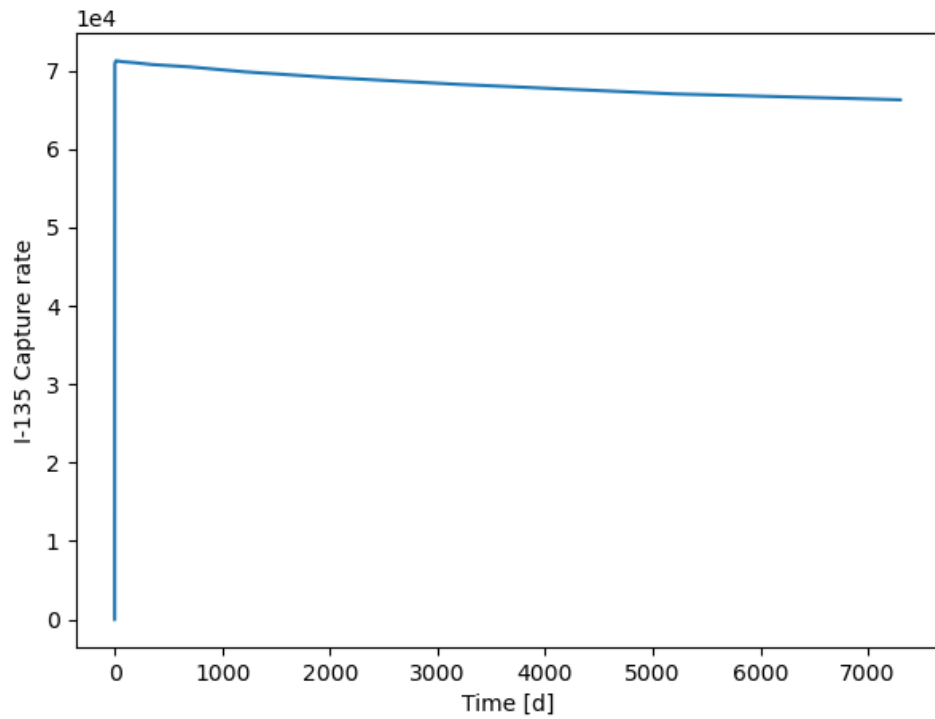


Figure 34: Reaction rate of I-135

The graph illustrates the I-135 capture rate, which shows a sharp initial rise followed by a stable plateau. This curve maintains the ideal shape, representing the rapid production of I-135 as a fission product and its subsequent equilibrium between neutron capture and decay into Xe-135. Initially, the capture rate sharply increases to around  $7.0 \times 10^4$  captures/s due to rapid I-135 buildup from decay processes. Following this initial transient, the capture rate slightly decreases and approaches a steady-state equilibrium, maintaining a stable value near  $6.7 \times 10^4$  captures throughout the reactor's operational lifetime. This steady behaviour indicates equilibrium between I-135 production, capture, and decay processes in the reactor core.

## 4.2 Full core

### 4.2.1 Core Layout:

The active core of the reactor is designed with a hexagonal geometry, similar to the Los Alamos National Laboratory (LANL) concept, featuring an inner central void that accommodates the emergency shutdown rod. This core design comprises a total of 462 fuel elements, strategically arranged to achieve optimal performance and safety. To plot and construct the geometry of this hexagonal fuel lattice, a nested lattice approach was employed.

In this approach, the fuel elements are arranged concentrically in successive ring layers around a central lattice. At the core of this arrangement, there is a single fuel lattice, which is surrounded by 6 additional fuel lattices in the first ring. This pattern continues with each successive ring expanding outward: 12 fuel lattices in the second ring, 18 in the third, followed by 24, 30, 36, 42, 48, 54, 60, 66, and finally 72 fuel lattices in the outermost ring. This ring-layer strategy ensures uniformity in spacing and criticality distribution throughout the core.

The necessity for this assembly strategy arises from the need to achieve a fully integrated and symmetric hexagonal core geometry. Such an arrangement ensures:

1. **Uniform Neutron Flux Distribution:** The concentric hexagonal layering minimizes flux peaking and supports a more even distribution of neutron activity across the core.
2. **Ease of Control Rod Placement:** The central void allows placement of the emergency shutdown rod, vital for reactor safety.
3. **Optimized Thermal and Neutronic Performance:** The symmetry and uniformity of the hexagonal lattice enhance both the heat transfer efficiency and the neutronic characteristics of the core.

This hexagonal fuel core is embedded in a beryllium matrix surrounded by an  $\text{Al}_2\text{O}_3$  reflector in a cylindrical shape. 12 rotating control drums are installed around the core to control the reactor core.

### 4.2.2 Flux Distribution of the Central Core:

Fast and intermediate neutron flux distribution was calculated for the center line of the core at 5MWt power, where a symmetric cosine-shaped curve with a maximum is at the center of the core. The energy range depicted in the flux distribution of the core is likely for fast and intermediate neutrons based on the higher magnitude of flux and the context of reactor flux analysis. This is

characteristic of an evenly designed reactor core where the central regions experience higher neutron production, and the edges are influenced by neutron leakage or reflective boundaries. Flux distribution of the Beginning of the Life (BOL) cycle has been plotted and shown in Figure 35.

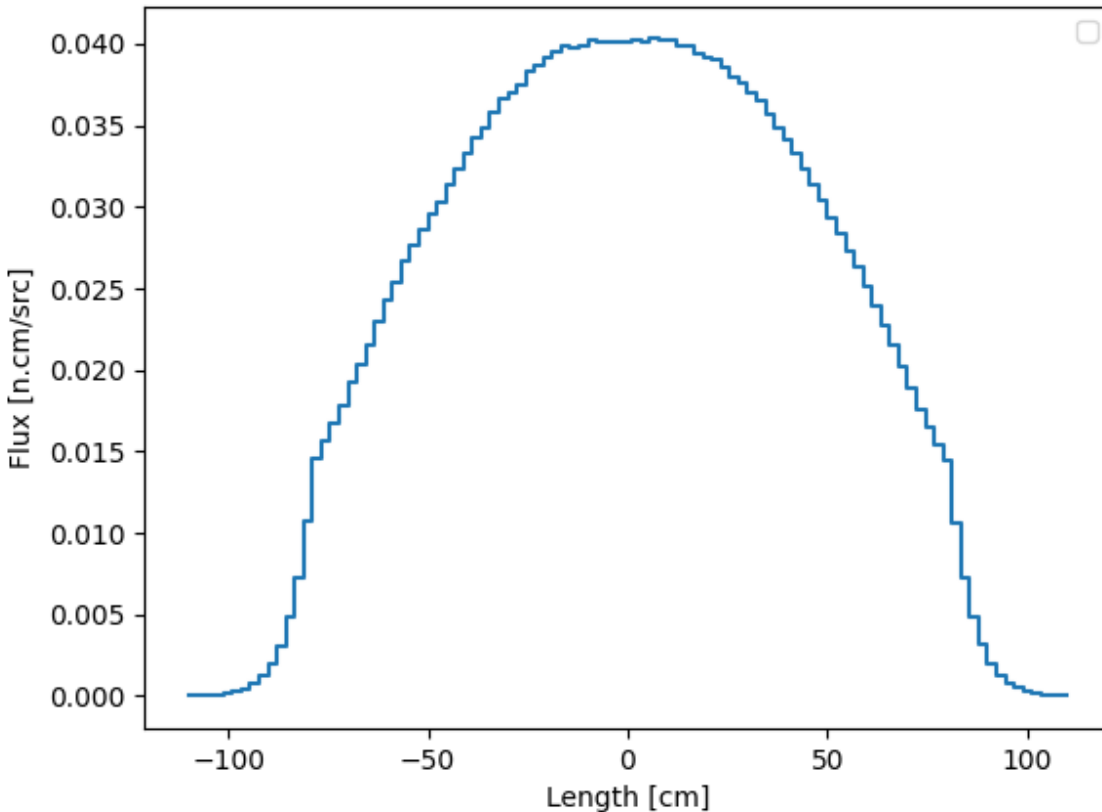


Figure 35: Radial flux distribution of the core at the BOL

In Figure 35, the one-dimensional radial flux distribution of the full core along the centerline is plotted for the fast neutron energy region, displaying a characteristic cosine-shaped profile. This radial flux distribution is expected to evolve over time, as each fuel element experiences different neutron flux levels depending on its position from the center to the periphery of the core. Consequently, the burnup behaviour varies between the core center and the outer regions, leading to different flux profiles at various stages of the reactor's life cycle, such as at the middle of life (MOL) and end of life (EOL).

Within the reactor core, millions of TRISO fuel particles are embedded, each undergoing burnup at different rates due to local flux variations. To accurately capture this spatially dependent fuel depletion, OpenMC provides a feature called 'diff\_burnable\_mats'. This functionality allows differentiation between materials that appear in multiple locations within the geometry. Without applying this method, using a single fuel material across the entire core would result in an averaged spectrum and reaction rate for all pins, incorrectly assuming uniform depletion behaviour. By enabling 'diff\_burnable\_mats', OpenMC creates distinct instances of fuel materials for different regions, ensuring that each fuel element depletes according to its local neutron flux. Due to the excessive resource-consuming power and the time-intensive nature of the simulation to treat each fuel compact separately to spatial flux change over burnup.

### 4.2.3 Optimization and Functionality of Absorbing Materials for Control Rods and Control Drums:

In the design of this Micro Nuclear Reactor (MNR), achieving precise reactivity control is essential to ensure safe, efficient, and reliable operation. To meet these objectives, neutron-absorbing materials were studied and optimized for use in the control rod and rotating control drums. The combination of these two mechanisms provides robust reactivity management and ensures the reactor remains subcritical under desired conditions, such as shutdown or emergencies.

**Control Drums: Design and Functionality:** Control drums are used to achieve reactor subcriticality. These rotating control drums are housed within the radial reflector, and each drum contains an annular sector of neutron-absorbing material. To analyze their effectiveness in achieving cold point subcriticality, 12 control drums were modelled in the radial reflector. Each drum has a radius of 14 cm and incorporates a 120° sector containing a 7 cm thick layer of Hafnium Hydride ( $\text{HfH}_2$ ), a strong neutron absorber of fast and intermediate neutrons.

**Control Rod: Centralized Reactivity Control:** The centrally located control rod complements the control drums. By inserting the control rod into the reactor core, a highly localized suppression of neutron activity is achieved. This mechanism is essential for rapidly reducing reactivity during startup, shutdown, or emergency conditions. The control rod's centralized position ensures uniform reactivity control across the core, addressing flux peaks and maintaining reactor stability.

The two mechanisms—central control rod and peripheral rotatable control drums—ensures a layered approach to reactivity management. Together, they provide the following benefits:

1. **Enhanced Safety:** The centrally placed control rod acts as a fail-safe mechanism, capable of rapidly shutting down the reactor if required, while the rotatable drums allow gradual reactivity adjustments to prevent abrupt changes.
2. **Operational Flexibility:** The rotatable drums provide incremental control over the reactor's power level, enabling operators to fine-tune the system for varying operational demands.
3. **Uniform Reactivity Management:** The central control rod ensures balanced reactivity control across the core, while the surrounding drums help maintain symmetry in neutron flux distribution, minimizing localized flux peaking.
4. **Redundancy in Reactivity Control:** The combination of the central control rod and the rotatable control drums provides redundancy, enhancing the reliability of the overall safety system.

**Absorbing Materials Evaluation and Optimization for Control Devices:** To optimize the absorbing materials used in the control rod and control drums, several candidates were studied, including hafnium hydride ( $\text{HfH}_2$ ), europium oxide ( $\text{Eu}_2\text{O}_3$ ), boron carbide ( $\text{B}_4\text{C}$ ), dysprosium titanate ( $\text{Dy}_2\text{Ti}_2\text{O}_7$ ), gadolinium oxide ( $\text{Gd}_2\text{O}_3$ ), cadmium (Cd), and Ag-In-Cd alloys. These materials were evaluated based on their effectiveness in reducing the effective multiplication factor ( $k_{\text{eff}}$ ) and corresponding reactivity changes under three key scenarios:

1. **Insertion of the Control Rod ( $k_1$ ):** Evaluating the suppression of reactivity due to the insertion of the control rod at the core center.

2. Rotation of Control Drums Inward ( $k_2$ ): Assessing the impact of rotating the control drums such that the neutron-absorbing material faces the core.
3. Combined Effect ( $k_3$ ): Analyzing the total reactivity reduction achieved when both the control rod is inserted, and the control drums are rotated inward.

The results of these evaluations are summarized in Table 6, highlighting the effectiveness of each material under different scenarios.

Table 6:  $k_{eff}$  and reactivity variation calculation for different absorbing materials.

Absorbing Material	Without absorbing material $k_{eff}$	$k_{eff}$ ( $k_1$ ) value Inserting the Control rod in the centre of the core	Change of reactivity $\rho_1$ (mk)	$k_{eff}$ ( $k_2$ ) value Rotating the Control drums inward the core	Change of reactivity $\rho_2$ (mk)	$k_{eff}$ ( $k_3$ ) value Inserting the Control Rod and rotating the Control Drums inward	Change of reactivity $\rho_3$ (mk)
Hafnium hydride (HfH <sub>2</sub> )	1.063	0.967	-93.03	0.996	-62.63	0.901	-169.5
Europium Oxide	1.062	0.989	-70.30	0.999	-60.06	0.907	-161.2
Ag-In-Cd	1.050	0.994	-53.73	1.010	-39.01	0.928	-124.9
Cd	1.063	1.014	-45.82	1.022	-39.7	0.969	-91.4
Gd <sub>2</sub> O <sub>3</sub>	1.059	1.007	-48.19	1.016	-40.36	0.936	-123.7
Dysprosium Titanate (Dy <sub>2</sub> T <sub>2</sub> O <sub>7</sub> )	1.057	1.013	-41.1	1.007	-47.27	0.943	-114.45
Boron Carbide (B <sub>4</sub> C)	1.040	1.001	-54.94	1.009	-48.30	0.916	-147.46

Analyzing Table 6:

1. Without Absorbing Material ( $k_{eff}$ ): This column provides the baseline  $k_{eff}$  value for the reactor without any absorbing material. This represents the reactor in an unperturbed state, where reactivity is at its maximum.

2.  $k_{\text{eff}}$  ( $k_1$ ) Value – Inserting the Control Rod in the Core Center: The insertion of the control rod into the center of the core significantly reduces  $k_{\text{eff}}$  by introducing a concentrated neutron-absorbing material.
3. Change in Reactivity ( $\rho_1$ ) Due to Control Rod Insertion: This column quantifies the reactivity suppression achieved by the control rod using the formula:

$$\rho_1 = \frac{(k_1 - k)}{(k_1 k)} \times 1000$$

Larger negative values indicate better performance in reducing reactivity.

4.  $k_{\text{eff}}$  ( $k_2$ ) Value – Rotating the Control Drums Inward: Rotating the control drums to face the absorbing material towards the core reduces  $k_{\text{eff}}$ , providing additional reactivity control at the periphery. This mechanism allows fine-tuning of reactivity during operation.
5. Change in Reactivity ( $\rho_2$ ) Due to Control Drum Rotation: Similar to the control rod, this column measures the reactivity change caused by rotating the control drums inward. It reflects the material's effectiveness in reactivity suppression at the core edges.
6.  $k_{\text{eff}}$  ( $k_3$ ) Value – Combined Effect of Control Rod Insertion and Control Drum Rotation: The combination of both mechanisms creates the most significant reduction in  $k_{\text{eff}}$ , achieving optimal reactivity control. This is crucial for ensuring the reactor can be safely shut down or transitioned to a subcritical state during emergencies.

Change in Reactivity ( $\rho_3$ ) Due to Combined Mechanisms: This column evaluates the combined effectiveness of the control rod and control drums in suppressing reactivity, with larger negative values representing superior performance.

- **Hafnium Hydride (HfH<sub>2</sub>):** Exhibits the highest change in reactivity across all scenarios, with  $\rho_3 = -169.537\text{mk}$  under combined control. This makes it a highly effective material for reactivity suppression.
- **Europium Oxide (Eu<sub>2</sub>O<sub>3</sub>):** Demonstrates strong neutron absorption capabilities, achieving a combined reactivity reduction of  $-161.151\text{mk}$ , making it another viable option for essential applications.
- **Boron Carbide (B<sub>4</sub>C):** Known for its stability and high absorption cross-section, B<sub>4</sub>C achieves a combined reactivity reduction of  $-147.460\text{mk}$ , making it an excellent alternative absorber.
- **Ag-In-Cd and Dysprosium Titanate (Dy<sub>2</sub>Ti<sub>2</sub>O<sub>7</sub>):** Provide moderate reactivity suppression, with  $\rho_3$  values of  $-124.945\text{mk}$  and  $-114.454\text{mk}$ , respectively.
- **Cadmium (Cd):** Shows the lowest suppression in combined control ( $\rho_3 = -91.4053\text{mk}$ ), indicating limited effectiveness compared to other materials.
- **Other Materials (Ag-In-Cd, Gadolinium Oxide):** While effective, these materials show moderate reductions in reactivity compared to HfH<sub>2</sub> and Eu<sub>2</sub>O<sub>3</sub>, making them more suitable for specific, less demanding applications.

Hafnium hydride's exceptional performance as a neutron absorber, combined with the strategic placement and functionality of the control rod and control drums, ensures precise reactivity control, safety, and efficiency. Now, the question arises why hafnium hydride acts as an effective control material in a fast and intermediate spectrum reactor. Hydrogen, being almost the same mass as a neutron, is the most effective moderator known in reactor physics. When fast neutrons collide with hydrogen nuclei, they undergo significant energy loss per collision, slowing down quickly:

- Hydrogen has an average logarithmic energy decrement ( $\xi$ ) close to 1, meaning neutrons lose a large portion of their energy in a single collision [37].
- In  $\text{HfH}_2$ , hydrogen atoms moderate the fast/intermediate neutrons locally within the absorber material, without needing an external moderator.

This moderation is especially important in reactors with a fast or epithermal neutron spectrum, where the raw fast neutrons would otherwise have a lower probability of being absorbed by Hf directly[38].

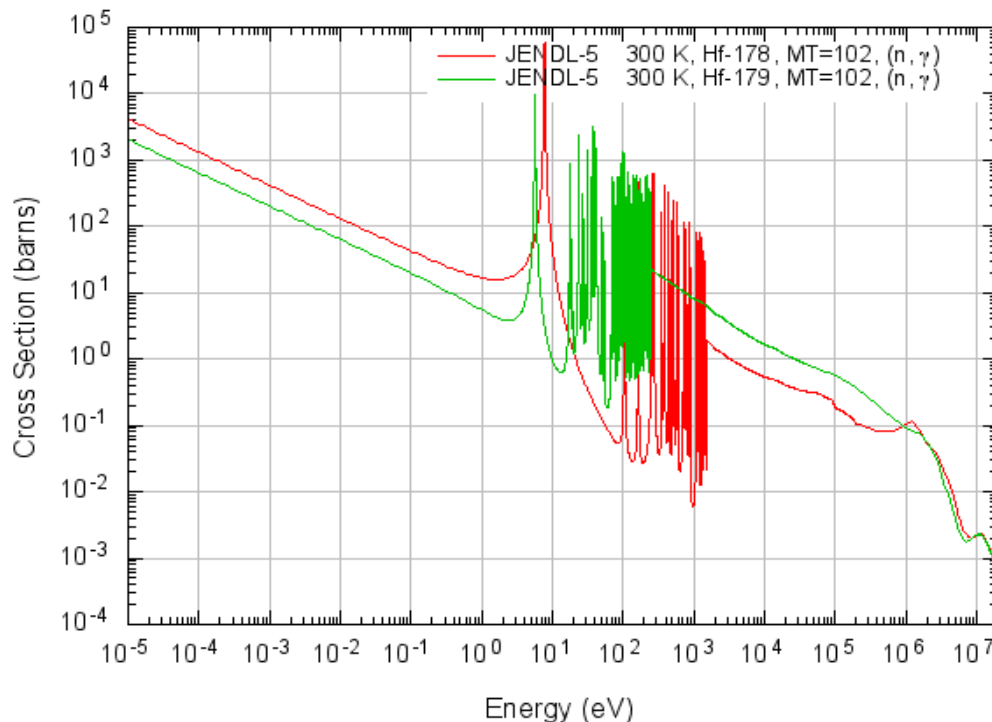


Figure 36: Absorption cross section of hafnium in  $\text{HfH}_2$  [39].

The plotted data shown in Figure 36 are sourced from JENDL-5:

- Hf-178 and Hf-179 both exhibit very high neutron capture cross sections in the thermal and epithermal regions, particularly in the range of  $\sim 0.1$  eV to 10 eV, reaching up to  $10^3$ - $10^4$  barns.
- In the fast energy range (above  $\sim 10^5$  eV), the absorption cross section is much lower, on the order of 1 barn or less, rendering pure hafnium less effective as an absorber in pure fast reactors.

However, due to the local moderation by hydrogen within HfH<sub>2</sub>, neutrons are slowed down in effectively shifting the neutron energy into the resonance and thermal regions, where hafnium's absorption cross section is highest. This coupling overcomes the inherent limitation of Hf in fast neutron fields.

### Implications for Reactor Design

The combination of a centrally placed control rod and rotatable control drums provides a robust mechanism for regulating the reactor's operation. Materials like hafnium hydride and europium oxide emerge as top candidates due to their superior performance in reducing reactivity. Now, control drum worth and control rod worth calculations are shown below-

$$1. \text{ Control drums worth} = \frac{\left(\frac{1}{k_2} - \frac{1}{k}\right)}{\beta_{\text{eff}}} = \frac{\left(\frac{1}{0.99621} - \frac{1}{1.06304}\right)}{0.004} = \$15$$

Where,

$\beta_{\text{eff}}$  = Effective delayed neutron fraction which is 0.004 in sodium-cooled fast reactors.  
 $k_2 = 0.99621$  (From Table 6 for hafnium hydride)  
 $k = 1.06304$  (From Table 6 for hafnium hydride)

Therefore, a single control drum is worth =  $\frac{\$15}{12} = \$1.25$

$$2. \text{ Control rod worth} = \left(\frac{1}{k_1} - \frac{1}{k}\right) / \beta_{\text{eff}} = \left(\frac{1}{0.96737} - \frac{1}{1.06304}\right) / 0.004 = \$23$$

The total control drum worth is \$15, meaning the full set of 12 control drums contributes to a significant negative reactivity insertion, with each drum worth \$1.25. The control rod worth is \$23.26, indicating it provides a stronger reactivity control than individual control drums, ensuring safe reactor shutdown.

#### 4.2.4 Impact of Control Rod and Control Drums on Reactor Flux Distribution:

To better understand the effect of the control rod and control drums on the neutron flux within the reactor core, additional calculations were carried out. The results of these analyses are presented in the figures below.

Figure 37 is the core layout of the micro nuclear reactor and depicts the spatial arrangement of key reactor components, including the central control rod, the hexagonal arrangement of fuel assemblies, and the surrounding control drums. The core is encased in a radial reflector, within which the 12 rotating control drums are housed. Each control drum features a 120° sector containing neutron-absorbing material (hafnium hydride), positioned to face the reactor core in this configuration. The control rod, inserted at the center, provides strong localized reactivity suppression, while the control drums contribute peripheral reactivity control. Under this configuration, the reactor achieves a  $k_{\text{eff}}$  value of 0.90365, indicating a subcritical state, which is essential for safe reactor operation during shutdown or controlled conditions.

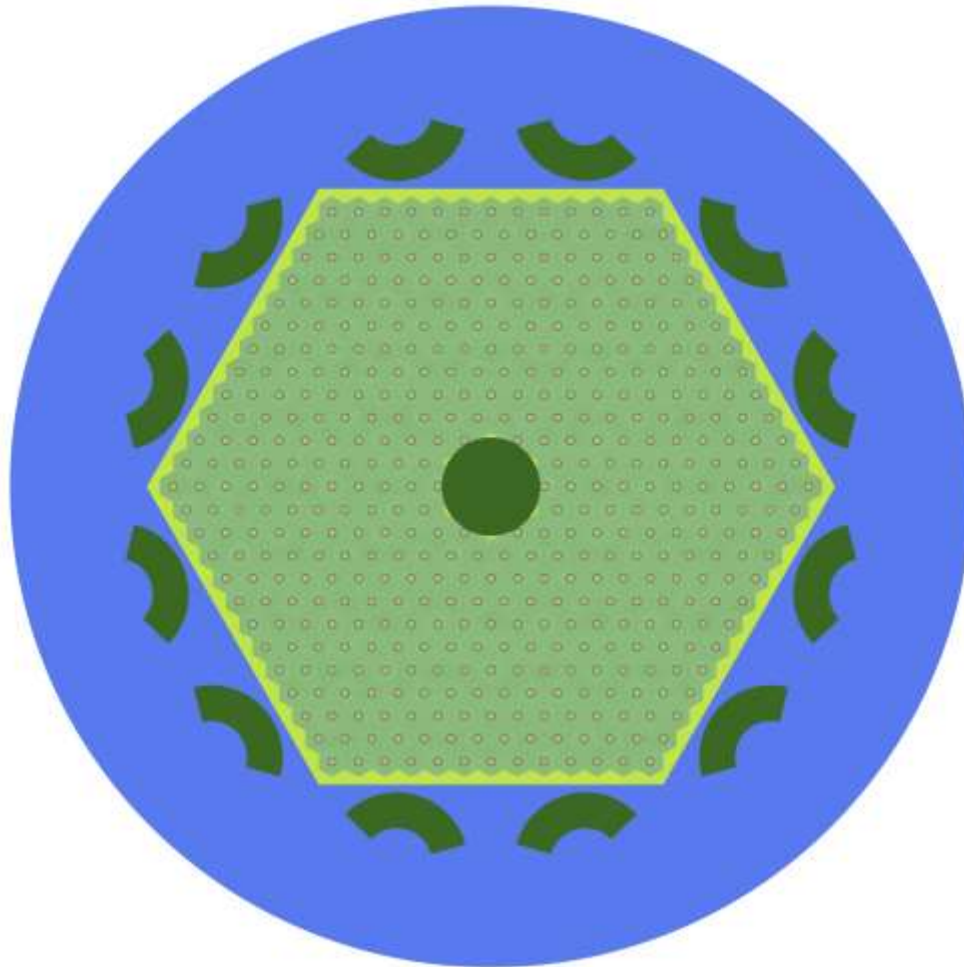


Figure 37: 2D MNR core layout with control rod inserted and control drum facing inward

This layout ensures balanced neutron flux control across the core, optimizing both operational efficiency and safety.

Figure 38 shows the 2D flux distribution plot of the core demonstrating the impact of the control mechanisms on neutron flux behaviour. The plot highlights a high neutron flux region forming a distinct ring between the central control rod and the surrounding control drums. The fully inserted control rod effectively suppresses neutron flux in the core center, ensuring reactivity reduction in essential regions. The flux decreases uniformly towards the core boundaries, indicating symmetric neutron flux suppression due to the inward-facing control drums. The effective performance of the control drums in reducing peripheral flux highlights neutron absorption near the core boundaries, preventing neutron leakage and maintaining a stable flux distribution.

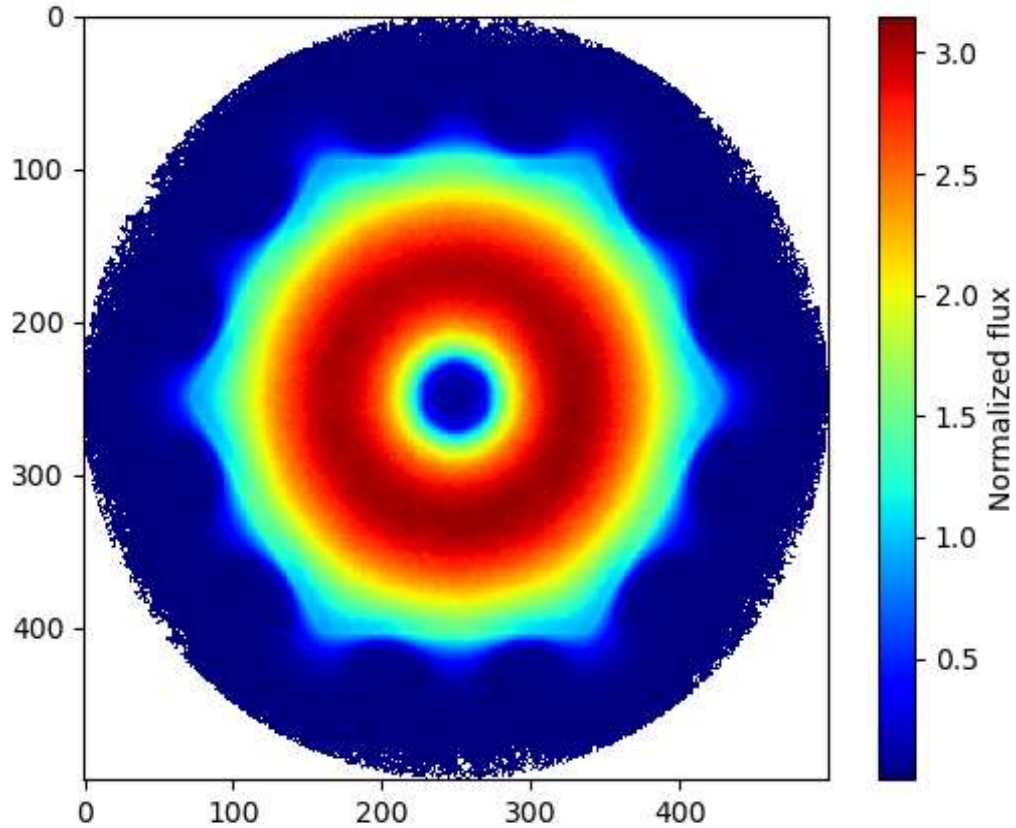


Figure 38: 2D plot of radial flux changes of the core inserting control rod in the middle of the core and rotating all the control drums facing inward the core.

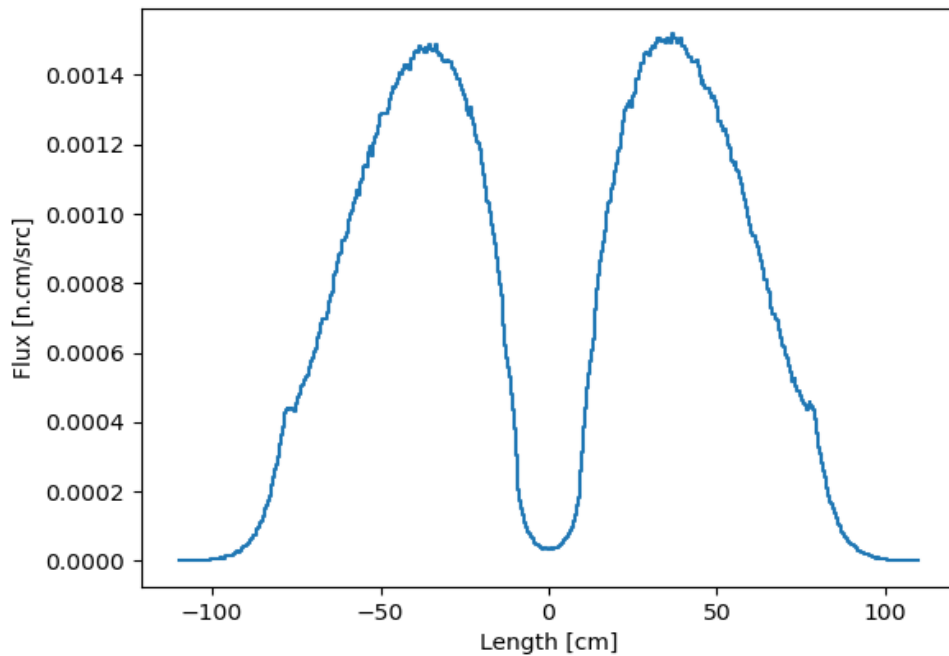


Figure 39: 1D plot of radial flux changes of the core inserting the control rod in the middle of the core and rotating all the control drums facing inward the core.

Figure 39, The 1D radial flux distribution plot provides a quantitative perspective on the neutron flux behaviour. The flux profile is observed to be symmetric, as expected. A sharp peak in neutron flux is seen at approximately 45 cm from the core center, corresponding to the high-flux region between the control rod and the control drums. This peak reflects the localized neutron population in the active region of the core. Beyond this point, the flux decreases consistently toward the edges of the core due to the neutron-absorbing effect of the control drums. The symmetry of the flux profile confirms the balanced configuration of the control mechanisms, ensuring uniform reactivity management.

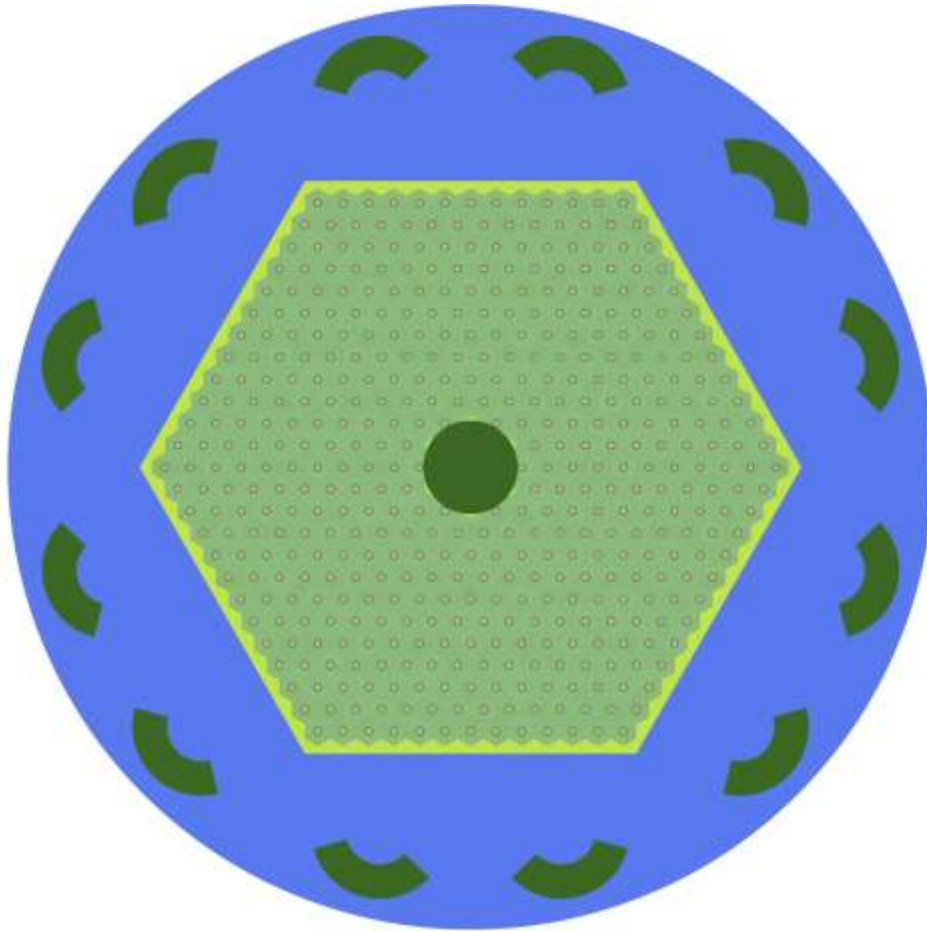


Figure 40: 2D MNR core layout with control rod inserted and control drum facing outward.

Figure 40 shows the core layout of the MNR with the spatial arrangement of the reactor's key components, including the central control rod and the hexagonal array of fuel assemblies, with 12 control drums housed within the radial reflector. In this configuration, the control drums are rotated outward, exposing the reflector material to the core. This reduces neutron absorption near the periphery of the core, allowing more neutrons to reflect back into the active region. The control rod remains fully inserted at the core center, providing localized neutron absorption to suppress central reactivity. In the condition where the control rod is inserted, the reactor achieves a  $k_{\text{eff}}$  value of 0.98703.

In Figure 40, the 2D flux distribution plot reveals the impact of the outward-facing control drums on neutron flux within the core. Compared to the inward-facing configuration, the neutron flux

spreads more broadly across the core, forming a wider flux profile. This is due to the reflector material of the control drums, which reflects neutrons back into the core instead of absorbing them.

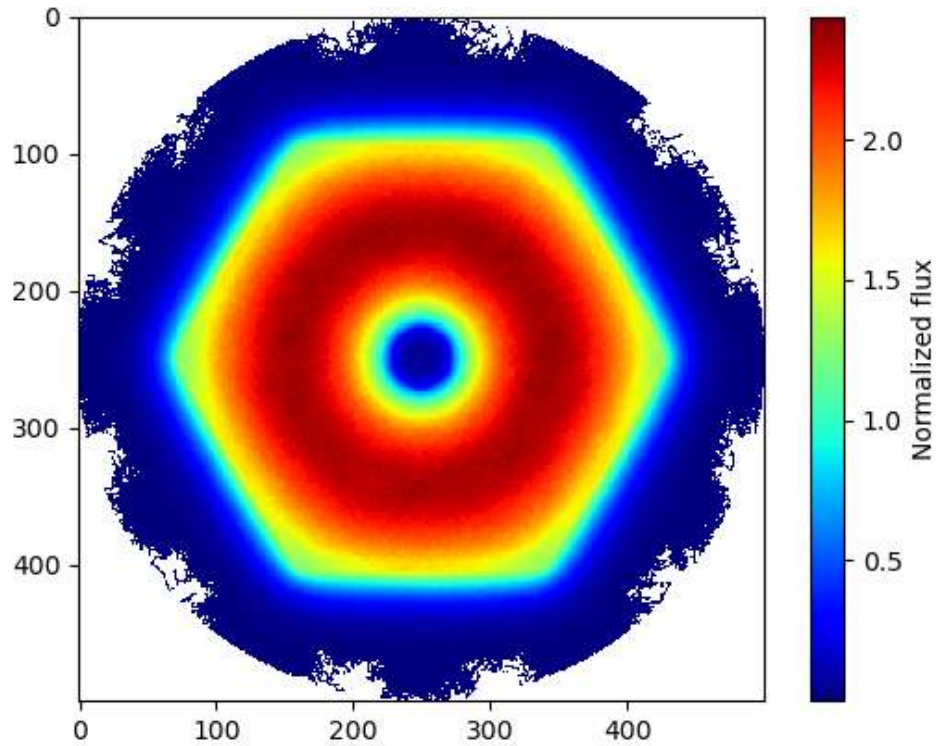


Figure 41: 2D plot of radial flux changes of the core inserting a control rod in the middle of the core and rotating all the control drums facing outward the core.

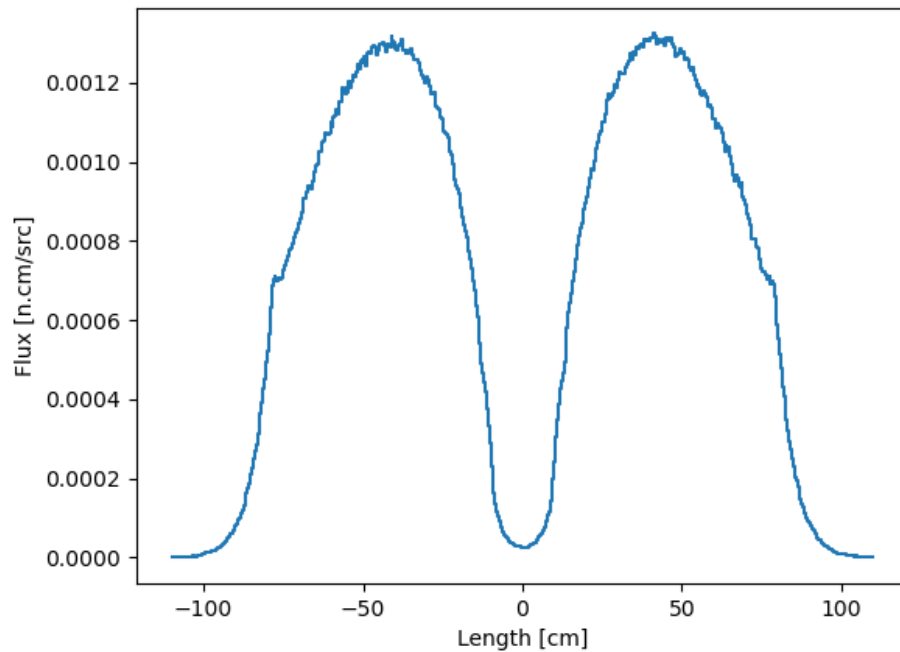


Figure 42: 1D plot of radial flux changes of the core inserting the control rod in the middle of the core and rotating all the control drums facing outward the core.

In Figure 42, the 1D radial flux distribution plot quantitatively highlights the broader flux behaviour under this configuration. The central region still exhibits a flux dip due to the presence of the fully inserted control rod, but the overall flux is elevated, especially near the core boundaries. A noticeable hump in neutron flux is observed at approximately 70–80 cm from the core center. This peak reflects the increased neutron activity caused by the reflector material of the outward-facing control drums, where the reflector materials of the control drums are facing the core and absorbing materials are facing outward from the core. Comparing Figure 40 with Figure 37 (inward-facing drums), the overall flux shape remains symmetric, but the peak flux in Figure 39 is slightly reduced due to the more distributed neutron behaviour.

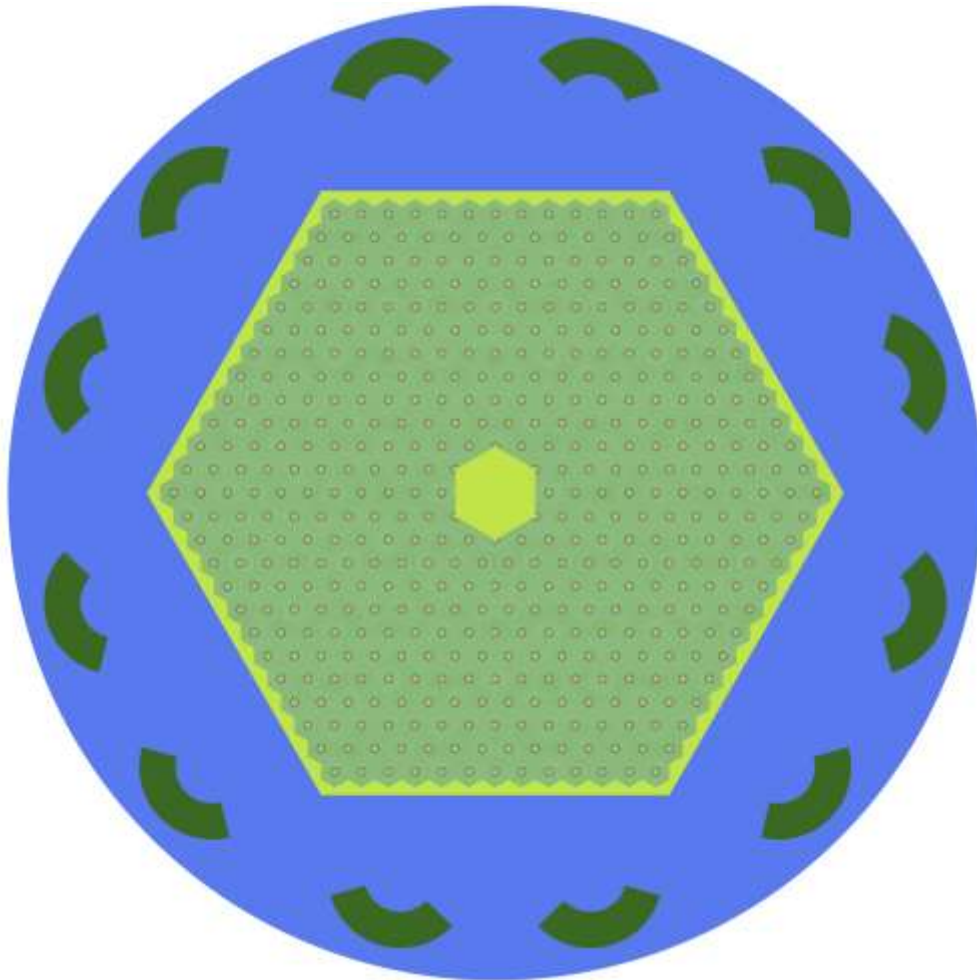


Figure 43: 2D MNR core layout with control rod withdrawn and control drum facing outward.

Figure 43 provides a 2D layout of the MNR core, illustrating the spatial arrangement of the hexagonal fuel assembly lattice, the central position of the control rod (withdrawn), and the 12 control drums within the radial reflector. The control drums are rotated outward, exposing their reflective material to the core. With the control rod fully withdrawn, neutron absorption at the core center is eliminated, and the outward-facing control drums reflect neutrons back into the core,

further increasing neutron population and flux. This configuration is expected to generate higher flux levels across the core due to minimal reactivity suppression mechanisms.

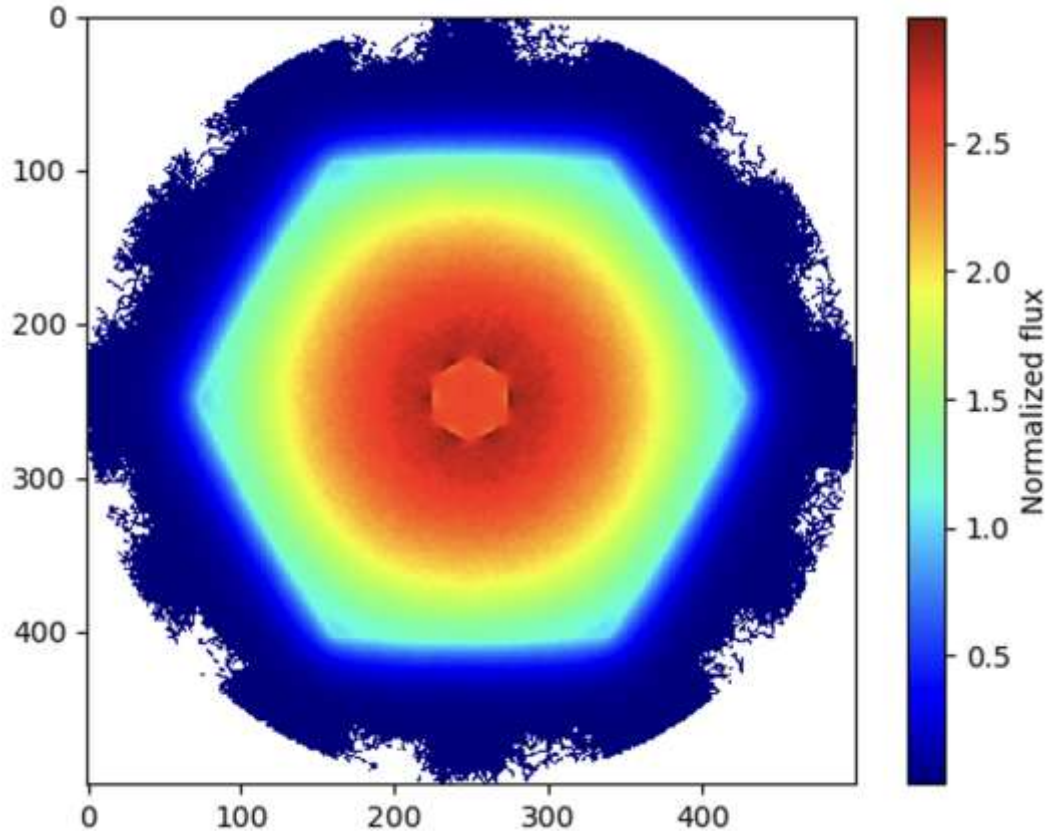


Figure 44: 2D plot of radial flux changes of the core withdrawing control rod in the middle of the core and rotating all the control drums facing outward the core.

Figure 44 shows the 2D radial flux distribution plot of the MNR core under this condition. Key observations from the plot include:

1. **Elevated Flux Across the Core:** The neutron flux is significantly higher throughout the core compared to previous conditions where the control rod was inserted. This is due to the absence of neutron absorption at the center and the reflective effect of the outward-facing control drums.
2. **Broader Flux Profile:** The flux distribution appears wider and more uniform, with the highest flux concentrated near the core center and gradually tapering off toward the periphery. This behaviour reflects the enhanced neutron reflection provided by the outward-facing control drums.
3. **Increased Core Reactivity:** The higher flux levels and the absence of significant neutron absorption led to a supercritical  $k_{\text{eff}}$  value of 1.06, indicative of elevated core reactivity in this configuration.

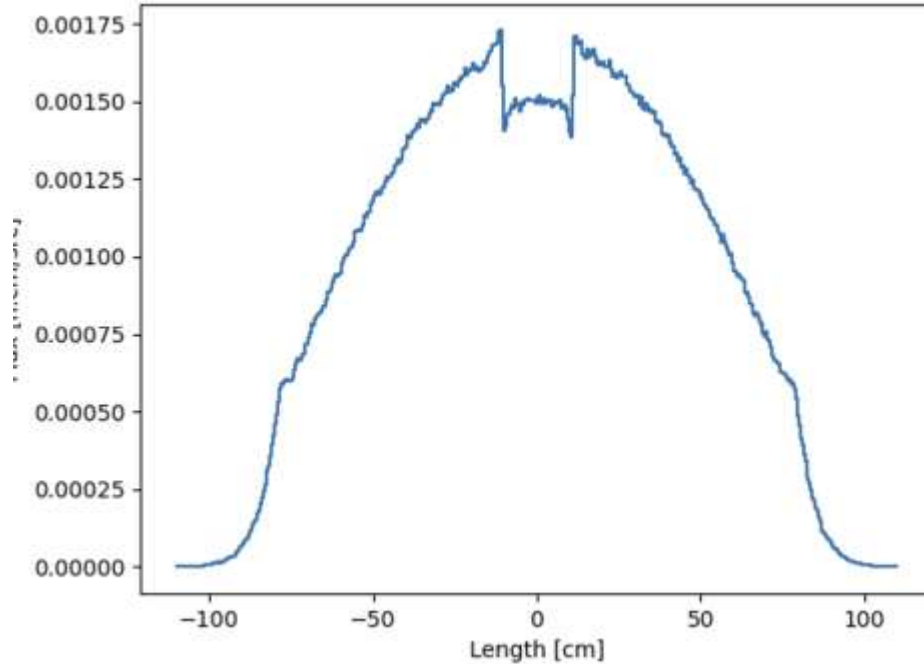


Figure 45: 1D plot of radial flux changes of the core withdrawing control rod in the middle of the core and rotating all the control drums facing outward the core. (250)

Figure 45 presents the 1D radial flux distribution plot, offering a quantitative analysis of neutron flux behaviour along a radial axis of the core. Key observations include:

The flux distribution exhibits a characteristic cosine shape, typical of a neutron flux distribution in a reactor core. The highest flux levels are observed near the central active region of the core, tapering off toward the edges. Despite the cosine shape, the peak is offset due to the absence of fuel rods in the very center of the core where the control rod was previously inserted (250 cm in the Y-axis). This results in reduced neutron production at the core center. This sharp dip corresponds to the area of reduced neutron multiplication, creating a noticeable valley in the otherwise smooth, cosine-shaped profile. The flux levels throughout the core are higher compared to conditions with inward-facing control drums, reflecting the increased neutron reflection and reduced neutron absorption.

Figure 46 presents a 1D radial flux distribution plot of the reactor core at a vertical axis position of  $Y = 220$  cm, where the core region consists entirely of fuel rods. Unlike the central plane ( $Y = 250$  cm), where the control rod or a helium gas gap introduces a dip in the flux profile, this section of the core is uniformly populated with fuel rods, resulting in a continuous and smooth flux distribution.

The flux distribution in this region exhibits a symmetric, cosine-shaped profile without any noticeable dips or valleys.

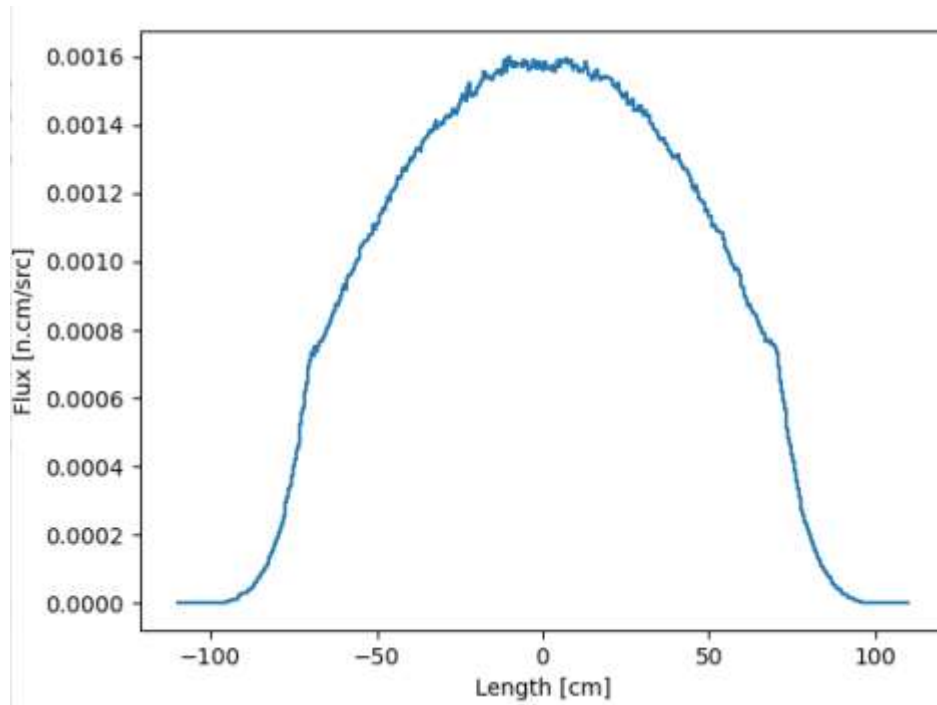


Figure 46: 1D plot of radial flux changes of the core withdrawing control rod in the middle of the core and rotating all the control drums facing outward the core. (220)

The presence of fuel rods throughout this region leads to a higher overall neutron flux compared to the central plane. The absence of neutron-absorbing materials, such as the control rod or helium gas gap, ensures that neutron interactions are maximized, resulting in a higher and more uniform flux profile.

At the boundaries of the core, the flux begins to taper off as neutrons interact with the radial reflector and are either reflected back into the core or absorbed. This behaviour is consistent with the expected neutron moderation and reflection dynamics in the reactor's design.

## 5. Discussion of Results

The neutronic design and optimization of the Micro Nuclear Reactor (MNR) presented in this study demonstrate the potential of advanced materials, innovative cooling mechanisms, and optimized reactor physics parameters in achieving a compact, efficient, and long-lifetime nuclear system. The study addressed several key challenges, including achieving criticality, optimizing the neutron economy, enhancing reactor safety, and ensuring the long-term sustainability of the fuel cycle.

### 5.1 Neutronic Optimization and Criticality Achievement

A significant aspect of the reactor design process was ensuring a sustainable neutron economy by selecting appropriate materials and configurations. The initial unit cell design, inspired by Los Alamos National Laboratory's (LANL) special-purpose reactor, faced substantial challenges due to high neutron absorption by stainless steel cladding. The replacement of stainless steel with a beryllium matrix not only mitigated neutron absorption losses but also enhanced neutron multiplication through (n,2n) reactions, thereby improving the reactor's criticality. The optimized unit cell with a 5.2 cm pitch and 20% fuel enrichment achieved a  $k_{\text{eff}}$  value of 1.15, ensuring excess reactivity for long-term operation. This result aligns with fast and intermediate reactor principles, where a balance between high neutron energy retention and effective utilization of fuel is crucial.

### 5.2 Fuel Burnup and Long-Term Reactor Viability

The burnup calculations indicated that the MNR exhibits a gradual depletion of U-235 while simultaneously breeding fissile isotopes such as Pu-239 from U-238. The evolution of fission product concentrations, particularly Xe-135, highlighted the reactor's ability to sustain stable reactivity over a 20-year operational lifespan. The observed reactivity swing over this period remained within manageable limits, demonstrating that the core design maintains sufficient reactivity margins without requiring refuelling. This capability is particularly advantageous for micro nuclear reactors intended for remote applications, where refuelling is impractical.

### 5.3 Neutron Flux Distribution and Core Performance

The neutron flux analysis provided key insights into the spatial behavior of neutron populations within the core. The 2D and 1D radial flux distributions confirmed a well-balanced neutron economy, minimizing localized power peaks and reducing the risk of hotspots. The fast and intermediate neutron spectrum was successfully maintained throughout the reactor's operational life, ensuring efficient utilization of TRISO fuel without significant spectral softening. The normalized lethargy flux spectrum further confirmed the reactor's fast and intermediate-spectrum operation, an essential characteristic for effective fuel utilization and waste minimization in next-generation nuclear systems.

## 5.4 Reactor Control Mechanisms

The implementation of dual reactivity control systems—comprising a centrally located control rod and surrounding control drums—demonstrated effective reactivity management. Hafnium hydride ( $\text{HfH}_2$ ) was selected as the neutron-absorbing material due to its superior neutron absorption properties compared to alternatives such as europium oxide. The control drum worth calculations indicated that a single drum contributed approximately \$1.25 of reactivity worth, while the full set of 12 drums provided a total worth of \$15. These values ensured that the control system could maintain reactor shutdown margins and accommodate reactivity fluctuations due to fuel depletion and fission product buildup.

## 5.5 Fuel Temperature Coefficient and Safety Implications

The reactor's negative fuel temperature coefficient of reactivity (FTC) is a crucial safety feature that enhances inherent stability. The calculated FTC values ranged from  $-6.85$  pcm/K at lower temperatures to approximately  $-4.35$  pcm/K at higher temperatures, confirming that an increase in fuel temperature leads to a corresponding decrease in reactivity. This behaviour is essential for mitigating transient power excursions, preventing runaway reactions, and ensuring passive safety under abnormal conditions. The results validate that Micro Nuclear Reactor (MNR) design incorporates robust negative feedback mechanisms, enhancing operational safety without reliance on active control systems.

## 5.6 Comparison with Existing Micro Nuclear Reactor Designs

A comparative assessment of the designed Micro Nuclear Reactor (MNR) with existing micro nuclear reactors revealed several distinct advantages. Unlike conventional solid  $\text{UO}_2$ -fueled microreactors, the integration of TRISO fuel embedded in a beryllium matrix significantly improved neutron economy while eliminating the need for fuel cladding. The use of sodium heat pipes for passive heat removal further differentiated this design from earlier concepts relying on liquid metal cooling. Additionally, the optimized core layout with a higher packing fraction of TRISO fuel particles demonstrated enhanced fuel utilization efficiency, reducing the required initial fissile inventory compared to traditional small modular reactors.

## 5.7 Challenges and Future Considerations

Despite the promising results, certain challenges warrant further investigation. The impact of rotating control drums at different angles and the change of power according to that should be studied in future work. Also, tracing every fuel particle, the burnup result for the full core of the designed micro nuclear reactor needs to be studied to measure the changing behaviour of material due to burnup with time. It is also important to study how the core flux changes with the reactor period.

## 5.8 Conclusion

This thesis presented the modelling, neutronic design, and optimization of a heat pipe-cooled Micro Nuclear Reactor (MNR) operating within a fast and intermediate neutron spectrum, tailored for long-term, self-sustaining operation in remote applications. The reactor concept, initially inspired by the Los Alamos National Laboratory's (LANL) Design A, underwent substantial modifications to meet the objectives of enhanced safety, higher reactivity margins, and efficient neutronic performance.

A unit cell design was developed based on a hexagonal fuel lattice, utilizing TRISO fuel particles embedded within a beryllium matrix. The removal of unnecessary stainless steel cladding and the replacement of the matrix material with beryllium significantly improved the neutron economy, allowing the reactor to achieve and maintain criticality. Further optimization of the fuel lattice pitch and fuel enrichment levels demonstrated that appropriate design adjustments could ensure excess reactivity margins for a 20-year operational lifespan.

Neutron flux distribution analyses, including 1D radial and 2D spatial flux profiles, confirmed that the reactor maintained a uniform neutron flux across the core, operating predominantly within the fast and intermediate energy ranges as intended. Comparative studies with traditional PWR and SFR neutron spectra validated the reactor's spectral behaviour.

The reactivity swing was manageable, and the reactor exhibited strong inherent stability, as indicated by the calculated negative Fuel Temperature Coefficient (FTC), which ranged between -4.8 to -6.8 pcm/K.

A full-core model was constructed with 462 fuel elements arranged in a concentric hexagonal pattern, ensuring symmetry and uniformity in neutron flux distribution. The control system design, consisting of a central control rod and 12 rotating control drums embedded with hafnium hydride (HfH<sub>2</sub>) absorbers, demonstrated effective reactivity management. Control rod worth and control drum worth calculations validated the system's ability to achieve subcriticality under shutdown conditions, ensuring robust operational safety.

Ultimately, the optimized MNR design successfully achieved all the intended goals:

- Sustained fast and intermediate neutron spectrum operation over a 20-year lifetime without refuelling,
- Inherent safety features through strong negative temperature feedback,
- Efficient reactivity control mechanisms using advanced absorber materials,
- Improved neutron economy and fuel utilization by employing TRISO fuel in a beryllium matrix,
- Compact, robust core geometry capable of supporting autonomous operation in isolated environments.

The work presented in this thesis contributes to the advancement of next-generation micro modular reactor designs, offering a promising solution for a reliable, long-term energy supply in off-grid, remote, or disaster-prone regions. Future studies may expand on this design by incorporating

thermal-hydraulic analysis, mechanical integrity assessments, and transient safety evaluations to further validate and refine the reactor's overall performance.

## Bibliography

1. Romano, Paul K., Nicholas E. Horelik, Bryan R. Herman, Adam G. Nelson, Benoit Forget, and Kord Smith. "OpenMC: A State-of-the-Art Monte Carlo Code for Research and Development." *Annals of Nuclear Energy* 82 (2015): 90–97.
2. Sterbentz, J. W. et al. (2018). Preliminary assessment of two alternative core design concepts for the special purpose reactor. Idaho National Laboratory. Available at: [https://inldigitallibrary.inl.gov/sites/sti/sti/Sort\\_8846.pdf](https://inldigitallibrary.inl.gov/sites/sti/sti/Sort_8846.pdf).
3. International Atomic Energy Agency. Research reactors: Purpose and future. Available at: <https://www.iaea.org/sites/default/files/18/05/research-reactors-purpose-and-future.pdf>.
4. ScienceDaily. High Flux Isotope Reactor named nuclear historic landmark. Available at: <https://www.sciencedaily.com/releases/2014/09/140911163106.htm>.
5. O'Rourke, R. Navy Columbia (SSBN-826) class ballistic missile submarine program: Background and issues for Congress. Congressional Research Service.
6. Australian Nuclear Science and Technology Organisation (ANSTO), "OPAL reactor,". Available: <https://www.ansto.gov.au/education/nuclear-facts/what-are-radioisotopes>
7. Till, Charles E., and Yoon Il Chang. *Plentiful Energy: The Story of the Integral Fast Reactor, the Complex History of a Simple Reactor Technology, with Emphasis on Its Scientific Basis for Non-specialists*. North Charleston, SC: CreateSpace Independent Publishing Platform, 2011.
8. Argonne National Laboratory. "Experimental Breeder Reactor-II (EBR-II)." Last modified March 15, 2013. <https://www.ne.anl.gov/About/reactors/firt.shtml>
9. Rahman, Mohammad Mizanur, Ji Dongxu, Nusrat Jahan, Massimo Salvatores, and Jiyun Zhao. "Design Concepts of Supercritical Water-Cooled Reactor (SCWR) and Nuclear Marine Vessel: A Review." *Progress in Nuclear Energy* 151 (2022): 104385. <https://doi.org/10.1016/j.pnucene.2022.104385>.
10. International Atomic Energy Agency. Fast reactors: Topics and resources. Available at: <https://www.iaea.org/topics/fast-reactors>.
11. World Nuclear Association. Fast neutron reactors. Available at: <https://www.world-nuclear.org/information-library/current-and-future-generation/fast-neutron-reactors>.
12. Japan Atomic Energy Agency, Nuclear Data Center. *JENDL-5 Neutron Cross Sections Graphs: Fission Cross Sections for Pu-239 and U-238*. Last modified 2023. [https://www.ndc.jaea.go.jp/ENDF\\_Graph/](https://www.ndc.jaea.go.jp/ENDF_Graph/).
13. Schneider, Mycle. "Fast Breeder Reactors in France." *Science & Global Security* 17, no. 1 (2009): 36–53. <https://scienceandglobalsecurity.org/archive/sgs17schneider.pdf>.
14. Wikipedia. "Monju Nuclear Power Plant." Last modified March 12, 2024. [https://en.wikipedia.org/wiki/Monju\\_Nuclear\\_Power\\_Plant](https://en.wikipedia.org/wiki/Monju_Nuclear_Power_Plant).
15. McClure, Patrick R., David I. Poston, Marc A. Gibson, Cheryl Bowman, John Creasy, Robert Reid, and Richard Kapernick. *Design of Megawatt Power Level Heat Pipe Reactors*. Los Alamos National Laboratory, LA-UR-15-28840, November 12, 2015. <https://doi.org/10.2172/1227259>.

16. Deng, J., Wang, T., Liu, X., Zhang, T., He, H., and Chai, X. (2023). Experimental study on transient heat transfer performance of high temperature heat pipe under temperature feedback heating mode for micro nuclear reactor applications. *Applied Thermal Engineering*, 230, 120826. doi: 10.1016/j.applthermaleng.2023.120826.
17. U.S. Nuclear Regulatory Commission. Heat pipe reactor concepts and their applications. Available at: <https://www.nrc.gov/docs/ML2215/ML22158A054.pdf>.
18. Oak Ridge National Laboratory. Nuclear data assessment for advanced reactors. Available at: <https://info.ornl.gov/sites/publications/Files/Pub157117.pdf>.
19. Powers, J. J. and Wirth, B. D. (2010). A review of TRISO fuel performance models. *Journal of Nuclear Materials*, 405(1), 74–82. doi: 10.1016/j.jnucmat.2010.07.030.
20. Wang, J. (2004). An integrated performance model for high temperature gas cooled reactor coated particle fuel. Thesis (Ph.D.), Massachusetts Institute of Technology. Available at: <https://dspace.mit.edu/handle/1721.1/28368>.
21. Ultra Safe Nuclear Corporation. TRISO and FCM fuel. Available at: <https://www.usnc.com/fuel/>.
22. U.S. Nuclear Regulatory Commission. TRISO-coated fuel particle performance. NUREG/CR-6844. Available at: <https://www.nrc.gov/docs/ML0406/ML040650057.pdf>.
23. ScienceDirect. "Monte Carlo Method – An Overview." Accessed April 2, 2025. <https://www.sciencedirect.com/topics/neuroscience/monte-carlo-method>.
24. Sekimoto, H. and Tech, T. Nuclear reactor theory. Tokyo Institute of Technology.
25. OpenMC. User guide: Depletion module. Available at: <https://docs.openmc.org/en/stable/usersguide/depletion.html>.
26. Johnson, T. et al. (2022). Advanced burnup algorithms in OpenMC. *Annals of Nuclear Energy*, 145, 12–25. doi: 10.1016/j.anucene.2022.107840.
27. Wilson, E. H. et al. (2019). Stochastic collocation for uncertainty quantification in burnup calculations. *Journal of Computational Physics*, 396, 678–692. doi: 10.1016/j.jcp.2019.07.022.
28. Smith, R. and Carter, E. (2021). Matrix exponential methods for nuclear depletion calculations. *Nuclear Science and Engineering*, 180(2), 235–247. doi: 10.1080/00295639.2021.1897397.
29. Aufiero, M. et al. (2015). Integration of depletion capabilities into the OpenMC Monte Carlo code. *Annals of Nuclear Energy*, 85, 245–256. doi: 10.1016/j.anucene.2015.06.019.
30. Carter, L. and Cashwell, E. (1975). Monte Carlo methods for nuclear applications. Los Alamos National Laboratory. Available at: <https://www.osti.gov/biblio/4167844>.
31. OpenMC User Documentation. Simulation methodology and energy spectra. Available at: <https://docs.openmc.org/en/stable/usersguide/index.html>.
32. Johnson, T. et al. (2022). Advanced burnup algorithms in OpenMC. *Annals of Nuclear Energy*, 145, 12–25. doi: 10.1016/j.anucene.2022.107840.
33. OpenMC User Documentation. User guide: Depletion module. Available at: <https://docs.openmc.org/en/stable/usersguide/index.html>.

34. Horelik, Nicholas, Bryan Herman, Benoit Forget, and Kord Smith. "Benchmark for evaluation and validation of reactor simulations (BEAVRS), v1. 0.1." In *Proc. Int. Conf. Mathematics and Computational Methods Applied to Nuc. Sci. & Eng*, vol. 7, pp. 63-68. 2013.
35. Stauff, N. E., T. K. Kim, T. A. Taiwo, L. Buiron, G. Rimpault, E. Brun, Y. K. Lee et al. *Benchmark for neutronic analysis of sodium-cooled fast reactor cores with various fuel types and core sizes*. No. NEA-NSC-R--2015-9. Organisation for Economic Co-Operation and Development, Nuclear Energy Agency-OECD/NEA, Nuclear Science Committee-NSC, 46, quai Alphonse Le Gallo, 92100 Boulogne Billancourt (France), 2016.
36. Lamarsh, J. R. (1977). *Introduction to Nuclear Engineering*. Addison-Wesley Publishing Company, 42–73.
37. Lamarsh, John R., and Anthony J. Baratta. *Introduction to Nuclear Engineering*. 3rd ed. Upper Saddle River, NJ: Prentice Hall, 2001.
38. Peterson, Per F., Charles F. Schleicher, and Tomasz Kozlowski. "Use of Hafnium Hydride in High-Temperature Gas-Cooled Reactors." *Nuclear Technology* 147, no. 3 (2004): 379–388.
39. Japan Atomic Energy Agency, Nuclear Data Center. JENDL-5 Neutron Cross Sections Graphs: Hf-178 and Hf-179 (n, $\gamma$ ). Last modified 2023. [https://www.ndc.jaea.go.jp/ENDF\\_Graph/](https://www.ndc.jaea.go.jp/ENDF_Graph/).